ISSN 1831-9424 (PDF)
ISSN 1018-5593 (Printed)

European Commission

Advanced design methods for BLAST Loaded steel structures

(ADBLAST)

Research and Innovation

EUR 27487 EN

EUROPEAN COMMISSION
Directorate-General for Research and Innovation
Directorate D — Key Enabling Technologies
Unit D.4 — Coal and Steel

E-mail: rtd-steel-coal@ec.europa.eu
RTD-PUBLICATIONS@ec.europa.eu

Contact: RFCS Publications

European Commission
B-1049 Brussels

European Commission

Research Fund for Coal and Steel

Advanced design methods for BLAST Loaded steel structures

(ADBLAST)

Benno Hoffmeister, Nicole Schillo, Carles Colomer
RWTH Aachen University
Institute for Steel Structures, 52074 Aachen, Germany

Ahmed Elghazouli
Imperial College of Science, Technology and Medicine
SW7 2AZ London, UK

Luca Nardini, Walter Salvatore
University of Pisa
56125 Pisa, Italy

David Lecompte, Bruno Reymen, Johnny Vantomme
Royal Military Academy – Patrimony
1000 Brussels, Belgium

Johan Maljaars, M. Schelland, Ton Vrouwenvelder
Nederlandse Organisatie voor toegepast-Natuurwetenschappelijk onderzoek - TNO
2628 VK Delft, The Netherlands

Renata Obiala
ARCELORMITTAL BELVAL & DIFFERDANGE S.A.
L-4009 Esch-Sur-Alzette, Luxembourg

André Dürr, Andreas Hemker
HOCHTIEF Solutions AG
60528 Frankfurt am Main, Germany

Grant Agreement RFSR-CT-2010-00030
1 July 2010 to 30 June 2013

Final report

Directorate-General for Research and Innovation

2015 EUR 27487 EN

Europe Direct is a service to help you find answers to your questions about the European Union

Freephone number (*)**:**

00 800 6 7 8 9 10 11

(*) Certain mobile telephone operators do not allow access to 00 800 numbers or these calls may be billed.

More information on the European Union is available on the Internet (http://europa.eu).

Cataloguing data can be found at the end of this publication.

Luxembourg: Publications Office of the European Union, 2015

Print	ISBN 978-92-79-52097-6	ISSN 1018-5593	doi:10.2777/155654	KI-NA-27-487-EN-C
PDF	ISBN 978-92-79-52096-9	ISSN 1831-9424	doi:10.2777/141025	KI-NA-27-487-EN-N

Printed in Luxembourg

PRINTED ON WHITE CHLORINE-FREE PAPER

Table of contents

1 Introduction

1.1 Motivation

In case of explosions severe consequences need to be expected – either in economical means or even worse in form of injuries or casualties. Several events in the past showed the necessity to protect structures and human health and safety by means of enhanced design rules against accidental or malicious blast loadings.

In view of the severe consequences of such events there is increased demand from clients and authorities for provision of appropriate design methods for blast resistance. This is particularly the case in important industrial facilities where such considerations are usually part of tender documents and contracts. Nevertheless, the formulation of these requirements as well as the definition of relevant actions remains ambiguous and the applicability and effectiveness of possible mitigation measures are largely unsubstantiated.

At present, there are few methods that deal with the design of structures under external or internal blast loading conditions. Existing methods have in common a very rough estimation of blast loads – usually assumed as equivalent static load – and missing consideration of the response characteristics of the structure and of structural elements. Consequently current design approaches typically result in high-mass demand and hence largely lead to heavy and bulky structures and components, which in turn favour concrete solutions. The same trend can be identified for façades and partitions design for which it is claimed that significantly higher blast resistance can be achieved by concrete elements in comparison to light weight steel cladding. Accordingly, although steel structures are still the preferred solution for various types of industrial buildings, the mass-based approaches required for the ever-growing demand for blast resistance are incompatible with the relatively light weight nature of steel construction.

Within ADBLAST it was aimed to develop safe and simple design methods allowing structural engineers to use the strategic advantages of steel constructions: material toughness and member ductility, large deformation capacity, material hardening due to high speed loading and membrane or catenary effects as well as customizable energy dissipation. The application of this developed method leads to improved blast resistance and hence to an enhanced competitiveness of steel structures.

1.2 Objectives

The research aimed at developing guidance for the design of steel structures with emphasis on procedures which are suitable for typical industrial buildings. Buildings under consideration were industrial buildings which are prone to possible blast load cases due to either storage of explosive materials or due to infrastructures (e.g. pipes, traffic).

The investigations involved blast tests on key non-structural and structural components together with their interactions, coupled with comparative quasi-static tests as well as analytical and nonlinear numerical assessments of local and global behaviour.

On the loading side, the project considered blast scenarios arising from external sources. Although the effects of an accidental explosion and a distant bomb explosion are comparable regarding their effects on buildings, the hazard scenarios were limited to accidental events as they are more likely in industrial facilities or along infrastructures. Close-to-surface explosions, e.g. from a bomb placed directly at a structural element were also not considered within this project. The effects from such explosion differ significantly from the effects caused by blast waves.

Internal explosions were excluded in an early stage of the project. Due to reflection and confinement phenomena, consideration of these loading scenarios would increase the complexity of the questions to be solved radically. For internal deflagrations however the approaches

developed within the project can be used provided that the time dependant development of the overpressure within a compartment is known.

On the response side, the project focused on the structural performance of key non-structural and structural components and their interaction on the local level as well as the global structural performance. The investigations were aiming at the predictability and control of the response of individual elements and groups of elements within a structure. Focus was laid on steel claddings and their supports. Comparative tests were conducted on trapezoidal sheets, liner trays and blank sheets. Dynamic interaction under blast loading on substructure level was accomplished with U-profiles, downscaled to fit the testing facility restrictions. These elements were used in static and blast tests, as well as in numerical simulations to ensure comparability.

Different connection types were investigated. Their resistance and structural behaviour have significant influence on the performance of the investigated elements. Different types of fastening were investigated in separate tests as well as in tests on the cladding elements. The test results were used to assess and to model the performance characteristics and the failure criteria for the cladding-support-subsystems. Main interest concerned self-tapping screws, as they are widely used in these structural applications. For the cladding to substructure connections also quasi rigid fasteners were used allowing for the separation of the contributions of the fasteners and the members to the response.

Of particular interest were also the failure modes governing the ultimate resistance of cladding and members and the deformations of members affected by the blast load. The post-blast damage-state was used to determine the required deformation capacity of members and of the residual resistance after the blast event.

The central idea of the project involves the provision of two main defence lines which are activated depending on the 'usually unpredictable' level of blast action. This approach enables, in a similar manner to approaches used in seismic resistance, the design of the structure such that it exhibits a gradual performance depending on the load level and type of action. This involves consideration of specific performance requirements as well as predetermined damage levels agreed with owners, users and/or authorities. The work therefore involved the following key constituents:

i. Development of action scenarios and classification of action types/models: development of a strategy involving limitation of action effects and the provision of a most favourable performance of the structure under the applied loading conditions.
ii. Response of non-structural elements: appropriate design of claddings or roof decking such that they fail at a specific blast load level and provide a ventilation effect. The maximum loads transferred to the main structures are therefore limited by the ultimate capacity of the claddings at the point of failure.
iii. Performance of the structural system: design and detailing of the main structure to respond in a ductile manner to the loads transferred from the non-structural components at the point corresponding to their ultimate capacity. Limitation of deformation for key members in order to ensure residual resistance and stability sufficient for the prevention of collapse or disproportional damage.

The results of experimental and analytical studies were aimed to use for a proposal for appropriate performance-based design procedures.

1.3 Research work

In the first step, typical industrial facilities and buildings were gathered and summarized, to identify typical structural components subjected to blast loading (e.g. span length, façade-systems, roof decking configurations, fastening systems etc.). This information was used to design the experimental test setups for static and dynamic investigations. A total number of 14 typical projects was identified, including

- Coal fired power plants
- Waste incineration plants
- Nuclear power plants and facilities
- Chemical facilities

Eight representative projects were studied in detail resulting in a set of typical roof/façade systems, cladding supports and main structure topologies. The studies comprised also the blast load scenarios and performance requirements specific for each project. As conclusion typical arrangement of trapezoidal claddings supported by secondary beams were selected for experimental and numerical investigations.

A survey on the safety and performance requirements revealed the direct correlation between blast scenario (internal or external explosion, type of explosive (e.g. single source), consequences classes and load assumptions. The consequences classes CC1, CC2 and CC3 refer to low, medium and high consequences as defined in the Eurocode EN 1990 Basis of Design (or EN 1991-1-7, Accidental actions) and are further described in the corresponding National Annexes for every individual country. Consequences may refer to economic losses, environmental disasters as well as to possible casualties. For some buildings the consequences may be confined to the building itself, for other structures the loss of function may have further consequences. Within a quantitative risk analysis approach, the probability of occurrence for a number of examples has been derived, using event tree analysis and numerical values based on Dutch data.

A framework for an explosion risk analysis was given and relevant statistical data for various explosion scenarios were gathered and made available. The risk analysis follows the principle of an event tree linked to the assessment of probabilities of occurrence for each branch.

Additionally, pressure-impulse scenarios were derived in dependence of risk/consequence class and blast sources. The results are based on the TNT-equivalent method, defining any load scenario (detonation or deflagration) as an effectively similar detonation type with corresponding weight [kg] of TNT (see deliverable D3). The derived values are depicted in the Design Guide.

The static and dynamic tests were designed in close cooperation with the industrial partners, to ensure realistic test setups. However, due to restrictions in the testing facilities, slight downscaling had to be accepted (see deliverable D4 – tests on cladding systems - and D5 – tests on claddings with substructure).

The comparison of static tests with blast tests (especially for structures with several elements and complex mass/stiffness distributions) showed decisive differences in failure modes, which made a transfer function from static to dynamic experiments ineffective.

Numerical simulations where used to compute the blast and static tests, in order to validate failure mechanism and compare them with the design approach developed within ADBLAST.

The test results were used for verification of existing design approaches, which proved to be very conservative and not taking advantage of considerable positive effects, such as energy dissipation properties of steel components, mainly combined with the activation of membrane action under extreme loading conditions.

Building upon approaches developed in the 50s and 60s of the last century, a dynamic reduction methodology was developed which allows for the inclusion of arbitrary boundary conditions, including joint properties. Thus, connectors can be explicitly modelled and their failure as well as membrane effects can be predicted. The solution is entirely analytically gained.

The solution has been derived additionally for normalized impulse duration and peak pressure values, so that general design aids could be produced as P-I diagrams, including an assessment of connector failure for typical steel cladding systems (see also in the Design Guide of this document).

With this method, the energy dissipation capabilities, and thus large deformation capacity and membrane effects of structural elements are exploited in a straight forward approach. This allows directly for a more efficient design of steel structures. Additionally, the formulation allows for an implementation in finite element codes, which open the possibility to more advanced parametric studies including full structural interaction.

The material behaviour assumed is based on a perfect elastic-plastic characterization and is directly connected to ductility requirements. It was aimed to find a link between existing ductility requirements of seismic codes and suggestions reasonable for blast loading. The basic needs for a structure exposed to on the one hand a cycling loading with relatively long loading times on more or less evenly spread at the whole structure, and on the other hand exposed to a very short impulsive loading on a part of the structure with transfer and change of the loading amplitude towards adjacent elements proved to be barely comparable. However, ductility requirements according to different codes and recommendations were gathered and can be found in deliverable D8 (transfer of seismic design rules to blast resistance) in the attached Design Guide.

Finally, a Design Guide was written by the partners, containing the main outcomes of the project reflected in selected examples.

2 Summary

In the first step, typical industrial facilities and buildings were gathered and summarized, to identify typical structural components (e.g. span length, façade-systems, roof decking configurations, fastening systems etc.). This information (Deliverable D1) was used to design the experimental test setups for static and dynamic investigations.

A survey on the safety and performance requirements revealed the direct correlation between blast scenario (internal or external explosion, type of explosive – e.g. single source), consequences classes and load assumptions. The consequences classes CC1, CC2 and CC3 refer to low, medium and high consequences as defined in the Eurocode EN 1990 Basis of Design (or EN 1991-1-7, Accidental actions) and further described in the corresponding National Annexes for every individual country. Consequences may refer to economic losses, contamination of the site or environment as well as to possible casualties. For some buildings the consequences may be confined to the building itself, for other structures the loss of function may have additional consequences. Within a quantitative risk analysis approach, the probability of occurrence for a number of examples has been derived, using event tree analysis and numerical values based on Dutch data.

A framework for an explosion risk analysis was prepared, and relevant statistical data for various explosion scenarios were gathered and made available (Deliverable D2).

Additionally, pressure-impulse scenarios were derived in dependence of risk/consequence class and blast source. The results are based on the TNT-equivalent method, defining any load scenario (detonation or deflagration) as an effectively similar detonation type with corresponding weight [kg] of TNT (Deliverable D3). The derived values are depicted in the Design Guide.

The static and dynamic tests were designed in close cooperation with the industrial partners, to ensure realistic test setups. However, due to restrictions in the testing facilities, slight downscaling had to be accepted (see Deliverable D4 – tests on cladding systems - and D5 – tests on claddings with substructure).

The comparison of static tests with blast tests showed decisive differences in failure modes, which made a direct transfer of results from static tests to dynamic performance ineffective.

The test results were used for verification of existing design approaches, which proved to be very conservative and not taking profit from considerable advantageous material and structural behaviour of steel.

Constitutive on analytical approaches developed in the 50s and 60s of the last century, a simplified model was developed which allows for the inclusion of different boundary conditions, load and stiffness distributions. The approach offers the possibility to explicitly model and calculate the connector forces in the system, which is a major advance in order to predict the dynamic response and ultimate limit states.

The scaling or normalization of impulse duration, peak pressure and ductility at failure allows for a relatively system-independent design aid, which is advantageous towards common PI-diagrams (see deliverable D6 and Design Guide). With this method structural elements can be designed with reduced efforts and increased efficiency. The exploitation of membrane effects (catenary action) allows for a more efficient and more accurate design of steel structures. An implementation into finite-element-codes is also possible, to allow for simplified calculation of full structures.

The material behaviour assumed is based on a perfect elastic-plastic characterization, and is directly connected to ductility requirements. It was aimed to find a link between existent ductility requirements of seismic codes and suggestions reasonable for blast loading. The basic demands for a structure exposed to cycling loading with relatively long loading times acting more or less simultaneously at the whole structure on one hand, and structures exposed to a very short impulsive loading acting on a part of the structure with transfer and change of the loading amplitude towards adjacent elements on the other hand proved to be barely comparable. However, ductility requirements according to different codes and recommendations were gathered and can be found in deliverable D8 (transfer of seismic design rules to blast resistance) in the attached Design Guide.

3 Scientific and technical description of the results

3.1 Main Aims

The project aimed to evaluate and develop design approaches and procedures suitable for different blast scenarios in terms of performance levels incorporating aspects such as:

- Characterization of resistance behaviour of facades/panels,
- Response characteristics for key and peripheral structural elements and global systems requirements.
- Determination of performance (e.g. deformation) demands
- Identification of limit states (failure) of members and of the entire structure

The investigation involved realistic blast tests on non-structural and structural components together with their interaction, complemented by comparative quasi-static tests as well as analytic and nonlinear numerical assessments. The results of experimental and analytical studies were used to propose appropriate performance-based design criteria and procedures.

On the loading side, the project considered blast scenarios arising from external, deliberate and accidental sources. On the response side, the project focuses on the structural performance of non-structural (façade-systems) and structural components (sub-structural elements).

The work involved the following key constituents:

i) Development of action scenarios and classification of action types or models: as the actions considered are of exceptional nature and typically exceed the level of other ordinary loads, it is necessary to develop a strategy involving a limitation of action effects and the provision of a most favourable performance of the structure under the applied loading conditions

ii) Response of non-structural elements. The maximum loads transferred to the main structures are limited by the ultimate capacity of the claddings at the point of complete failure (e.g. due to rupture of fastenings)

iii) Development of safe-sided, simple design aids for structural engineers. Thus enabling them to use ductile properties of steel for blast loaded structures.

3.2 Comparison of initially planned activities and work accomplished

The first Workpackage (WP 1) "Representative structures and safety requirements" was aiming at (i) classification of user performance and safety requirements for industrial and similar low redundancy structures, (ii) to identify typical industrial facilities and buildings which may be subject to blast action and (iii) to select typical façade as well as roof decking configurations. For this purpose structural configurations as well as safety and performance requirement of past practice projects were collected and evaluated. Furthermore, structural configurations of industrial buildings as well as cladding and roof decking typical for the European market were identified. The outcome was a catalogue of structures and cladding types, which was the basis for the selection of case studies. The subsequent workpackages based on the outcome; the experimental tests were designed according to these information. The outcomes of this WP 1 are supplied as stand-alone report (deliverable 1). The complete contribution was uploaded to the Circa Server as Deliverable 1.

The aims of WP 2 "Risk assessment and definition of actions" were (i) the development of a risk assessment procedure for exceptional loads, (ii) the assessment and definition of blast scenarios and (iii) the determination of blast load parameters. A multi-level framework was developed for providing blast loads on structures including models for risk calculation of explosions. Furthermore, a catalogue of blast scenarios was prepared, where their frequencies of occurrence were estimated based on available statistical data as well as recent data from evaluated

newspapers. For each type of blast scenario models for determination of the blast load were prepared. The complete background documentation was made available as Deliverable 2 and 3.

In WP3 "Performance of steel claddings – experimental investigations" the ultimate performance of cladding and roof element under blast loads were investigated. Especially the determination of the load transfer function to the supporting members as well as the blast absorption by cladding elements were of major interest. Based on the results of WP1 and WP2 a testing program for static tests and blast tests was defined. Extensive material tests and tests on connections were conducted to calibrate material and structural performance of the connections to implement in finite element models. These tests were supplemented by material and connection tests considering strain rate effects.

Blast tests on claddings were conducted and analysed. The results were used as input for the development of simplified models in WP5 and WP6. The detailed description of static and dynamic tests can be found in deliverable D4.

WP4 "Performance of substructures – experimental investigations" dealt with the evaluation of the member-structure interaction under blast loads due to different boundary conditions.

Static tests with varying loading scheme on substructures were performed, and failure modes investigated. The bearing of the substructure element was varied to evaluate the influence of different bearing stiffness. With finite element calculations a model was created to investigate the possibility of performing the blast tests on the substructure in Brussels by RMA instead of Oberjettenberg, as was initially planned. Although the blast loading capacity in Brussels is restricted compared to the German facility, the testing facility was more flexible with regard to expected changings in the test-setup; such modifications could be more easily applied in case they are needed. The calculations supported the assumption that the pressure-impulse loading of Brussels could be sufficient in terms of achievable plastic deformation. Preliminary tests were conducted successfully and subsequently, tests were conducted in Brussels. The results of these tests were analysed and used as input for the development of simplified models in WP5 and WP6. An extensive background documentation can be found in deliverable D5.

The aim of WP5 "Performance of steel claddings – numerical investigations" was the numerical determination of the load transfer functions from claddings/roof decking to the main structure. Based on these simulations simplified methods for the design of claddings/roof decking against blast loads shall be developed. However, the computations showed decisive dependencies on modelling aspects. Moreover, the complexity of the structural elements as trapezoidal sheet decking and light gauge wall claddings, lead to very complex transfer functions, which were very system specific and not applicable on general systems. Research focus was therefore oriented towards the possibilities to reduce and simplify systems and find transfer functions in a general approach which are directly usable for designers and their needs.

In WP6 "Performance of full structures – numerical investigations" the performance and ductility demands on structures under blast loads, the interaction between the affected member and the global structure was investigated in numerical simulations. Different stages of model accuracy – from modelling a whole frame-structure down to just several cladding elements including substructure were evaluated to judge the behaviour and influence of smaller parts of the system. Similar to the research focus shift in WP5, the ADBLAST-team concentrated with increased intensity on the analytical derivation of a simplified model in comparison to the proposal, where the focus was more concentrated on numerical studies. Numerical studies were nonetheless conducted for chosen cases, whereas the analytical approach is applicable for general use.

A detailed description of the simplified ADBLAST design approach as well as the numerical studies can be found in deliverable D6 (D6 and D7 were merged to one document due to the similarity in the calculation approach).

The objective of WP7 "Transfer of seismic design rules to blast resistance" was related to identification and modification of existing seismic design rules for blast loads. For this purpose

European and US seismic standards were evaluated with regard to relevant design principles for blast loads. In the deliverable D8 the most relevant tables from ASCE-SEI 59/11 "Blast protection of buildings", where ductility requirements for structural steel members (end rotations) are stated, were extracted. These values can be directly compared with ductility limits for seismic design (from EN 1998-3 or ASCE-SEI 41/06).

In WP8 "Design Guidance and examples" the main results of the project are provided in a guideline for blast resistant steel structures. It includes as first step the risk assessment procedure and derivation of pressure-impulse load amplitude, followed by the design according to different standards and the ADBLAST approach. The Design Guide is attached as Annex to this document.

It can be concluded that although some ways and means as described in the proposal were modified considering the progress of the research project, the main aims:

- to give inside in risk assessment procedures
- to give advice how to assume blast load scenarios on actual structures
- to give simplified design aids to structural engineers
- to implement steel specific advantages

were fully achieved.

3.3 Actual work/ description of activities and discussion

3.3.1 Representative structures and safety requirements

Altogether 14 examples for industrial facilities were collected and evaluated in regard to typical design:

- Coal fired power plants
- Waste incineration plants
- Nuclear power plants and facilities
- Chemical facilities.

The investigation revealed a direct correlation between blast scenario, safety and performance requirements, as depicted in Table 1. The table also contains the typical structural types depending on the specific safety and performance level.

Generally the assessment of scenarios, risk, hazard and load models are case specific and needs consultation with authorities and owner of the structure.

Regardless of whether an internal or external blast scenario is considered, the most common safety requirement is to prevent the collapse of the building. Therefore, the structural stability has to be assured for example by local and global redistribution capabilities. For an internal explosion it might be necessary to reduce the maximum loads transferred to the main structures by an appropriate design of the cladding or roof decking such that they fail a specific blast load level providing a ventilation effect, preferably through the roof (scenario 1A). If the complete integrity of the structure must be assured for an internal explosion e.g. in order to avoid contamination by pollution release and damages at neighbouring buildings, then the application of a standard steel structure with light steel cladding and roofing systems is not reasonable (scenario 1B). In those cases usually heavy concrete structures are used which are not analysed within the project ADBLAST.

Also for the collapse prevention due to an external explosion it might be reasonable to reduce the load transferred to the main structure through a predictable failure of the cladding and plastification of secondary members (scenario 2A). For external blast waves combined with safety requirements for the humans and the technical equipment within the building, standard steel structures are only used if the blast wave is not too large (scenario 2B).

Table 1: Correlation blast scenario and requirements on structures

Explosion Scenario	Safety Requirement	Performance Requirement	Typical Structure	ADBLAST
1 Internal Explosion	A No collapse of the building Prevention of secondary explosions No domino effects No damages outside the building Investment protection	Structural stability of the structure Moderate damage of the structure **Ventilation through failure of defined area in roof or cladding** (or assembly of special products like pressure release openings)	Standard steel structures and cladding / roofing systems	Partly Considered
	B See A Prevention of pollution release	Integrity of structure and cladding	Concrete structures	Not considered
2 External Explosion	A No collapse of the building No domino effects Investment protection	Structural stability of the structure Moderate damage of the structure Pressure reduction through defined failure of cladding	Standard steel structures and cladding / roofing systems	Considered
	B See A Prevention of pollution release Protection of humans Protection of process control systems	Integrity of structure and cladding Moderate damage of structure and cladding	Small Blast Wave Standard steel structures and cladding / roofing systems	Considered
			Large Blast Wave Concrete Structure Double-wall system	Not considered

In general, regardless of whether an internal or external blast scenario is considered, the classification of performance requirements is also dependent on the defined safety requirement and the probability of occurrence as given in the chapter risk assessment.

The investigation of the case studies also revealed typical configurations of cladding system, fasteners and substructure/ frame. These were considered in the static and dynamic tests in the subsequent work.

Table 2: Typical systems identified from case-studies for use in experimental studies

System		Dimensions	Profile type
1	Single-skin cladding (non-insulation)	▪ Profile depth: approx. 85 mm Thickness: 1,00 to 1,25 mm	▪ TRP 85/280 ▪ TRP 35/207 ▪ TRP 45/333
2	Single-skin roofing (non-insulation)	▪ Profile depth: approx. 85 to 100 mm Thickness: 0,88 to 1,25 mm	▪ TRP 85/280 ▪ TRP 100/275
3	Double-skin cladding (insulation)	▪ Liner tray: Profile depth: approx. 130 mm Thickness: 0,88 mm ▪ Insulation: approx. 100 mm ▪ Weather sheet: Profile depth: approx. 85 to 100 mm Thickness: 0,88 to 1,00 mm	▪ K 600/130 ▪ TRP 35/207
4	Double-skin roofing (insulation)	▪ Liner tray: Profile depth: approx. 135 to 150 mm Thickness: 1,00 to 1,25 mm ▪ Insulation: approx. 100 mm ▪ Weather sheet: Profile depth: approx. 35 to 45 mm Thickness: 0,75 to 0,88 mm	▪ TRP 135/310 TRP 150/280 ▪ TRP35/207 TRP 45/333

3.3.2 Risk assessment and definition of blast scenarios

3.3.2.1 Introduction

The objectives were to provide a risk based framework for the design of buildings with steel claddings under blast loading with an emphasis on the design blast pressure for buildings in the vicinity of a single blast source as well as buildings within industrial plants. The starting point for the derivation of design values and or design procedures is the Eurocode EN 1990 Basis of Design [2] in combination with Eurocode EN 1991-1-7 on Accidental design situations [1].
This chapter defines relevant *design scenarios* and corresponding *design loads* for blast loadings on industrial buildings with steel structures and steel claddings.

A *scenario* refers to a set of site related physical characteristics and events like (for blast loading) the type and amount of possible explosive materials, the release process, ignition, the resulting pressure waves and temperatures, etcetera. All aspects of such a scenario involve a degree of scatter and uncertainty, starting from the probability that in the period under consideration an explosion occurs at all. But in general also items like the exact amount (mass) of explosive material, time and location of the explosion, the turbulence inside a vapour cloud will be unknown to the designer. A rational way out is to estimate likelihood's and make best guesses, depending on the specific circumstances. Given those models one may strive for an optimal design where costs of mitigating measures are in balance with risk reduction.

Additionally there is a need to keep the design process simple, in particular if one may expect relative low explosion pressures and low failure consequences. The designer simply wants to find *design values* for peak blast pressures and blast duration in a similar way as for instance wind or impact loads are defined in the Eurocodes. An extensive Quantitative Risk Analysis (QRA) as described above should only be carried out for environments with a relatively high explosion danger and possible very serious consequences. In other cases some general classification should

be sufficient to obtain design values in tables that are optimal in some average sense and correspond to a defined level of acceptable damage.

In the ADBLAST project internal as well as external explosions are relevant. For internal gas and dust explosions [1] and the corresponding background documentation [Background Document EN 1991-1-7, COST-TU0601-documents] give adequate requirements for a meaningful design, also for industrial buildings. The basic idea is to reduce the load values by proper venting conditions.

The sources for external industrial explosions considered in this project are:

- Storage of explosives
- Warehouses / no explosives
- Stationary pressurised tanks and vessels
- Stationary atmospheric tanks and vessels
- Gas cylinders
- Pipes
- Road tankers
- Tank wagons (trains)
- Ships

Most information is based on the Background documentation of the Dutch quantitative risk assessment method for industrial sites and infrastructure [Purple Book, RIVM, Netherlands] as well as calculations provided by ADBLAST partner RMA. The principle design aim is to prevent or limit the damage to the structure for reasonable design pressures. Note that, if not fixed for other reasons, distance is a very important design variable. Also a defined limited failure load of the cladding may be helpful to protect the structure. However, this is not always possible as the building may be intended to protect humans and technical equipment inside.

A third relevant blast category considered is the terrorist attack. In order to find some information on these loads UK and Dutch newspapers have been studied of 2009 and 2010. However, most information available from newspapers concerns blasts in residential areas. Information about explosions on industrial plants is very limited. In addition, it is unknown whether this information gives a reliable overview, since it is expected that not all industrial explosions be documented in newspapers. Finally, the quantitative size of the blasts is difficult to obtain from newspaper information. For this reason the information from newspapers is used mainly to obtain a qualitative overview of blast sources.

3.3.2.2 Design Procedure

Formally speaking, each blast scenario has a certain probability of occurrence and of effects in terms of the *peak pressure* and *duration*, given its occurrence. In order to determine economically justified design values of the blast loads, the scenarios and effects (that is the Quantitative Risk Assessment) need to be performed in conjunction with the cost of mitigation measures.

More in detail, the main elements for a Quantitative Risk Assessment (QRA) are given by:

- The available type and amount of possible explosive material;
- The possible release and ignition processes;
- The development of the explosion;
- The location of the source in relation to the building;
- The resulting pressures on the structure;
- The structural response analysis;
- The estimation of the damage and casualties.

For all items models and quantities in statistical terms need to be specified. We then may derive the risk for a given design by:

$$Risk = \lambda(H) \cdot P(D|H) \cdot C(D) \quad (1)$$

Where $\lambda(H)$ is the occurrence rate of the triggering event, *P* stands for probability, *D* is the damage given the event has occurred, and *C* the related costs. The intention of the design should be to minimize the sum of the mitigating costs and risk.

$$C_{tot} = C_0 + \sum Risk_i/(1+r)^i \quad (2)$$

C_o are the initial costs, *r* the real annual discount ratio, $Risk_i$ the risk related to year *i.* In some cases additional limits due to human safety (individual safety, social safety) may be important.

3.3.2.3 Simplifications / Eurocode type

Elaborating all possible scenarios for a specific building – including relevant parameters like the distance to roads, pipelines and other buildings on the plant – may be time-consuming and is not practical for many low-risk industrial buildings. The suggestion is to provide the designer with more general or more detailed models and information, depending on the probability of explosion and the consequences of the explosion. This is shown in Table 3.

Table 3: Example of general models depending on consequence class (CC) and type of activity

Probability of explosion	CC1	CC2	CC3
single source	Design pressure	Design pressure	Use formulas to determine pressure
industrial area	Design pressure	Design pressure	Perform a Risk Analysis

In normal situation, i.e. without presence of specific dangerous objects, the normal robustness rules of Eurocode EN 1991-1-7 apply. A low probability in general may be related to design situation involving only one dangerous object. A high probability corresponds to buildings on or very close to industrial areas having large amounts of gas vessels or other stored or transported explosive materials.

The consequence class in Table 3 is defined by the possible damage *C* and the number of fatalities N_d. Given the consequences class the required reliability level may be defined and design pressure p_d derived.

3.3.2.4 Models to quantify blast loads on structures

The free air overpressure *p* [kPa] depends on the amount of available energy *E* [GJ] and the distance R [m] and may be found using models like the Multi Energy, CFD or TNT equivalent. In this project the latter has been used (RMA-WP2 Task 2.2 Report "Classification of blast scenarios and methods for determination of corresponding blast parameters").

Obstacles in the vicinity of the blast source are known to have a significant effect on the blast wave in some cases; in particular in case of delayed ignition where the obstacle is situated inside the vapour cloud at the moment of ignition. This effect, although significant, is still difficult to quantify with a simple (analytical) model. For this reason, and for the time being, this effect is not explicitly modelled in WP2, but considered to be part of the random scatter. In a later stage we can decide whether or not the models should be updated to include this effect.

Obstacles in between the building to be designed and the blast source – i.e. other than obstacles inside the vapour cloud – may have a 'shielding effect' on the building to be designed. However, research has shown that the shielding effect is only significant if the obstacle is situated very close to the building and is substantially large. For these reasons the presence of shielding obstacles is not considered in this study.

It is convenient to translate the (free) pressure diagram to a triangle having a peak load value *p* and a duration Δt, as indicated in Figure 1.

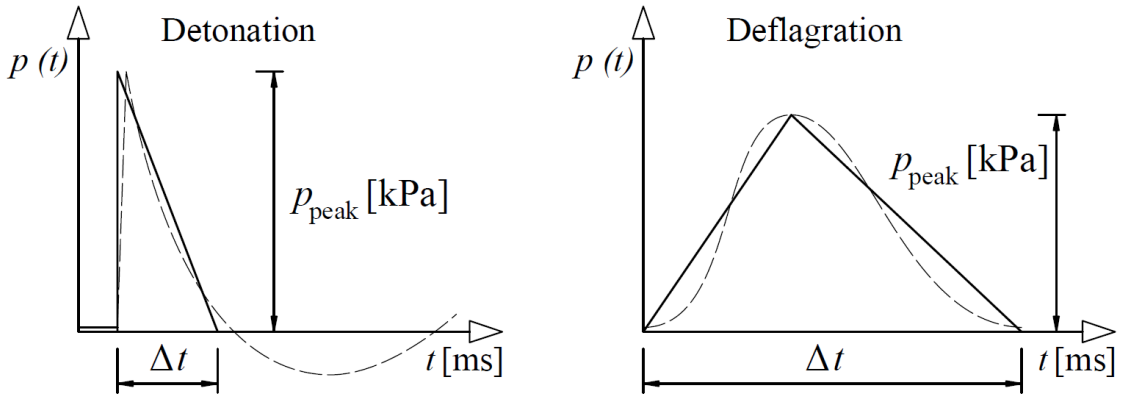

Figure 1: Triangular pressure-time model

Alternatively, the pressure and impulse values may be presented. In the case of a triangle we have simply:

$$I = 0{,}5 \cdot p_{peak} \cdot \Delta t \; [Pa \cdot s] \qquad (3)$$

When the blast wave reaches the building a complex pattern of reflection and interaction occurs. In some cases this may lead to much higher pressures on the building facades then the free value. For larger distances the factor of reflected pressure compared to the free field pressure is about 2, for shorter distances it my go up to 7.

3.3.2.5 Models / Examples for the external explosion risk calculation

3.3.2.5.1 Specific examples for stationary situations

In ADBLAST, the following specific examples were considered:

1. An LPG station with an underground storage tank of 20 m^3 and a pump machine.
   - 1.1 Blast source = storage tank.
   - 1.2 Blast source = road tanker (50 m^3) present on the site
2. A stationary atmospheric vessel containing solvents, e.g. ethanol.
   - 2.1 Content per vessel is 10 m^3
   - 2.2 Content per vessel is 100 m^3
3. A stationary pressurised vessels containing flammable, liquefied gases, e.g. propane.
   - 3.1 Content per vessel is 100 m^3 (45 000 kg)
   - 3.2 Content per vessel is 2000 m^3 (900 000 kg)
4. A storage site for explosives, e.g. fireworks. Blast source = explosives.
   - 4.1 Total mass of fireworks per container = 500 kg
   - 4.2 Total mass of fireworks per container = 10000 kg

The distance between the building to be designed and the stationary blast source was defined as 10 m, 100 m and 500 m. The probability of an explosion was analysed and gave the blast loading on the building in terms of pressure and impact. Table 4 shows an overview of the main results. First the estimated amount of effective blast energy is mentioned (in general 5% of the theoretical available energy). It is expressed both in [GJ] and in the equivalent [kg TNT] (column 2 and 3).

The next column mentions the distance between the building (that is the considered façade – column 8 and 9) and the centre of the explosion. It is followed by the calculated free air pressure, the positive phase duration and the impulse as computed by the computer program ConWep in column 5 to 7. Also the maximum pressure on the façade is given as well as the total pulse. For large distances the difference in pressure is about a factor 2. These values allow for the design of adjacent structures. The probability of occurrence per year is given in the last column.

Varying the distance R (column 4), it can be observed that pressure and impulse reduce significantly with increasing distance of the explosion source to the respective structure. The reflected pressure/impulse is of course much higher than the free air pressure/impulse correlation, however, the ratio is also highly depending on the energy set free (column 1 and 2).

Table 4: Results for specific examples

1	2	3	4	5	6	7	8	9	10
	E_{eff} [kg TNT]	E_{eff} [GJ]	R [m]	p_{free} [kPa]	Δt [ms]	I_{free} [Pas]	p_{fac} [kPa]	I_{fac} [Pas]	λ [1/a]
underground LPG tank	160	0.8	10	340	11	800	1364	786	2E-6
	160	0.8	100	6,7	32	90	13.8	170	
	160	0.8	200	2,4	39	40	4.9	76	
road tanker pumping	12700	63.5	10	6000	6	4000	52500	69900	5E-7
	12700	63.5	100	60	80	1600	139	3500	
	12700	63.5	500	6	140	340	11	620	
ethanol vessel with protective outer shell	260	1.3	10	500	13	1100	2200	3100	4E-5
	260	1.3	100	8	35	130	17	234	
	260	1.3	250	2	45	50	4.8	89	
	380	1.9	10	660	16	1400	3200	4200	
	380	1.9	100	10	40	160	20	300	
	380	1.9	300	2	50	60	4.8	100	
propane vessel	200	1	10	400	12	900	1670	2500	1 E-6
	200	1	100	7	33	100	15	195	
	200	1	200	2,4	41	46	4.8	81	
	3000	15	10	2400	10	2600	16900	17000	3E-7
	3000	15	100	20	60	550	49	1080	
	3000	15	500	2	90	110	5.2	200	
	800	4	10	1100	20	2000	6500	7300	1E-6
	800	4	100	13	45	260	28	500	
	800	4	500	2,4	66	73	4.8	129	
	12000	60	10	6000	6	4000	50000	66000	3E-7
	12000	60	100	50	80	1500	132	3300	
	12000	60	500	5	140	330	11	600	
Storage of explosives	500	2.5	10	800	18	1600			1E-5
	500	2.5	100	11	40	200			
	500	2.5	300	2	55	60			
	10000	50	10	5000	6	3600			
	10000	50	100	50	80	1300			
	10000	50	500	5	130	300			

NOTE: The road tanker case is based on a leak in a pipe; there is also a possibility of a leak in a hose: in that case we have a smaller explosion but a larger probability.

3.3.2.5.2 Specific examples for transport systems

For vapour clouds resulting from transport lines (roads, railways, waterways, pipelines) the cumulative effect of the total chain has to be considered. In the next sections the various types of possible external explosions will be considered. The values presented are based on a literature review and on engineering judgement.

Transport of explosive materials considered in this project consist of trucks, trains, ships and pipeline transport. In these cases the occurrence rate λ has to be specified "per transport unit and per km" or "per km pipeline". Given the intensity of the traffic one can then calculate the expected number of explosions per year.

Five specific transport blast scenarios are considered:

1. Highway. Number of road tankers containing GF3 substances (e.g. LPG) per year = 700
2. Highway. Number of road tankers containing GF3 substances (e.g. LPG) per year = 7000
3. Rail track (single track) with no crossing and one point. Number of tank wagons per year = 10 000.
4. Rail track (double track) with two crossings and two points. Number of tank wagons per year = 2000.
5. Underground gas transport pipeline. Diameter = 500 mm, pressure = 66 bar.

In the case of transport we may subdivide the road or river into a number of segments. For each segment the probability of an explosion may be calculated given the occurrence rate per vehicle kilometre, the number of transport units per year (see Figure 2).

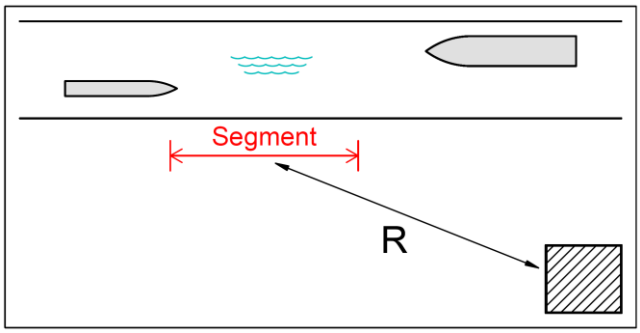

Figure 2: Procedure in case of transport explosive material on a waterway.

3.3.2.5.3 External vapour cloud explosion on a chemical plant

In order to deal with these types of loading in a risk approach one needs the explosion rate λ [1/a], the probability density of the amount of energy E [J] for an arbitrary and a probability distribution for the distance R [m] as the explosion may occur anywhere on the plant.

The probability of an accidental explosion somewhere will depend on the area A and the type of activities. In the Netherlands there is a major explosion about once per 10 years. Assuming about 100 relevant industrial areas this leads to λ = 0.001/a for an industry park. If we assume on average about 100 installations in one industrial area this corresponds to $\lambda = 10^{-5}$/a for one installation. This is in the order of magnitude of most cases in Table 4. We will use $3 \cdot 10^{-6}$/a for one installation and $3 \cdot 10^{-4}$/a for a plant. In a more refined risk analysis the exact number of installations could of course be considered.

The energy of a stoichiometric mixture is about 3.5 MJ/m^3. Given a large vapour cloud of r = 30 m we have a gas air volume of V = 50 000 m^3 which correspondents to 200 GJ. Of course, smaller values are possible, but also larger ones, in particular if chain reactions will start. We may arrive at a lognormal Weibull distributions with V = 1.0 as coefficient of variation. Note that in most cases only a small amount of 2 - 20 % this amount of energy will be converted into explosion energy, depending on the actual mixture conditions and the confinement properties of the

environment. So the effective blast energy E_{eff} is average about 10 GJ. The resulting distribution is presented in Figure 3. The result looks reasonable if we look into the calculated values in Table 4: many events in the region 1-5 GJ and some higher extremes (15 and 60 GJ) with lower probabilities.

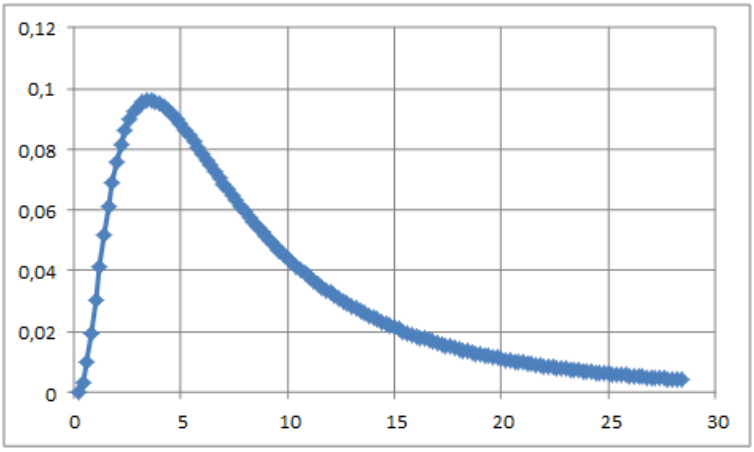

Figure 3: Probability-density function for the effective amount of energy E_{eff} [GJ]

Assuming a circularly shaped industrial area ($A = \pi \cdot R_0^2$) and the building of interest in the centre, the probability of *R* is:

$$f_R(r) = 2\pi r/A = 2r/R_0^2 \text{ for } 0 < r < R_0 \quad (4)$$

In consequence, large values of the distance *R* are more likely. In addition a minimum value of e.g. *R*=20 m may be appropriate.

3.3.2.5.4 Design pressures

The design pressures for the situation of both single source cases and industrial plants environments are presented in Table 5. The first line shows the target reliability index β for the period of one year according to the Eurocode EN 1990, Annex B, for the consequence classes CC1, CC2 and CC3. Using the table of the normal distribution, the corresponding annual failure probability P(F) = Φ(-β) can be found. Next the acceptable target failure probability given the occurrence of an explosion is found from:

$$P(F \parallel H)target = P(F)target/\lambda_H \quad (5)$$

where λ_H is the occurrence rate of an explosion following from Table 4 (last column) for the single source hazard. The target is already met by the low probability of having an explosion at all. For CC2 a low conditional target reliability index is received (β = 0,3). For CC3 it is recommended to use the detailed information of Table 4.

For the single source CC2 we assume:

- For the effective explosion energy level E a mean value of 10 GJ and a coefficient of variation of V=1.
- For the distance R a distribution according to Table 4 with R_{min} = 20 m and R_{max} = 500m.
- For the model uncertainty a mean value 0,7 and coefficient of variation V=0,5 as the model is considered to be a bit pessimistic.

For the CC3 class more case specific information is recommended.

The calculation of the mean and standard deviation of the pressure p and the impulse I have been performed using a simplified model (tuned to Table 4) and Monte Carlo.

Assuming a lognormal distribution for p the design value p_d follows from:

$$p_d = \frac{\mu}{\sqrt{1+V^2}} e^{\{\beta\sqrt{(\ln(1+V^2)}\}} \quad (6)$$

For small values of V the equation simplifies to:

$$p_d = \mu e^{\{\beta V\}} \cong \mu(1+\beta V) \quad (7)$$

The values for Δt can simply be calculated using $\Delta t_d = I_d/p_d$.

The design pressures for two cases, a single source containment tank of ethanol and the case of storage of explosives in an industrial plant are derived in Table 5. The target reliability β (row 4) increases with the increasing Consequence Class (CC), while the failure probability (row 5) is aimed to decrease. The actual failure probability $P(H)$ (row 6) for single containment tanks ethanol and storage of explosives is about a factor 10 higher and a shift by one CC category should be made: CC1 should be considered as CC2 and CC2 as CC3. It may depend on the circumstances whether at the design pressures local damage is allowed or not. If no special thread is present one may follow the standard robustness rules of the Eurocode. Depending on the amount of energy released of an explosion (row 9) and the assumed distance to the structure evaluated (row 11 to 13), the mean values as peak pressure p and impulse I, as well as the final design values can be derived (row 16 to 24).

The resulting pressures from the model may be considered as being rather conservative; therefore a mean value for the model uncertainty of 0.7 (row 14) has been used. The calculation of the mean and standard deviation of the pressure p and the impulse I have been performed using a simplified model (tuned to Table 4) and Monte Carlo Method.

Table 5: Calculated load-functions in dependence on risk class

1			Single source			Industrial plants		
2		Unit	CC1	CC2	CC3	CC1	CC2	CC3
3								
4	β(F) target		4.2	4.7	5.2	4.2	4.7	Risk Analysis necessary
5	P(F) target	[1/a]	1.3e-5	1.3e-6	1.0e-7	1.3e-5	1.3e-6	
6	P(H)	[1/a]	1.0e-6	3.0e-6	Table 4	3.0e-4	3.0e-4	
7	P(F|H) target		1	0.4		0.04	0.004	
8	β(F|H) target		-	0.3		1.7	2.6	
9	Mean(E_{eff})	[GJ]		10	Table 4	10	10	
10	V(E_{eff})			1.0	0.5	1.0	1.0	
11	R	[m]		(Table 4)	Actual	Table 4	(Table 4)	
12	R_{max}	[m]		500	-	500	500	
13	R_{min}	[m]		20	-	20	20	
14	Mean(Model uncertainty)			0.7		0.7	0.7	
15	V(MU)			0.5	0.5	0.5	0.5	
16	Resulting load-values for design							
17	Mean(p)	[kPa]		6	To be calculated	6	6	
18	Mean(I)	[Pas]		200		200	200	
19	Mean (Δt)	[ms]						
20	V(p)			1.3		1.3	1,3	
21	V(I)			1.3		1.3	13	
22	p_d	[kPa]	0	5		20	50	
23	I_d	[Pas]	0	160		600	1600	
24	Δt_d	[ms]	0	64		64	64	

3.3.3 Classification of blast scenario's and methods for the determination of corresponding blast parameters

The scenarios were defined in a joint effort of RMA and TNO. 5 types of industrial incidents were defined and for each type 2 examples selected. Determination of the blast parameters – incident and reflected pressures and impulses were derived for several cases. Three cases are summarized exemplarily here:

1. Internal Blast: for a gas and a dust explosion.
   - As these kind of explosions take place in confined areas, the overpressure due to a deflagration reaches a maximum as a function of the concentration of the gas/fuel/dusts. The rise time of this overpressure depends on the volume. The pressure-decrease after reaching a maximum is a function of the exchange of heat between the heated pressurized gases in the vessel and the outside world.
2. Station of liquefied gas, underground storage and road tanker failure.
   - LPG is a liquefied gas by means of a decrease in temperature and an increase in pressure. It leads to a thermodynamic equilibrium between vapor pressure and the liquid in the container. The pressure depends on the composition and the temperature, but a mean value of 10 bar is a good approximation. The composition is a mix of different gases, but the two main elements are butane and propane gas.
   - However, in case of the road tanker, the liquid will partly evaporate before reaching the ground surface and forming a pool. It is possible to calculate the evaporating rate before it reaches the ground, and it is also possible to estimate the size of the pool and the evaporation rate of the pool. Besides, the distance is of utter importance, as can be seen for an example in the following Table 6, where the pressure decreases significantly with the distance:

Table 6: Overpressure and Impulse Values depending on the distance according to TM5-855

	Overpressure (kPa)	Positive phase duration (msec)	Impulse (kPa·msec)	Reflected overpressure	Reflected impulse
At 10 m	665.9	16.01	1367	3244	4193
At 100 m	9.662	38.46	164	20.13	305.9
At 287 m	2.394	51.62	56.96	4.833	101.4
At 500 m	*Too far to calculate with formula in TM5-855*				

3. A chemical ethanol plant of different sizes
   - It has to be first determined, if the ethanol evaporates instantaneously or not. This is depending of geometry of the vessel, the weight of the released product, temperature and the location of the leaking hole. Also weather conditions and wind take their influence and decide if a vapour cloud explosion will take place or not.

These examples show the divers assumptions and possibilities to take into account in each scenario and give also information of different approaches to calculate blast scenarios in dependence of the blast action. A comprehensive understanding of the constraints of each case are therefore of utter importance.

General examples for classification, which were used for the case study selection, are given in Table 7.

Table 7: Examples for blast scenarios

Scenario	Internal or external scenario	Source for probability of occurrence or blast model
Vapour cloud explosion	Internal	[1]
Dust explosion	Internal	[1]
Storage of explosives	Internal or external	[3]
Stationary pressurised tanks and vessels	Internal or external	[3]
Stationary atmospheric tanks and vessels	Internal or external	[3]
Gas cylinders	External	[3]
Pipes	External	[3]
Warehouses	External	[3]
Road tankers	External	[3]
Tank wagons (trains)	External	[3]
Ships	External	[3]
Terroristic attack: bombs/explosives packed in backpacks / cars	Internal or external	Estimate based on information from newspapers
Nuclear explosions	Internal or external	Not to be considered [1)]

For some of them, the models for blast parameter determination are dependent on the product contained and not the type of containers. A ship, a tank wagon or a road tanker, can be considered as types of containers containing a given product under given conditions. The only difference lies in the quantity and the nature of the contained product. The distinction between the different possible scenario's in this report is based on the nature of the containment (dust, liquids, gas or vapour, pressurized or under atmospheric pressure).

The main reference used in ADBLAST was the manual on 'Methods for the calculation of physical effects – due to releases of hazardous materials (liquids and gases)' or 'Yellow Book' [4]. It is internationally recognized as a standard for calculations of physical effects of accidents. It was developed in 1997 by TNO. The latest version has been revised in 2005.

For the determination of blast loads (on industrial buildings), two main methods can be identified: the TNT-equivalency method and the Multi-Energy Method. The first method is the most frequently used due to the fact that it is the simplest method. The second method is more versatile but needs more input values.

Due to the general approach of the study, a lot of information cannot provided precisely or is unknown. Details like the disposition of the installation, the buildings round the site, are essential information for this method to allow for a detailed determination of the blast parameters. Therefore the Multi-Energy Method was not used within ADBLASTADBLAST. The method adopted for the calculations was the TNT-equivalency method.

The assumed loading was simplified as a triangular pressure-impulse loading; an example is shown in Figure 4, which was used for the case study on an internal explosion of propane gas in a 500m³ tank.

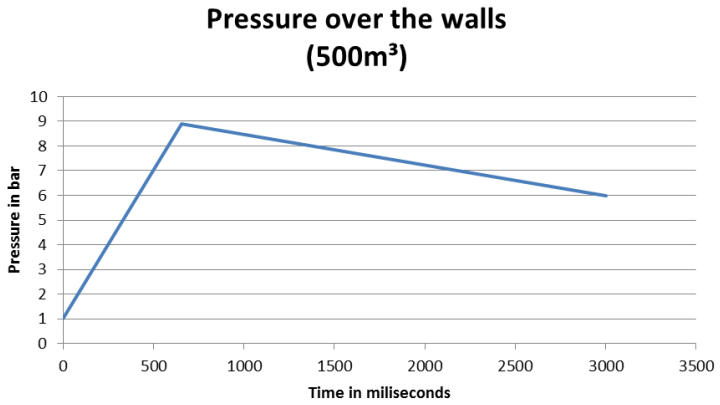

Figure 4: Pressure due to an internal explosion of propane gas in a 500 m³ tank

3.3.4 Experimental investigations

3.3.4.1 Introduction

Based on the results of Work Package 1, for cladding systems 3 types were chosen:

1. TR84/273 (trapezoidal sheet) with 0.75mm, 1mm and 1.5mm thickness
2. TR35/207 (trapezoidal sheet) with 0.75mm and 1mm thickness
3. K110/600 (liner trays)

And for the U-profile used as substructure element:

1. U60 and U100

The U-profiles are usually larger in full-sized structures, but in order to achieve a significant deformations they had to be downscaled for testing purposes due to testing-rig restrictions.

For fasteners, two types were used

1. M12 for assumed rigid connections (abbreviated with M12)
2. S-MP 52Z 6.3x25 (self-tapping screws, kindly provided by HILTI) (abbreviated with ST).

The test matrix for static and blast large scale tests are summarized in Table 9, Table 10, Table 13 and Table 14.

3.3.4.2 Material characterization

Cladding materials and fasteners were tested in regard to their static resistance, and also to their behaviour under high speed loading.

With the results of static tests on the connectors in shear and pull-through direction, the bearing stiffness was calculated and used in the recalculation of tests in the simplified models.

The test-setup for the high-strain rate tests can be seen in Figure 5. The specimen/coupon was loaded with a dynamic load cell in tension. a Phantom V201 high-speed camera operating with a resolution of 1278x718 pixels was used for strain monitoring in medium (MS) and high-speed (HS) tests,. Recording rates of 200 and 2000 fps (frames per second) were employed for medium and high-speed tests, respectively. A purpose built in in-house MatLab script was employed for video processing in order to obtain mean strain measurements along the gauge length of the coupon. Additional strain gauges were utilized in selected specimens for corroboration of the measured strain ranges. Average strain rates of 0.005/s (slow speed), 0.23/s (medium speed) and 2.3/s (high speed) were studied.

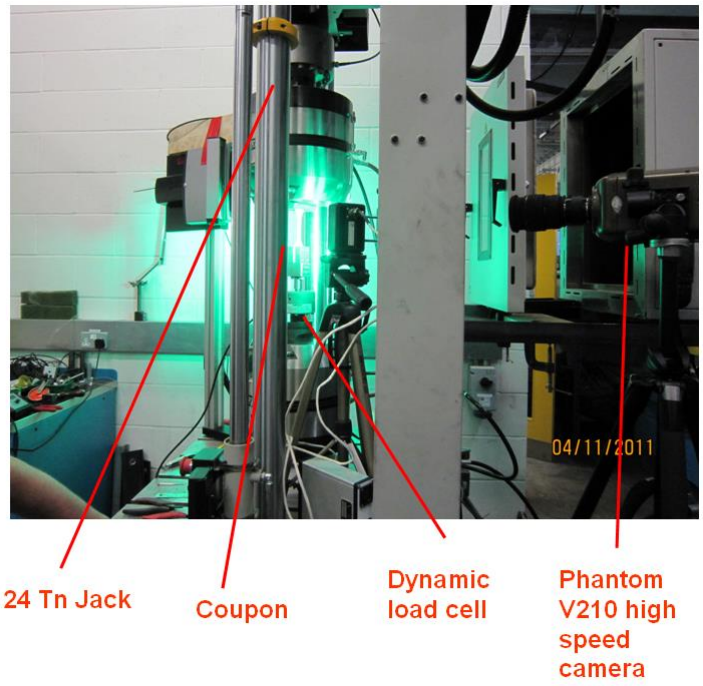

Figure 5: Test set-up for medium (MS) and high-speed (HS) coupon tests

Figure 6 compares the stress-strain curves for two different thickness materials at different loading rates exemplarily.

Table 8 presents a summary of the observed material properties in terms of mean engineering stress at yield, median maximum engineering stress after yield and mean strain at fracture together with their corresponding standard deviations. The results are obtained from slow-speed (SS), medium-speed (MS) and high-speed (HSS) tests on all cladding types studied (e.g. TR84 of 0.75, 1 and 1.5 mm thickness and TR35 of 1 and 0.75mm thickness). Mean engineering stress values and their corresponding standard deviations are calculated for constant levels of engineering strain up until failure of a specimen. It can be observed that the strain rate-dependent overstrength ratio is not constant over all strain levels with larger strength increments observed near the plastic plateau than in the strain-hardening region.

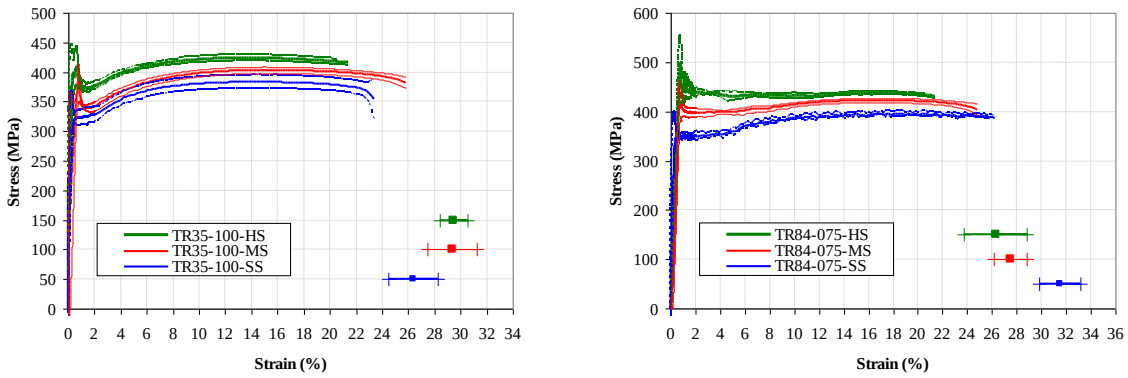

Figure 6: Mean stress-strain relationships for TR35-100 (left) and T84-075 (right)

Table 8: Summary of material properties

Cladding Type (Thickness)	Rate	Yield Stress (MPa)		Maximum Stress (MPa)		Strain at fracture (%)	
		Mean	σ	Mean	σ	Mean	σ
TR 35/207 (0.75 mm)	SS	343.57	9.70	383.78	9.25	28.09	1.01
	MS	373.20	7.41	395.97	3.05	29.25	1.62
	HS	411.89	11.67	414.97	3.72	29.80	3.20
TR 35/207 (1 mm)	SS	323.62	12.47	383.42	11.65	26.37	1.92
	MS	348.24	4.61	403.51	5.34	29.36	1.91
	HS	376.23	8.11	424.11	4.50	29.47	1.08
TR 84/273 (0.75 mm)	SS	351.37	9.75	396.08	5.33	31.48	1.68
	MS	398.11	8.56	422.73	4.28	27.51	1.35
	HS	439.15	9.87	437.83	3.03	26.30	2.55
TR 84/273 (1 mm)	SS	353.04	9.08	410.00	8.06	25.50	1.68
	MS	399.95	8.75	435.05	2.28	26.91	2.26
	HS	438.22	13.33	452.03	9.04	27.24	4.18
TR 84/273 (1.5 mm)	SS	365.31	3.52	418.216	2.095	28.15	0.87
	MS	409.82	9.09	448.85	2.37	27.04	1.16
	HS	420.36	13.74	464.61	2.35	29.26	2.13

Figure 7 compares the mean overstrength values with the corresponding predictions of three commonly used steel strain-rate-functions [6] [7] [8]. Comparisons are presented for mean yield and ultimate strength values. Here mean yield strengths correspond to an average strain rate of 2/s for HS tests and 0.2/s for MS samples. Similarly, the mean ultimate strength was determined at around 14% strain with a rate of 2.3/s in HS tests and 0.23 in MS specimens. It can be observed from Figure 7 that the CEB model [7], offers a reasonably good estimation of overstrengths at yield for the cladding materials here employed. Nevertheless, the material maximum overstrength is significantly overestimated by the Soroushian and Choi [6] as well as the CEB [7] steel strain-rate models while the Bodner and Symonds [8] equation underestimates the overstrength in all cases.

The results of high strain material tests were used for the numerical models on parametric studies for claddings and in substructures for the assessment of *P-I*-diagrams.

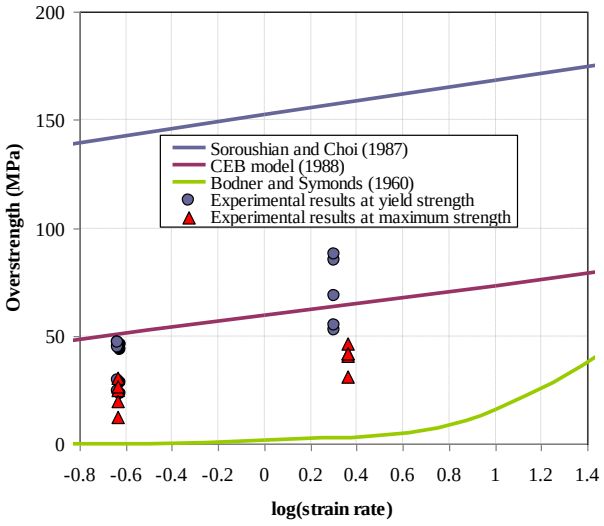

Figure 7: Comparison of strain rate-dependent overstrength and empirical predictions

3.3.4.3 Large scale static tests – tests on trapezoidal and blank sheets

Three different types of tests were performed:

1. 4-point bending tests on single and double span specimens with trapezoidal sheet
2. 4-point bending tests (single span) on cassettes
3. Elaborate tests with up to 9 actuators for tests on trapezoidal sheets including substructure

Of special interest was the ultimate load-bearing capacity beyond the first local failure due to buckling. For the static tests on trapezoidal sheets the failure mode was bearing at the supports. This mode was accompanied by high deformation of the sheets as indicated in Figure 8. Large deflections lead to increasingly high longitudinal forces in the sheet, or membrane effects, which loaded the fasteners in shear. However, in the investigated cases mostly bearing of the sheet itself was governing the ultimate resistance.

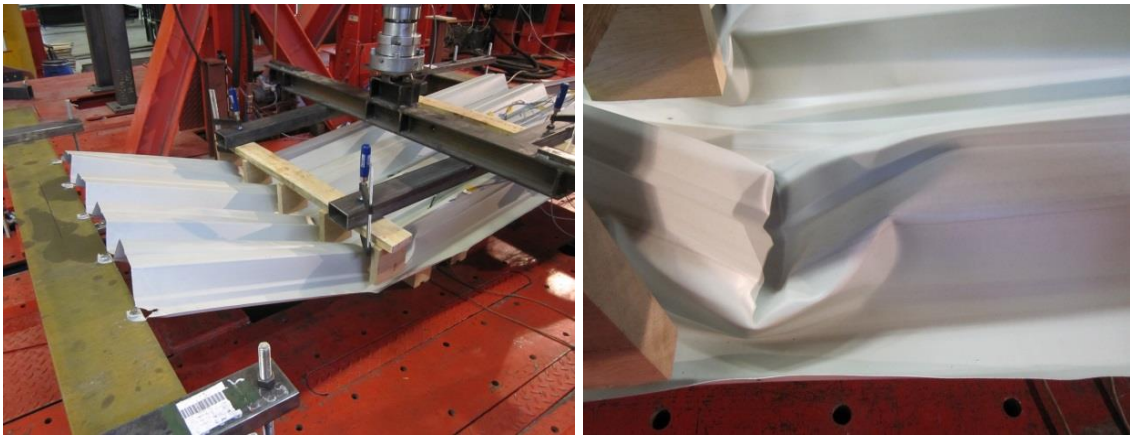

Figure 8: Local buckling in midspan (A) and connection bearing-failure at the supports induced by membrane effects

Additional tests with blank sheets were conducted to identify the influence of the trapezoidal forming. The result is shown in Figure 9 where the local failure and post-failure strengthening due to membrane effects can be identified, whereas in blank sheets the membrane effect occurs right from the start.

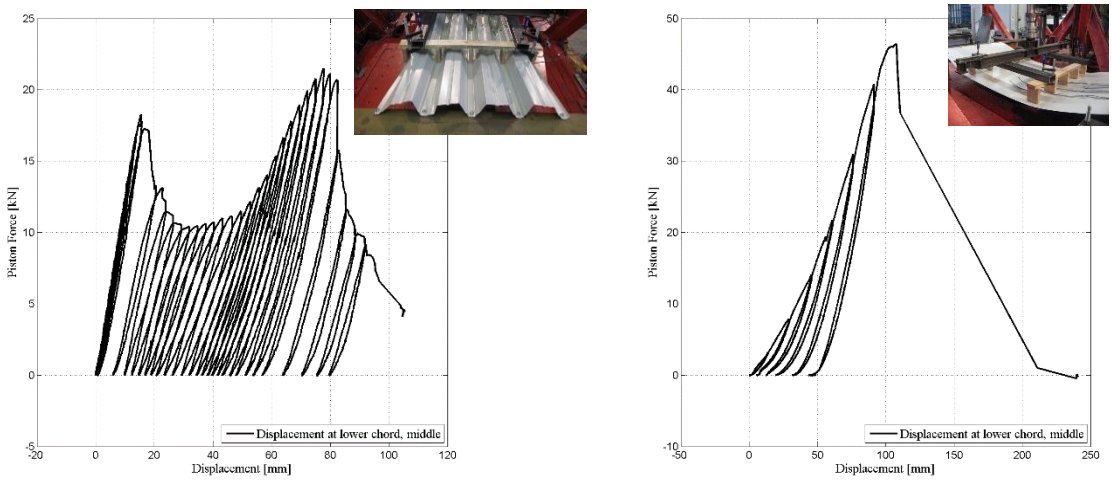

Figure 9: Comparison load-deflection curve of trapezoidal sheet (left) and blank sheet (right)

The angle of the sheet at the support at ultimate load was investigated to evaluate the corresponding rotational requirements (Table 9). It could be shown, that a minimum rotation of 5.79° was reached, where in in current American design aids [9] a minimum of 4° is required under consideration of membrane effects for cold-formed panels.

Although a potential postbuckling behaviour can be exploited with trapezoidal sheet, the collapse-failure is defined by failure at the connection. Use of M12 compared to self-tapping screws increased significantly this collapse-load.

Table 9: Test results of trapezoidal (TS) and blank sheets (BS), static loading

Specimen (Fastener_ thickness_ System_ Span_no)	Buckling onset		Ultimate resistance state					Failure mode of fasteners	
	Buckling load [kN]	Deflection at mid-span [mm]	Ultimate load [kN]	Deflection at mid-span [mm]	Deflection at quarter-span [mm]	angle	Horizontal Force per bolt	Bearing	Shear
M12_075_ BS_250_1	-	-	16.2	142.41				X	-
M12_075_ TS_250_1	18.26	19.61	21.48	138.26	75.28	6.87	17.83	X	-
M12_150_ BS_250_1	-	-	46.44	107.71	111	10.07	26.15	X	-
M12_150_ TS_250_1	52.68	47.9	67.32	283.79	156.35	14.04	26.91	X	-
ST_075_B S_250_1	-	-	12.24	140.48	131.74	11.90	5.81	X	-
ST_075_TS _250_1	14.61	22.18	14.48	119	63.35	5.79	14.29	X	-
ST_075_TS _250_2*	16.7	24.95	16.73	202.42	101.21	9.20	10.33	X	-
ST_150_B S_250_1	-	-	35.46	154.09	147.7	13.30	15.01	-	X

3.3.4.4 Large scale static tests – tests on cassettes

The testing programme performed by the University of Pisa consisted in a series of nr. 8 experimental static tests on cladding elements, summarized in Table 10.

Table 10: Test matrix cassettes

Denomination	Sheet	Thickness [mm]	Fastener	Length
TR84/2500/ETAG	TR 84/273	1	S-MP52Z 6,3x30	2500
TR84/2500/4POINTS	TR 84/273	1	S-MP52Z 6,3x31	2x2500
K110/2500/ETAG	K110/600 and TR35/207	0.88(K110); 0.75 (T35)	S-MP52Z 6,3x32	2500
K110/2500/4POINTS	K110/600 and TR35/207	0.88(K110); 0.75 (T35)	S-MP52Z 6,3x33	2x2500
TR84/5000/ETAG	TR 84/273	1	S-MP52Z 6,3x34	2x2500
TR84/5000/4POINTS	TR 84/273	1	S-MP52Z 6,3x35	2x2500
K110/5000/ETAG	K110/600 and TR35/207	0.88(K110); 0.75 (T35)	S-MP52Z 6,3x36	2x2500

Measured were end rotation and displacements at several positions, see Figure 10.

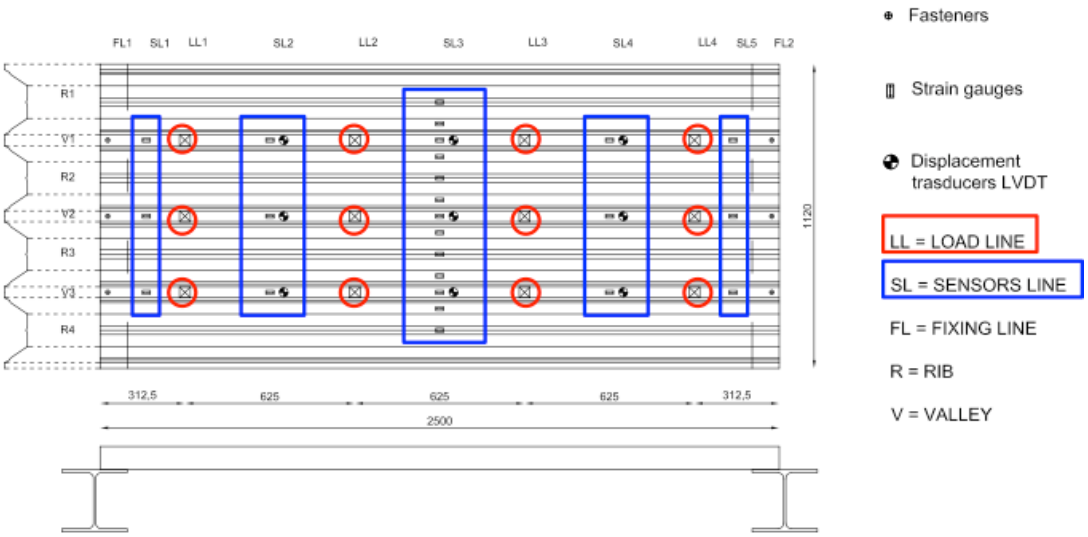

Figure 10: Measurements at cassette tests

The results of the test on K110/600+TR35/207 liner tray (cassette), 2500 mm length, loaded according to ETAG scheme (Figure 8) are shown in Figure 11. It is noticeable that the behaviour is governed by the buckling of vertical flanges of K110 profiles, but also the top horizontal flanges manifest local instability. From the beginning the cross section started to distort and flatten with the top trapezoidal profile remaining substantially not deformed with the exception of the proximity of the screws. Local plastic deformation can be then observed at supports. As can be observed in the *F-d* diagram after a very steep initial branch the curve presents a rapid decrease with large deformations and a further load recovery. The test was terminated because the loading frame touched the cladding.

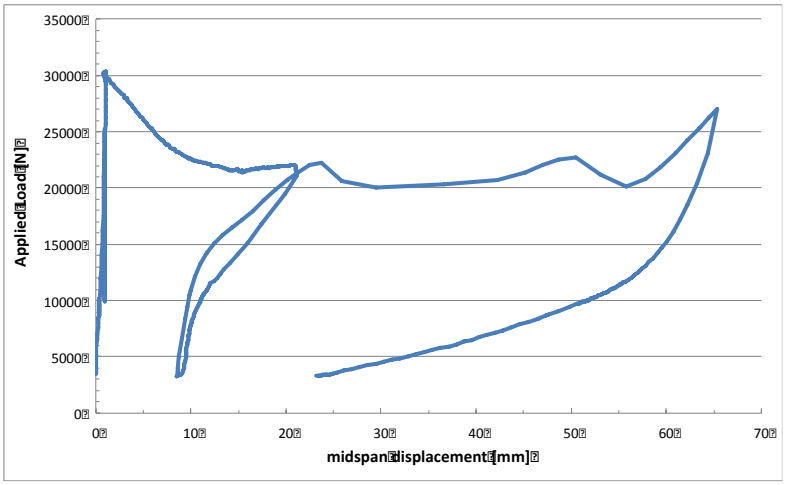

Figure 11: Example test results on cassettes

In order to quantify the plastic deformation capacity of cassette claddings, the end rotations time histories were evaluated near the supports.

In Figure 12 are reported the end rotation time histories for K110/2500/ETAG specimen and in Table 11 are listed the end rotation values corresponding to the "yielding point" θ_y and to "ultimate (lower)" load value θ_u. It should be noted that the definition of this two points is anything but clear and can vary a lot between one sensor to the others. As can be observed in Table 11 also the ductility evaluated on the basis of these end rotation values presents large variations.

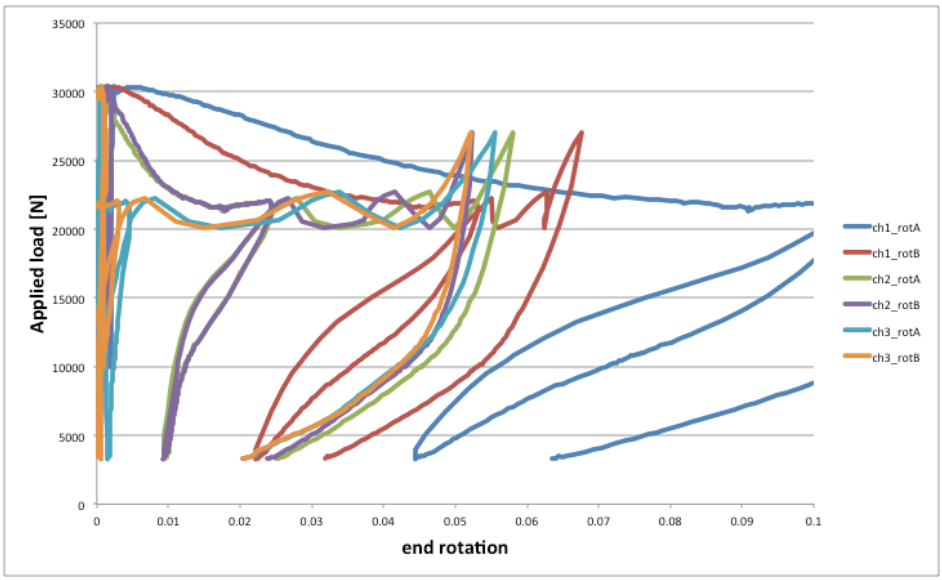

Figure 12: End rotation K110/2500/ETAG

Table 11: End rotation measurements for K110/2500/ETAG

	ch1_rotA	ch1_rotB	ch2_rotA	ch2_rotB	ch3_rotA	ch3_rotB
θ_y	0.0020	0.0011	0.0009	0.0020	0.0003192	0.00096
θ_u	0.0900	0.0450	0.0165	0.0165	0.0413	0.044
μ	45.00	40.91	18.75	8.25	129.39	45.83

Similar observations can be drawn from Figure 13 and Table 12 corresponding to K110/2500/4POINTS specimen. Also in this case the end rotation values present very large variation.

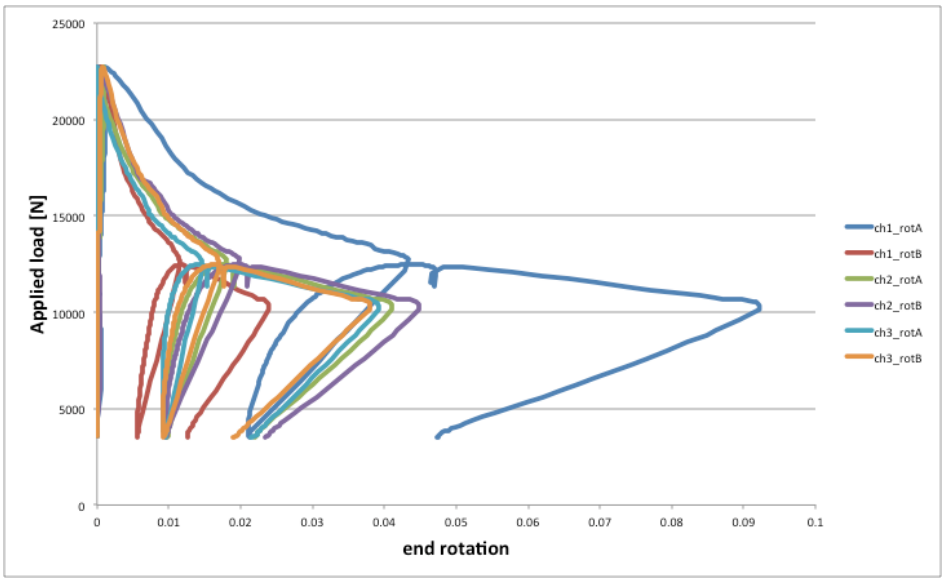

Figure 13: End rotation K110/2500/4point

Table 12: End rotation measurements for K110/2500/ETAG

	ch1_rotA	ch1_rotB	ch2_rotA	ch2_rotB	ch3_rotA	ch3_rotB
θy	0.000867	0.0005	0.0005	0.0003	5.28E-06	0.00033
θu	0.0913	0.0237	0.0417	0.0444	0.0387	0.0377
μ	105.31	43.80	77.28	134.45	7329.55	114.24

Due to local buckling and cross section flattening, the behaviour of these cassette cladding is not beam-like: thus the attempt to extract beam-like ductility information seems to be not appropriate. It should be also noticed that the tested specimen do not contain any internal insulation layer, simulating the real case with very soft rock wool panel. Conversely if a stiff insulation layer is inserted into the U profile K100/600, the global behaviour of the cassette could change substantially because the local buckling and distortion of cross section is avoided or postponed and then a beam-like behaviour can take place.

3.3.4.5 Large scale static tests – tests on substructures

In order to evaluate the member-structure interaction, six sub-structure tests as well as an additional three partial sub-structure tests, were performed with varying loading and boundary conditions. An overview of the testing matrix is given in Table 13. A purpose-built test-rig was constructed to facilitate a versatile experimental assessment. The layout and frontal view of the test-rig is depicted in Figure 14 while the lateral view is shown in Figure 15, respectively. Figure 16 presents a general view of the experimental set-up. Nine Enerpac Jacks were employed to apply vertical loads at selected regions within the cladding-purlin-beam subassemblies as denoted with the shaded areas numbered 1 to 9 in Figure 14. Each Enerpac Jack employed had a maximum stroke of approximately 230 mm and a capacity of nearly 100 kN Figure 16 presents the load-distribution system employed to transfer the vertical loads from each of the actuators to the cladding sub-assemblage. Plates of 40 mm thickness were used to distribute the load to a pair of 3/2”x3” wood laths of 400 mm length resting on alternate troughs of the corrugated cladding sheet. The plate was connected to a load cell and vertical actuator through a spherical pin in order to allow rotations. A 50 t load cell was employed to monitor forces at the tip of each of the nine Enerpac Jacks employed. The actuators were connected to a common manifold to enforce an even distribution of pressure among all cylinders.

Table 13: Testing matrix substructures

Denomina-tion	sheet	Thick-ness [mm]	Fastener	Length	Edge Purlin	Middle Purlin	Edge Connect ion	Purlin connect ion
A-TR35-100	TR35/207	1	S-MP52Z 6,3x25	2x1270	U100	U100	P1	P1
B-TR35-100	TR35/207	1	S-MP52Z 6,3x26	2x1270	U100	U100	P1	P1
C-TR35-100	TR35/207	1	S-MP52Z 6,3x27	2x1270	SHS 100x10	U100	P2	P1
D-TR35-100	TR35/207	1	S-MP52Z 6,3x28	2x1270	SHS 100x10	U60	P2	P2
E-TR35-075	TR35/207	0.75	S-MP52Z 6,3x29	2x1270	SHS 100x10	U60	P2	P4
F-TR35-100	TR35/207	1	S-MP52Z 6,3x30	2x1270	SHS 100x10	U60	P2	P5
S1	TR35/100		S-MP52Z 6,3x31	2x1270	SHS 100x10			
S2	TR84/100		S-MP52Z 6,3x32	2x1270	SHS 100x10			
S3	TR84/100		S-MP52Z 6,3x33	2x1270	SHS 100x10			

The cladding-purlin sub-structure specimens consisted of four standard cladding sheets spanning over two 1.27 m spans. The cladding was fixed to the purlins by means of S-MP52Z 6,3x25 self-taping screws.

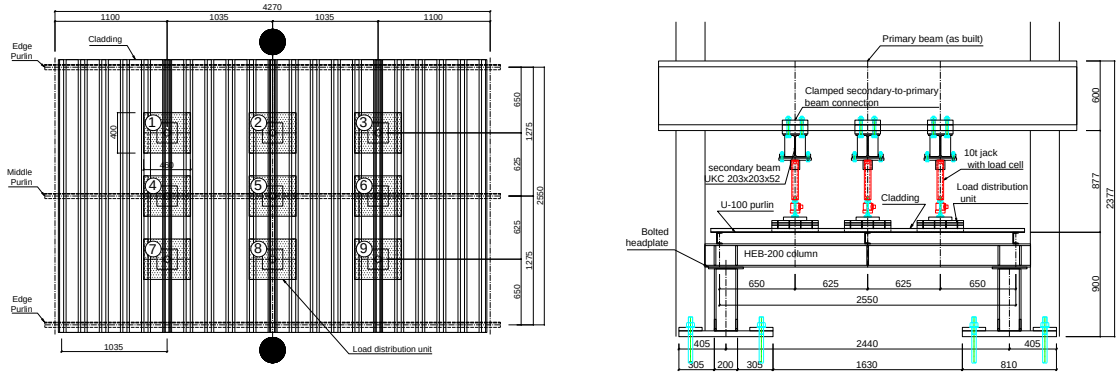

Figure 14: Test-rig layout (with numbered actuators) and Test-rig front view

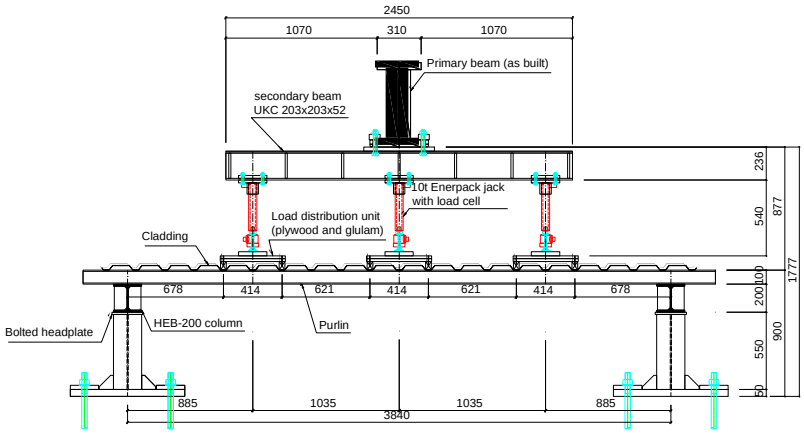

Figure 15: Test-rig lateral view

Figure 16: General view of the test-rig

A total of nine sub-structure tests were performed with varying load and boundary conditions. These boundary conditions were varied in regard to rigidity (amount of fasteners, for SHS connections also welded plates, see Figure 17.

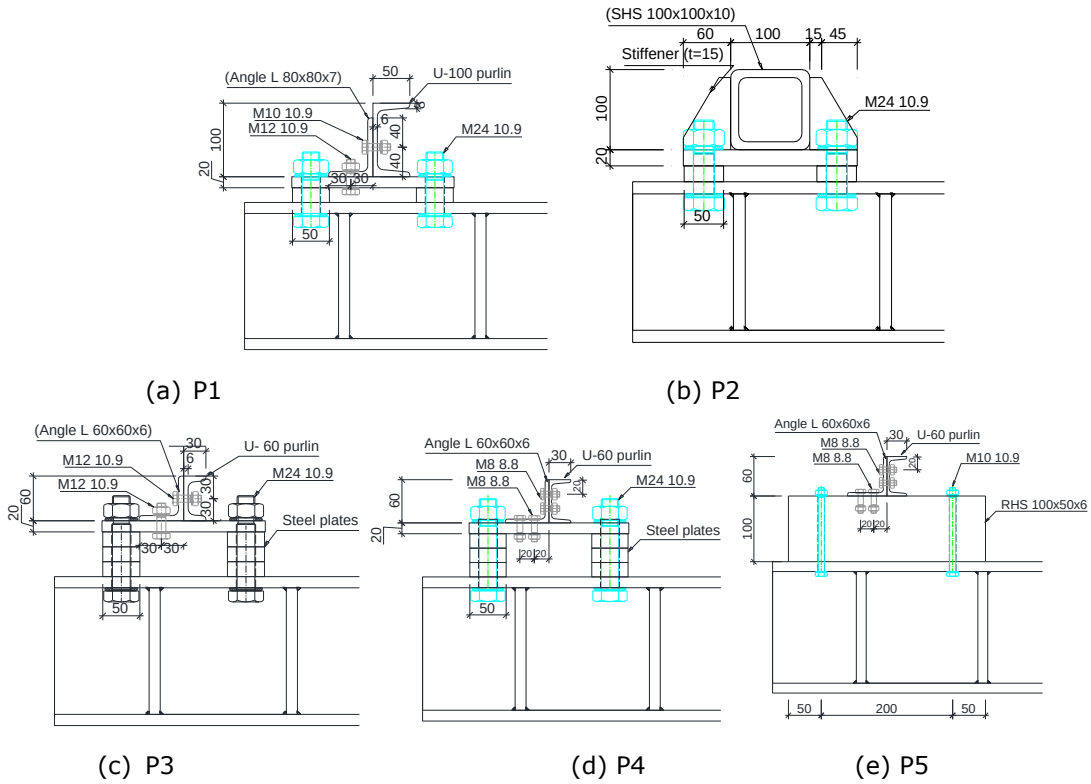

(a) P1 (b) P2

(c) P3 (d) P4 (e) P5

Figure 17: Connection details

In all cases, coupon tests were conducted in order to characterise the material properties of the different components of the sub-assemblages. The deformations on the cladding-purlin system were monitored via nine string transducers placed vertically within the actuator's line of action under the cladding sheet (for actuators 1 to 3 and 7 to 9) or below the central purlin (for actuators 4 to 6). Additional displacement transducers were employed to check vertical and horizontal deformations at one end of the middle purlin and at the mid-point of a lateral purlin. Finally, two Accustar analogue inclinometers were attached to the cladding edge to monitor inclinations in the borders. The tests were conducted under force control conditions. The forces in the actuators were uniformly increased up to failure of the specimen or up to the maximum displacement capacity of the transducers at approximately 230 mm. Attention was placed to maintain a reasonably even distribution of forces over all actuators.

The results of tests performed on twelve sub-structures representing industrial cladding systems under extreme loading conditions are presented in deliverable D5 in detail. Based on the results obtained, the main conclusions are as follows:

i. The sub-structure test set-up and testing procedure have been verified. Also, a largely uniform distribution of forces over all actuators has been proved possible;

ii. The degree of restraint provided by the purlins has been identified as an important parameter on the response of cladding sub-structures. When significant torsional deformations on the edge purlins are prevented, failure of the screws connecting them to the cladding near the purlin extremes was observed, and failure also occurs in the screws located in the middle purlin that occurred when torsionally more flexible edge purlins were provided;

iii. The provision of weak purlin to column connections, leads to bolt failure and limits the overall capacity of the cladding sub-structure;

iv. Importantly, the experimental results presented in D5 provide valuable information for the validation of numerical models.

3.3.4.6 Large scale blast tests – tests on claddings

A total of 12 blast tests on single-span cladding systems were conducted in Brussels. A summary of all performed tests is given in Table 14. The experimental test set-up and the chosen positioning of the sensors is shown in Figure 18.

Table 14: Overview of the executed tests

Test	Cladding Type (*)	Charge	Date
1 (*)	3 x TR84 - 1.50 mm	1.5 kg C4 at 3.5 m	23/08/2012
2 (*)	3 x TR84 - 1.50 mm	1.5 kg C4 at 3.5 m	23/08/2012
3	3 x TR84 - 1.50 mm	0.5 kg C4 at 3.5 m	12/12/2012
4	On the same plates	1.0 kg C4 at 3.5 m	12/12/2012
5	3 x TR84 - 1.50 mm	0.5 kg C4 at 3.5 m	12/12/2012
6	On the same plates	1.0 kg C4 at 3.5 m	12/12/2012
7	3 x TR84 - 0.75 mm	0.5 kg C4 at 3.5 m	13/12/2012
8	3 x TR84 - 0.75 mm	1.0 kg C4 at 3.5 m	13/12/2012
9	3 x TR84 - 0.75 mm	0.5 kg C4 at 3.5 m	13/12/2012
10	3 x TR84 - 0.75 mm	1.0 kg C4 at 3.5 m	13/12/2012
11	3 x TR84 - 0.75 mm	1.5 kg C4 at 3.5 m	13/12/2012
12	3 x TR84 - 0.75 mm	1.5 kg C4 at 3.5 m	13/12/2012

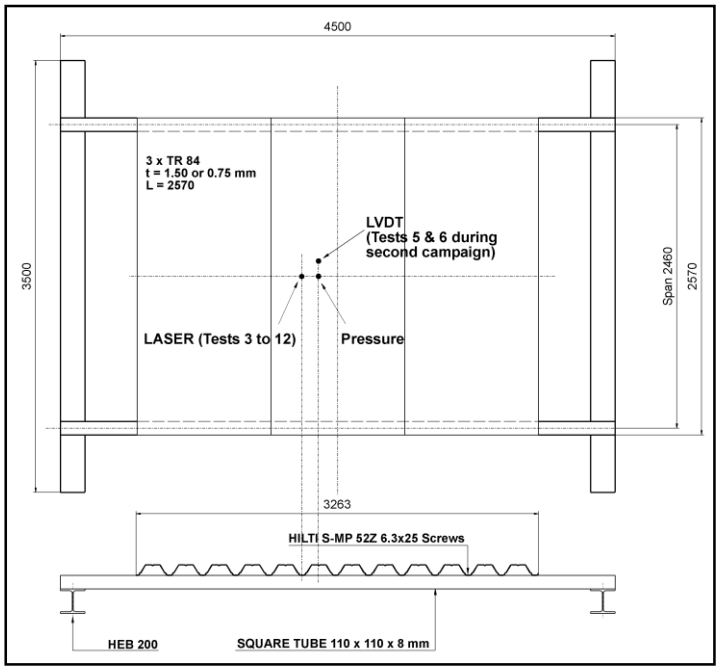

Figure 18: Set-up final test campaign on TR84 cladding panels

The tests gave information about the dynamic behaviour of the cladding under explosive loading, which is in fact a complex process because of the divers failure-modes possible: geometry of the

trapezoidal sheets tends to local buckling and tearing at the connection, while fasteners can pull out or lead to bearing and thus to localized plastic modes.

The results of the tests are given in Table 15 and could be used for comparison with the test results of blast tests on sub-structural assemblies (consisting of cladding and purlin) with similar boundary and loading conditions. Table 15 shows the results of the measured peak pressure, impulse, first dynamic deflection and the final plastic deformation measured at the mid-span of the cladding.

Table 15: Results explosion tests on cladding panels

Test N°	Charge & Cladding Thickness	Reflected Peak Pressure [kPa]	Reflected Impulse [kPa.ms]	First Dynamic Deflection [mm]	Plastic Deformation [mm]
1 (~)	1.5 kg - 1.5 mm	319	180	+52 (*)	+30
2 (~)	1.5 kg - 1.5 mm	341	182	+71 (*)	+19
3	0.5 kg - 1.5 mm	112	84	-22	0
4	1.0 kg - 1.5 mm	205	142	-34	0
5	0.5 kg - 1.5 mm	(#)	(#)	(#)	(#)
6	1.0 kg - 1.5 mm	194	170	-41	(?)
7	0.5 kg - 0.75 mm	124	73	-50	+4
8	1.0 kg - 0.75 mm	214	212	-76	+14
9	0.5 kg - 0.75 mm	135	(?)	-40	+7
10	1.0 kg - 0.75 mm	205	151	-71	+23
11	1.5 kg - 0.75 mm	315	196	-110	-13
12	1.5 kg - 0.75 mm	168	162	-101	+6

(*): Obtained by 15 Hz LP filtering

(~): These are test 5 & 6 from the preceding campaign

(#): No Signal

3.3.4.7 Large scale blast tests – tests on substructures

A total of 12 tests were conducted on sub-structural assemblies composed by claddings and a purlin (meaning underlying comparable soft U-beam as middle-support) in Brussels. A summary with all tests and the main results are given in Table 17. Within the substructure test-series, also restraint conditions of the mid-purlin was varied, with fixed support (fitting bolted connection) and "free" support (slotted hole connection). The fixings were conducted as in the static tests.

The tests results provided information about the dynamic behaviour of the cladding, which is in fact a complex structure because of the trapezoidal shape (elastic response, plastic deformations, local buckling failure) and the functioning of the fasteners under blast loads (plastic transformation of the holes in the deck into oval holes, deformations or failure of the fasteners).

Charges of 250 g, 500 g, 1000 g and 1500 g C4 (plastic explosive) were positioned at a fixed distance of 3.5m above the middle of three panels as shown in Figure 19.

Deflection measurements as well as measurements with load cells under the support were taken.

Exemplarily, a displacement-time curve is shown in Figure 20, together with the corresponding pressure-time evaluation.

Figure 19: Positioning of the explosive, cladding test-setup

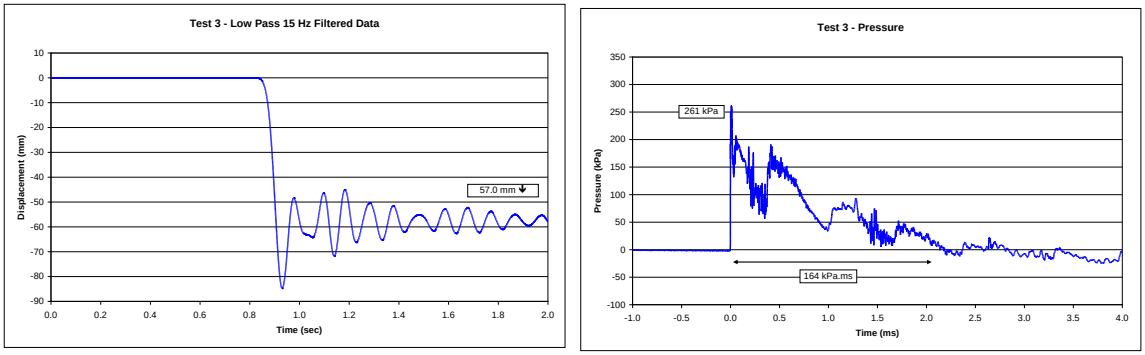

Figure 20: Results of blast test on cladding: load-displacement (left) and pressure-time evaluation (right)

Figure 21 shows exemplarily the setup for a substructure test, with the detail of the fastening of the U-beam used as purlin equivalent. Figure 22 and Table 16 show the results for the measured reflected pressures and impulses in the middle of the specimen.

Table 16: Reflected pressures and impulses

Test	Cladding	Support	Reflected Peak Pressure (kPa)	Reflected Impulse (kPa.ms)
3	4 x TR 35 - 1.00 mm	Fixed	209	215
4			266	165

Figure 21: Construction of the substructure (left), detail fixing of U-beam (right)

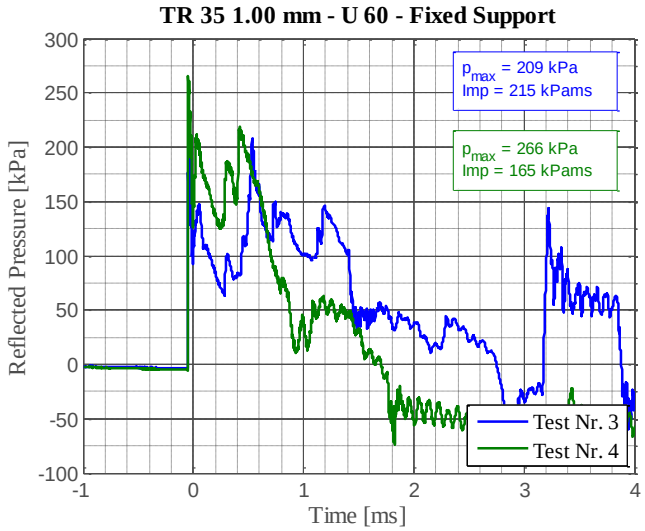

Figure 22: Reflected pressure and impulse in Tests Nr. 3 and 4

After the test, the remaining plastic deformation of the substructure was measured. Also the failure behaviour of the fasteners, the bearing at end supports was investigated.

The deformation behaviour can be summarized as follows:

The deformation process of the structural assembly after the detonation of 1.5 kg of C4 in 3.5 m height shows the same hard-to-predict behaviour as it could be observed in the explosive test on stand-alone claddings.

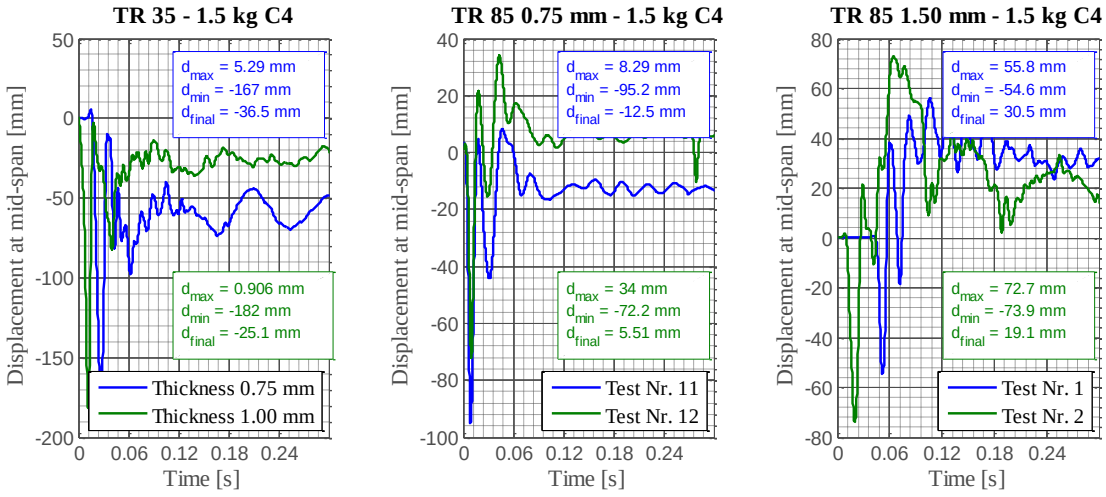

Figure 23: Deformation behaviour of the claddings (without substructure) under same explosive load, TR 35 (left), TR 85-0.75mm (middle), TR 85-1.50mm (right)

From an analysis of both the observed behaviour on single claddings (see Figure 23) as well as on complete substructure assemblies we can conclude that:

- the softer the cladding, the higher the initial deformation peak.
- the post-impact behaviour was determined by local buckling phenomena that appeared during the first loading.
- the stiffness and resistance dropped down suddenly as buckling happens, leading to final deformation states that cannot be predicted by classical elastic-plastic assumptions, i.e. the cladding type TR 85 with 1.50 mm thickness lifts up in all tests performed.

– the measurements were affected by local buckles that deform locally the measurement spot (see Figure 24).

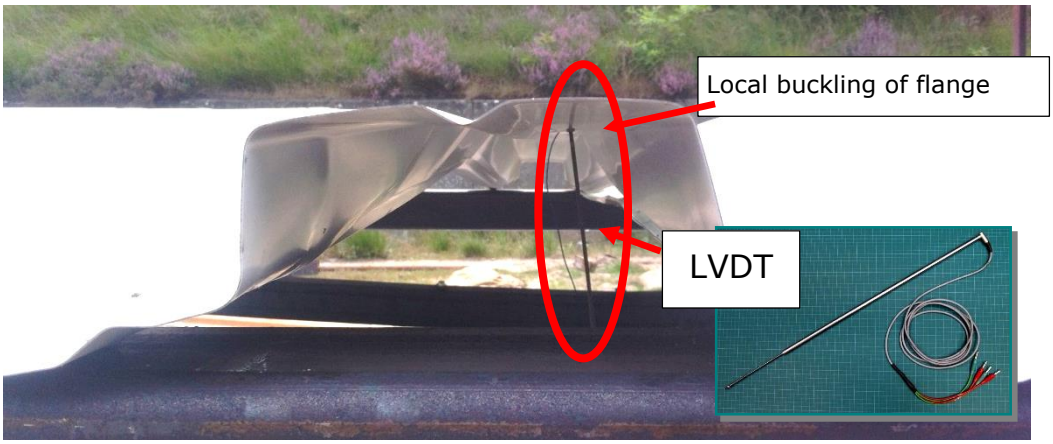

Figure 24: Local buckles affecting the precision of the measurements

The behaviour of the substructure was very strongly affected by the cladding response against the explosion. In the chosen experimental set-up, the mechanical properties (mass and stiffness) of the assembly were dominated by the cladding.

A particular effect was observed when the connectors were detached by pull-through failure. Here the beam received the shock-impulse from the claddings. Soon after that, the connectors failed so that the beam undergoes large plastic deformations, as the cladding cannot contribute anymore to the dissipation of the impulse energy. This uncoupled load bearing mechanism was observed in several tests and are analysed in more detail in the next clause (transferred forces). Only in these tests, a clear nonlinear behaviour of the substructure could be activated. At the deformational level, no significant differences could be appreciated between the fixed and free support.

Transferred Forces:

An important aspect for the assessment of impulsive loaded structures is the duration of the applied impulse on the main structural members. Especially for members that are not directly affected by the reflected pressure wave, a significant increase in the loading duration (slightly larger than the natural period of the load transferring member) is to be expected.

Since the total impulse is conserved during the whole process (Newton's Momentum Conservation law), the peak force transmitted to the support will be significantly decreased by the presence of intermediate members between the pressure wave and the support (in this case trapezoidal claddings and the U-beam).

Seen from the practical point of view, for a given impulsive loading, the transmitted impulse will always have a larger duration and a smaller pressure peak.

Cladding detachment:

By means of numerical simulation with simplified models according to FABIG [10] and Norsok [11] (see Figure 25), an estimation of the transferred force from the cladding to the beam can be obtained. Here it can be observed, that a rebound force (in pulling direction) equal to the elastic capacity in the cladding is to be expected.

The pull-through resistance of the self-tapping screws per meter length can be estimated at 24.4 kN/m (assuming 4 fasteners per meter). The numerical simulation shows an expected pull-through action of between 25.4 and 28.9 kN/m, which explains the detachment of the cladding.

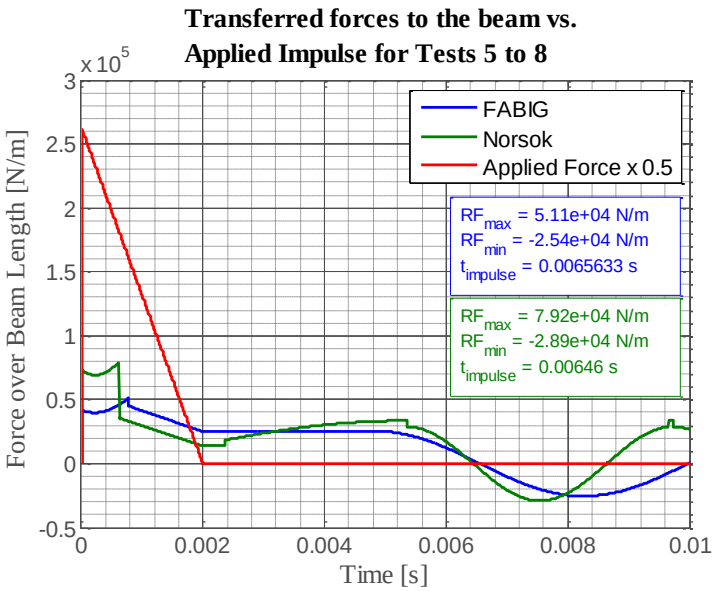

Figure 25: Transferred force from the cladding to the beam (applied load-time function for Test Nr. 5 to 8), Numerical Simulation according to Fabig and Norsok

Impulse transmitted by the beam element:

The transmitted impulse between the beam and the main structure (here the main supporting construction) was measured. The results can be associated in 2 behaviours: without cladding detachment and with cladding detachment.

In tests without cladding detachment, the measured total absorbed impulse by the beam support barely reached 10 % of the total impulse. In these test, the impulse was mainly transmitted by the cladding to the stiff main structure.

In tests with detachment, the total impulse transmitted reaches higher values of 20-25% of the total impulse. After detachment, the cladding cannot contribute to the dissipation of the impulse, which must be absorbed solely by the beam, thus leading to higher plastic deformations.

Summary of blast tests:

A summary of all tests is given in Table 17. Here, the reflected peak pressure and impulse, as well as the first dynamic deflection during the load-deformation cycle was taped. The plastic deformation of trapezoidal sheet (vertical) and plastic deformation vertical and lateral of the mid-purlin is shown. With help of load pressure cells the transferred loads at connection of the mid-purlins were recorded, too. The results were re-evaluated with the "simplified method" developed within this project. Comparative results are shown in the previous figures (e.g. Figure 25).

Table 17: Blast Test results

Test	Cladding-type and thickness	Sup-port	Reflected Peak	Reflected Impulse	First Dynamic Deflection	Plastic Deformation	Transfer Load F1	Transfer Load F2	Plastic Deformation vertical U 60 (*)	Plastic Deformation lateral U 60 (*)
			[kPa]	[kPa·ms]	[mm]	[mm]	[kN]	[kN]	[mm]	[mm]
1	4 x TR35 - 1.00 mm	U 60 x 30 x 6 Free	164	169	-94	-35	9.3	-	-25	0
2			257	164	-97	-30	5.6	-	-26	0
3		U 60 x 30 x 6 Fixed	209	212	-84	-24	10.9	13	-10	0
4			266	161	-94	-36	11.3	10.8	-16	0
5	4 x TR84 - 0.75 mm	U 60 x 30 x 6 Fixed	231	330	-71	11	16.3	17.7	-143	87
6			289	163	-82	5	17.4	19.2	-150	87
7		U 60 x 30 x 6 Free	267	165	-75	22	11.5	14.2	-120	43
8			236	309	(?)	12	11.6	12.9	-143	120
9	4 x TR84 - 1.50 mm	U 60 x 30 x 6 Free	182	334	-45	5	11	10	0	0
10			289	361	-49	6	8.8	8.1	0	0
11		U 60 x 30 x 6 Fixed	307	116	-45	6	8.3	9.2	0	0
12			167	164	-40	8	11	11	0	0

3.3.5 Numerical simulations

Numerical studies were undertaken, static as well as dynamically loaded. The main conclusions are summarized here, for detailed information the reader might refer to deliverable D6.

3.3.5.1 Numerical simulations on trapezoidal sheets

A numeric parametric study was conducted to investigate the influence of changing impulse and constant impulse with varying peak pressure on single-span and two-span systems. Failure time was defined as the time were a given resistances value at the respective outer screw/bolt represented by a constraint material in the model was exceeded. The resistance of the assumed connection failure was derived for this model from previous material and connection tests conducted within the project.

The comparison of static and dynamic analysis is shown in Table 18 and Table 19. The vertical displacement and strain energy S_E at connection failure was evaluated and compared. Within the different load histories (LH1 to LH4) the peak pressure was varied +/- 10% while the impulse was kept constant. The impulse was varied between the different load histories.

In Table 18 the time at rupture (critical time t_c) is evaluated for the numeric simulations and the strain energy S_E at that time. The strain energy in the static test was evaluated for the corresponding deflection with the Simpson-integral. Comparison of both values is shown in the last row of Table 18. The deviation between both results was found to be high (between 31 and 23%) but surprisingly constant. However, it has to be kept in mind that the values are valid within one structural system.

Table 18: Comparison of Static Experiment and Dynamic Simulation relating to the Strain Energy

	LH1	LH1 +10	LH2 -	LH2	LH2 +10	LH3 -	LH3	LH3 +10	LH4	LH4 +10
Time t_c [ms]	0.749	0.704	0.961	0.899	0.849	1.11	1.04	0.976	1.25	1.16
Strain Energy at time t_c [kJ]	0.314	0.313	0.35	0.36	0.37	0.36	0.37	0.36	0.37	0.38
Strain Energy static experiment. at same Vertical Displacement [kJ]	0.074	0.074	0.092	0.090	0.087	0.110	0.100	0.096	0.112	0.110
S_E_Exp./S_E_Numerical Model [%]	77	77	74	75	75	69	72	73	70	71

Table 19: Overview of critical Time, Energies and Deformation Results; time t_c: bearing failure occurs

Single Span	Load History 1		Load History 2			Load History 3			Load History 4	
Peak Pressure Variation	0	+10%	-10%	0	+10%	-10%	0	+10%	0	+10%
Impulse	421.2		288.21			246.75			207.15	
[MPa] [MPa]	0.26	0.286	0.191	0.213	0.234	0.158	0.175	0.193	0.141	
[ms] [ms]	3.24	2.95	3.02	2.71	2.46	3.12	2.82	2.56	2.93	2.66
Critical time t_c [ms]	0.749	0.704	0.961	0.899	0.849	1.11	1.04	0.976	1.25	1.16
Total Energy at t_c [kJ]	6.23	6.12	5.00	5.40	5.76	4.32	4.65	4.92	3.97	4.20
Strain Energy at t_c [kJ]	0.314	0.313	0.35	0.36	0.37	0.36	0.37	0.36	0.37	0.38
Deviation [%]	0.3		2.9		2.8	2.7		2.7	2.6	
Displacement at Mid Span at critical time t_c [mm]	3.26	3.09	4.17	3.88	3.50	5.63	5.02	4.07	7.25	6.17
Deviation [%]	5.5		7.5		8.6	11		18	18	
Maximum Kinetic Energy [kJ], respectively	25.06	26.23	12.37	12.88	13.29	8.96	9.37	9.69	6.52	6.77
Kinetic Energy at time t_d [kJ]	24.54	25.53	11.88	12.92	13.06	8.51	8.53	9.25	6.31	6.65
Strain Energy at time t_d [kJ]	6.95	7.01	3.20	3.02	2.86	2.27	2.38	2.19	1.45	1.32
Deviation [%]	0.8		2.7		1.6	4.8		8.5	9.8	
Total Energy at time t_d [kJ]	32.42	33.45	15.77	16.19	16.46	11.37	11.7	12.7	8.08	8.32

With decreasing impulse, the ratio of t_c/t_d increases, which means that the time of failure gets closer to the end of loading time. While the total energy in the system decreases with decreasing impulse (for an impulse of 421 MPa·s (LH1) 6.29 kJ was achieved, for 207 MPa·s (LH4) 3.97 kJ), the percentage of the strain energy absorbed by the structure increases: here from 0.314 kJ to 0.37 kJ. This might be contributed to the strain hardening of the structure, as a stiffer structure deforms less and contributes thus less to plastic work. The variation of the peak pressure was of minor influence.

The deformation at the critical time t_c shows that with increasing impulse the structure reacts more delayed due to the inertia of mass. While for the maximum Impulse 3.26 mm deformation where achieved at t_c, the minimum Impulse lead to 7.25 mm deformation at t_c.

The deviations of strain, kinetic and total energy at t_c between LH_X +/- 10% to LH_X are presented in the respective rows in Table 19. It can be concluded that with decreasing impulse, the deviations increase, while for changing peak loads but constant impulse the variations are considered to be low.

Deformation and strain energy were evaluated and – in case of the single span system – compared with the static tests. The conclusions are summarized below.

- The deviation from the strain energy observed for the experimental tests to the numerical model ranges between 69 and 77 %. As there are significant differences between static and dynamic loading, the deviation is plausible, but rather constant in the investigated impulse range.
- With decreasing impulse, the ratio of t_c/t_d increases, which means that the time of failure gets closer to the end of loading time.
- The deformation at the critical time t_c shows that with increasing impulse the structure reacts more delayed due to the inertia of mass.
- For the continuous system in regard to the strain energy, not only the impulse but also the peak load is of importance.
- The two-span system absorbs more strain energy due to plastic work because of the additional middle support. The constraint confines the deformation of the sheet and crinkling also occurs at the mid flange, supplying more area to deform plastically. Depending on the fasteners more strain energy could be absorbed, especially with the two span system.

3.3.5.2 Numerical simulations on static substructure tests

3.3.5.2.1 Calibration of models

A summary of investigations is given here, the complete documentation of the results was prepared as deliverable D6.

Finite element models were developed by means of the commercial FE software ABAQUS [17], see Figure 26 and Figure 27. The models were used to gain an understanding of the structural response of steel cladding assemblages, as well as lap splice connection models. These FE models were validated against selected results from the static sub-structure tests and small scale tests. Finally, the models were employed to perform a number of sensitivity studies and the corresponding results were summarized.

Material strain-rate effects were accounted for by means of the Cowper-Symonds overstress power law defined as:

$$\dot{\varepsilon}^{pl} = D(R-1)^n \tag{8}$$

where $\dot{\varepsilon}^{pl}$ is the equivalent plastic strain rate, R is the ratio of the yield stress at nonzero strain rate to the static yield stress, and D and n are material parameters. A value of D=223.83 and n=2.52 were assumed in accordance with the material coupon and strain rate tests.

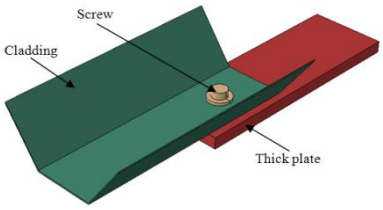

Figure 26: FE solid model for lap-splice connections

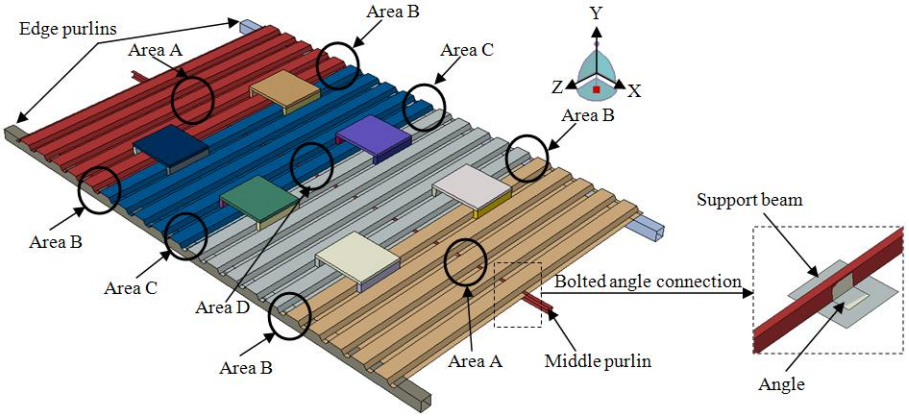

Figure 27: FE shell model for cladding substructures

The finite-element-calculations and the experimental tests showed very good compliance, as can be seen e.g. in Figure 28.

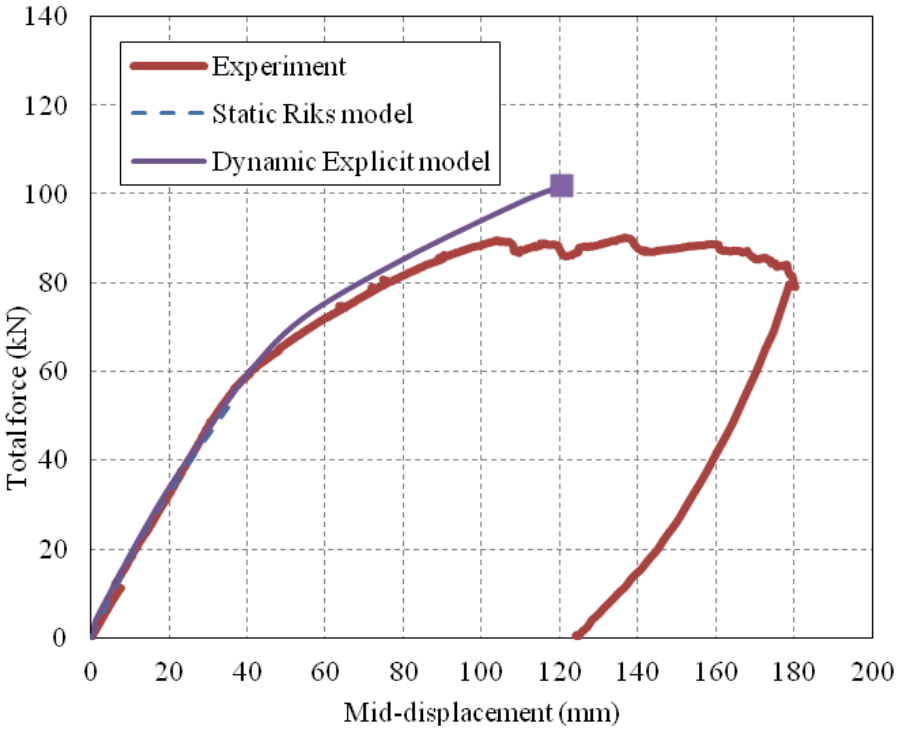

Figure 28: Comparison of experimental and numerical total force-to-mid-displacement relationship for Specimen A-TR35-100

To provide some insight into deformation patterns observed in the tests and simulated in the analysis a number of comparisons are shown hereafter. The experimental and numerical deformation patterns for Specimen C-TR 35-100 at the end of the test are depicted in Figure 29, while the comparison of the deformation in the purlin-to-column connections for Specimen D-

TR35-100 is presented in Figure 30. It is evident from both figures that the deformations and plastic mechanisms are replicated reasonably well by the proposed FE model.

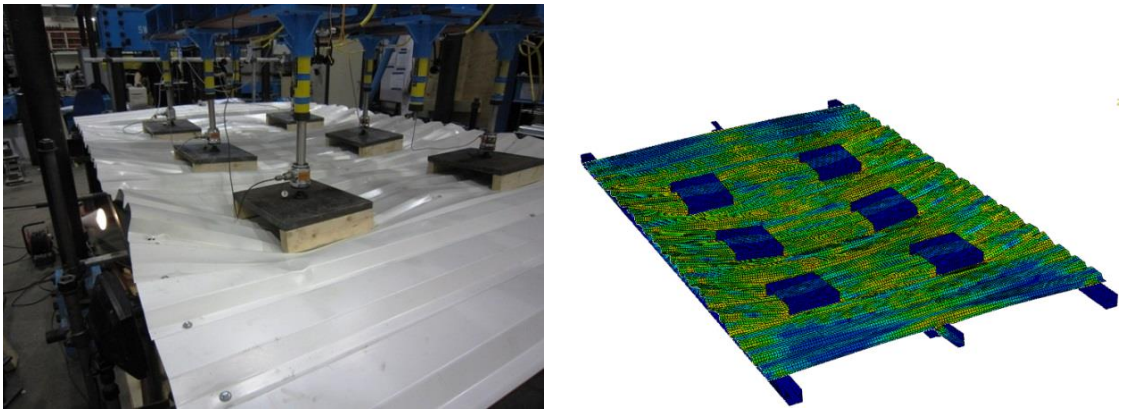

(a) Experiment (b) FE model

Figure 29: Comparison of deformation patterns between experiment and FE model for Specimen C-TR35-100 at the end of the test

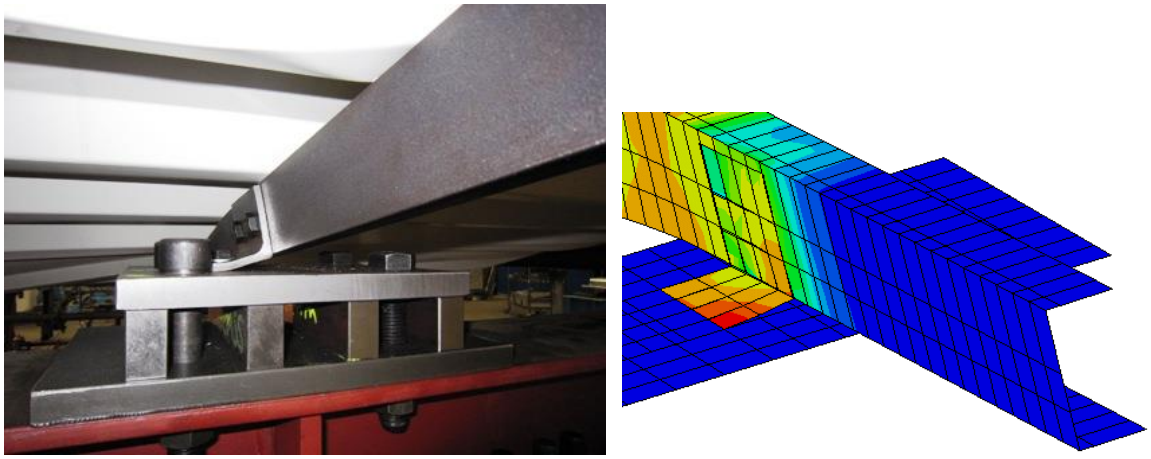

(a) Experiment (b) FE model

Figure 30: Comparison of deformation in the purlin-to-column connections for Specimen D-TR35-100

Figure 31 and Figure 32 present comparisons between the experimental and numerical response of the partial sub-structure Specimens S1-TR35-100 and S2-TR84-100. It can be noted from Figure 31 that reasonable estimates of the initial stiffness and yield capacity from the Static Riks and Dynamic Explicit analysis for Specimen S1-TR35-100 were obtained. Significant differences between the experimental results and numerical simulations were observed from a displacement of 100 mm, where an evident local buckling occurred abruptly in the cladding. Notably, instantaneous slippage occurred in the range from 100 mm to 110 mm mid-displacement in the experiment whereas a gradual and sustained accumulation of deformations was noticeable in the FE models. Close estimation of the ultimate capacity was also obtained between the experimental and Dynamic Explicit FE model within a difference of around 8 kN at a similar mid-displacement of 175 mm, although the Static Riks model provided overestimated failure force at a displacement of about 180 mm. Similarly, it is worth noting that in the case of Specimen S2-TR84-100 (Figure 32), an abrupt drop occurred at a load of around 46 kN in the experiment whereas a more gradual displacement was observed in the FE models. This can be attributed to the sudden local buckling deformation in the cladding during the test, which is difficult to capture in the FE modelling.

Overall, it can be appreciated that the general behaviour, elastic and post-elastic response, are closely represented by the numerical model, although the numerical models predicted higher failure force and displacement when compared with the results of the test. This good agreement with the tests shows that the detailed FE model can closely simulate the real response of the sub-structures.

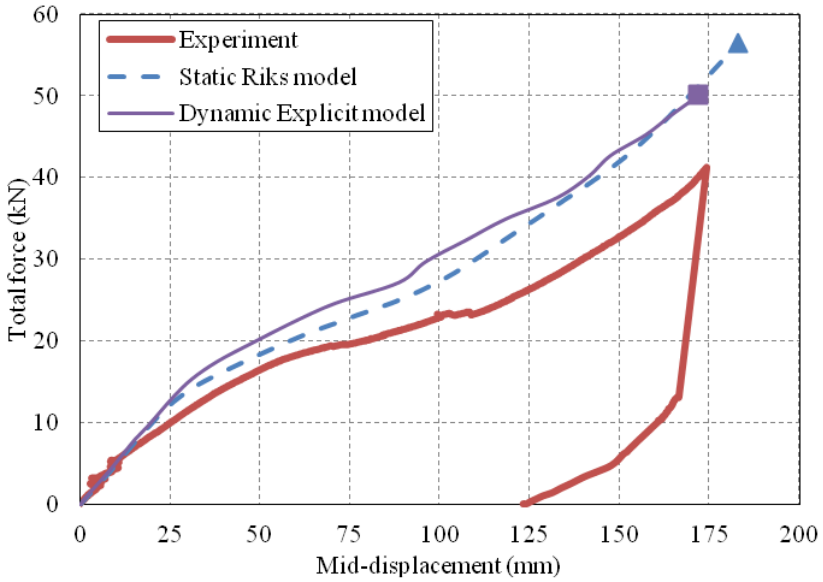

Figure 31: Comparison of experimental and numerical total force-to-mid-displacement relationship for Specimen S1-TR35-100

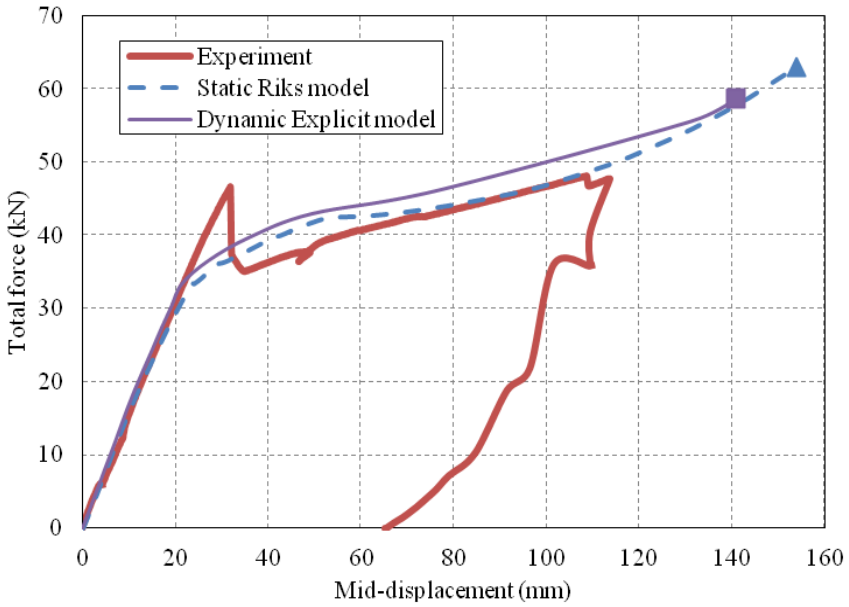

Figure 32: Comparison of experimental and numerical total force-to-mid-displacement relationship for Specimen S2-TR84-100

Figure 31 and Figure 32 compare the experimentally observed plastic deformations in Specimens S1-TR35-100 and S2-TR84-100 against their numerical predictions, respectively.

(a) Experiment

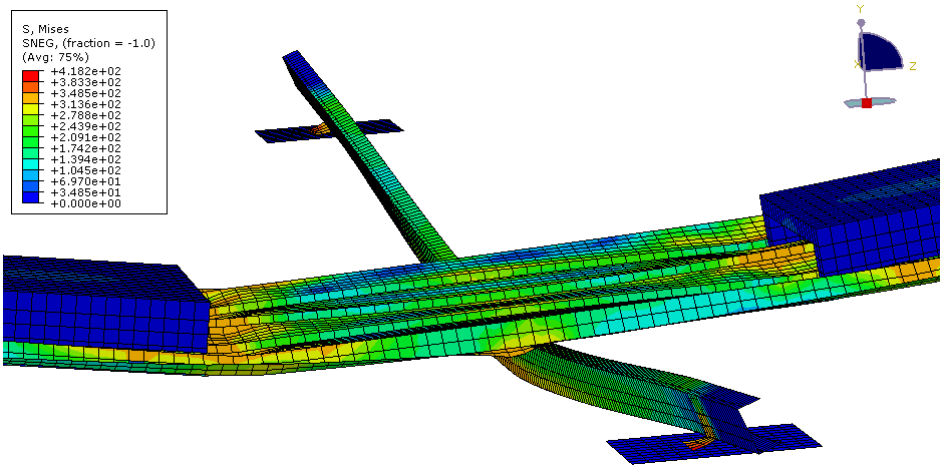

(b) FE model

Figure 33: Comparison of deformation patterns between experiment and FE model for Specimen S1-TR35-100 at the end of the test

(a) Experiment

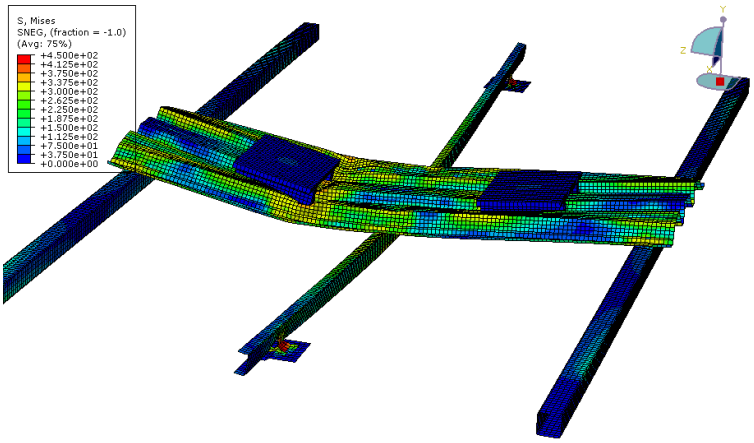

(b) FE model

Figure 34: Comparison of deformation patterns between experiment and FE model for Specimen S2-TR35-100 at the end of the test

It is evident from the above figures and associated discussions that the proposed FE models are able to replicate the observed plastic deformation modes, such as the local buckling in the cladding, the rotation of the middle purlin as well as the deformation of the angles in purlin-to-beam connections.

3.3.5.2.2 Sensitivity Studies

Sensitivity studies were carried out regarding the behaviour of cladding substructures, varying:

- Boundary conditions

  Six specimens with different purlin boundary conditions were studied in order to examine the effect of changes in the connection details on the static response of cladding substructures. Three types of boundary definitions were applied to the purlins, i) bolted angle connections for U purlins (the details replicate the bolted angle connections used for Specimen C-TR35-100), ii) simply supported, and iii) full fixed. These details are summarized in Table 20.

Table 20: Summary of specimens accounting for the influence of the boundary conditions and their failure mechanisms

Specimen	Middle Purlins	Edge Purlins	Screw Failure*	Force at Failure (kN)	Mid-deflection at Failure (mm)
Ma-Sf	Angle connection	Fully fixed	Shear fracture in X direction of screws in Area A	126	101
Mv-Sf	Simply supported	Fully fixed	Shear fracture in X direction of screws in Area A	110	108
Mf-Sf	Fully fixed	Fully fixed	Shear fracture in X direction of screws in Area A	152	102
Ma-Sv	Angle connection	Simply supported	Shear fracture in X direction of screws in Area A	127	119
Mv-Sv	Simply supported	Simply supported	Shear fracture in X direction of screws in Area A	112	127
Mf-Sv	Fully fixed	Simply supported	Shear fracture in X direction of screws in Area A	157	120

* The screw areas (Areas A, B, C and D) as well as the global directions are indicated in Figure 27.

The comparison of total force-displacement relationships for these six specimens is presented in Figure 35. It is shown that when the edge purlins are fully fixed, the stiffness and capacity of Specimens Mv-Sf, Ma-Sf and Mf-Sf were improved proportionally when the boundary conditions are varied from simply supported, bolt angle connection and fully fixed on the middle purlin. It can be also appreciated from Figure 118 that simply supports at the ends of edge purlins in the last three specimens (Specimens Mv-Sv, Ma-Sv and Mf-Sv) led to lower stiffness and higher ductility when compared with the specimens having the same boundary definition in the middle purlin (Specimens Mv-Sf, Ma-Sf and Mf-Sf), respectively. Importantly, the failure load keeps relatively constant, as demonstrated in Table 20 and Figure 35. As expected, the boundary conditions have a significant and direct effect on the stiffness and capacity of the cladding structures subjected to static loadings.

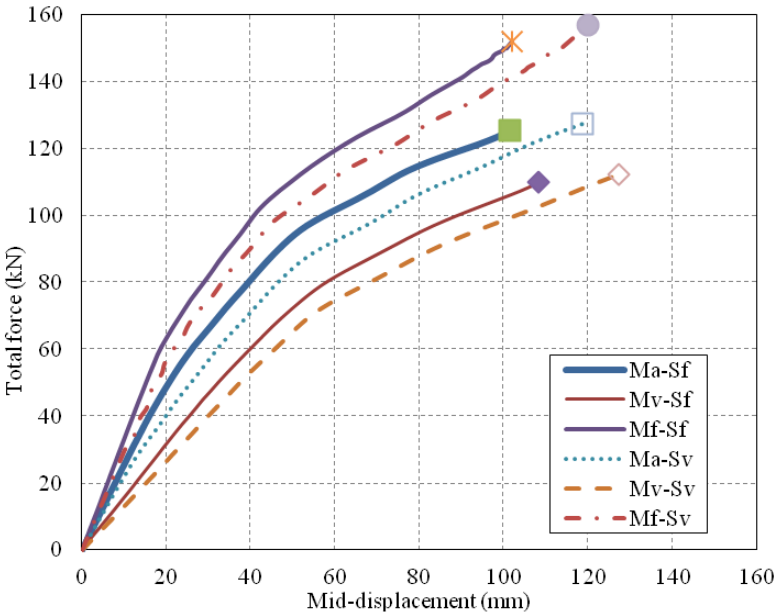

Figure 35: Influence of boundary conditions on cladding substructures under static loads

– Purlin size

The influence of the purlin sizes on the static response of the cladding substructures are explored by comparing the total force-displacement relationships and failure mechanisms of the ten specimens summarized in Table 21. U sections of dimensions 60×30×6, 100×50×6 and 150×75×6 were used for the middle purlins for Specimens U60-S100, U100-S100 and U150-S100, whereas SHS of dimensions 100×100×10, 100×100×5, 60×60×5 were used for Specimens S100-S100, S100(5)-S100 and S60(5)-S100. These six specimens incorporated with edge purlins of SHS 100×100×10, coupled with the above six different sections for the middle purlins. On the other hand, the last four specimens have edge purlins of U 60×30×6 and U 100×50×6 sections. Table 21 presents the details of each specimen as well as their failure mechanisms, while Figure 36 shows the corresponding results in terms of total force-mid-displacement relationships.

The direct influence of the purlin sizes on both the cladding structure stiffness and capacity is evident from the observation in Figure 36. It is shown from Figure 36 (a) that strong purlins (SHS 100×100×10) in Specimen S100-S100 are associated with higher stiffness and capacity. The failure of Specimen S100-S100 occurred at a total force of 250 kN due to the shear fracture of the middle screws in the edge purlins, whereas the specimen with relatively flexible purlins (U 60×30×6) presents lower failure capacity. Specimen U60-S100 exhibits about 150 kN less failure capacity when compared with that of Specimen S100-S100. Also, it is observed from Figure 36 (a) that the middle purlin of U 150×75×6 section for Specimen U150-S100 provide improved stiffness and capacity when compared with that for Specimens U100-S100 and U60-S100.

Table 21: Summary of specimens accounting for the influence of the purlin sizes and their failure mechanisms

Specimen	Middle Purlins	Edge Purlins	Screw Failure*	Force at Failure (kN)	Mid-deflection at Failure (mm)
U60-S100	U 60×30×6	SHS 100×100×10	Shear fracture in X direction of screws in Area A	128	93
U100-S100	U 100×50×6	SHS 100×100×10	Shear fracture in X direction of screws in Area A	110	124
U150-S100	U 150×75×6	SHS 100×100×10	Shear fracture in X direction of screws in Area A	121	112
S100-S100	SHS 100×100×10	SHS 100×100×10	Shear fracture in Z direction of screws in Area B	249	129
S100(5)-S100	SHS 100×100×5	SHS 100×100×10	Shear fracture in X direction of screws in Area A	178	127
S60(5)-S100	SHS 60×60×5	SHS 100×100×10	Shear fracture in X direction of screws in Area A	173	175
U60-U60	U 60×30×6	U 60×30×6	Shear fracture in X direction of screws in Area A	117	326
U100-U60	U 100×50×6	U 60×30×6	Shear fracture in X direction of screws in Area A	187	437
U150-U60	U 150×75×6	U 60×30×6	Shear fracture in X direction of screws in Area A	187	396
U100-U100	U 100×50×6	U 100×50×6	Shear fracture in X direction of screws in Area A	124	313

* The screw areas (Areas A, B, C and D) as well as the global directions are indicated in Figure 27.

It is also important to note from Figure 36 (b) that when more flexible U sections are used as edge purlins (Specimens U60-U60, U100-U60, U150-U60 and U100-U100) as compared with the stiffer SHS employed in Specimens U60-S100, U100-S100 and U150-S100, the stiffness decreases but the failure displacement increases to more than 400 mm. This is particularly evident in Specimens U60-U60 and U100-U60.

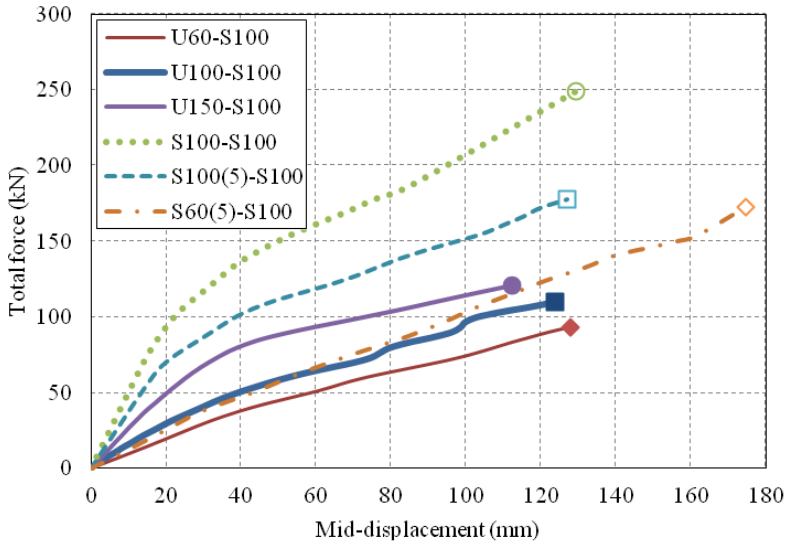

(a) Coupling with SHS edge purlins

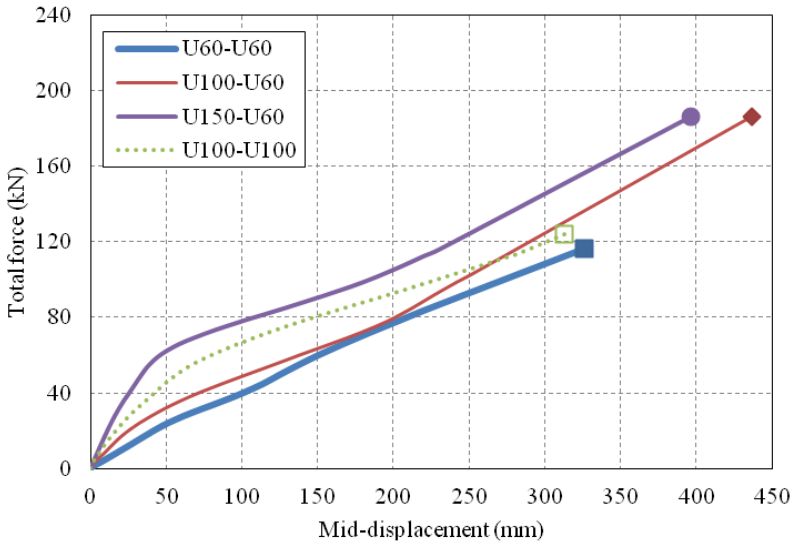

(b) Coupling with U section edge purlins

Figure 36: Influence of purlin sizes for cladding substructures under static loads

– Cladding thickness

The influence of cladding thickness on the substructure behaviour is evident by comparing the results of specimens TR35-075, TR35-100 and TR35-150 in Figure 37. It can be appreciated from this figure that the initial stiffness increases proportionally to the cladding thickness. However, Specimen TR35-075 exhibits higher capacity and larger failure displacement compared with Specimen TR35-100. This can be attributed to the different failure mechanisms observed in the former specimen. The more flexible cladding of Specimen TR35-075 fails in the shear fracture of the middle screws in the edge purlins rather than the fracture of the edge screws in the middle purlin as observed in Specimen TR35-100. Furthermore, the deep cladding TR 84/272 provides higher stiffness and capacity when compared with TR 35/207 in the same thickness, as illustrated in Figure 37.

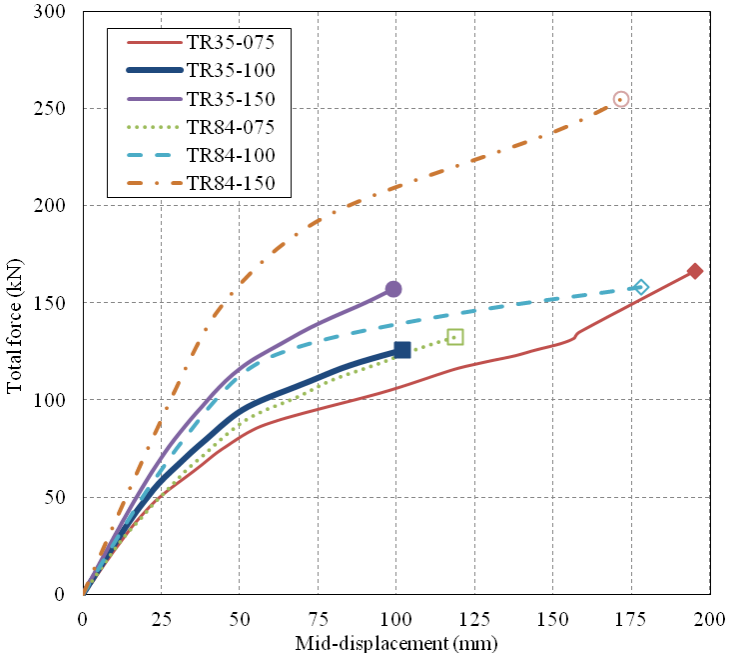

Figure 37: Influence of cladding types for cladding substructures under static loads

– Purlin span

The behaviour of the five specimens depicted in Table 22 is studied herein in order to examine the effect of the purlin span (the distance between two purlins) on the substructure response. Purlin spans of 750 mm, 990 mm, 1275 mm, 1500 mm and 1800 mm are considered. The total force-mid-displacement relationships of these five specimens are presented in Figure 38 with the indication of the failure points, whereas the corresponding failure mechanisms are summarised in Table 22. As expected, the stiffness and capacity of the cladding substructures decrease proportionally to the increase of the purlin span. It is also observed that all of the specimens failed due to the shear fracture of the screws in the edge of the middle purlin (Area A indicated in Figure 27) at a displacement of about 120mm.

Table 22: Summary of specimens accounting for the influence of the purlin spans and their failure mechanisms

Specimen	Purlin Span	Screw Failure*	Force at Failure (kN)	Mid-displacement at Failure (mm)
Span 750	750 mm	Shear fracture in X direction of screws in Area A	160	149
Span 990	990 mm	Shear fracture in X direction of screws in Area A	135	128
Span 1275	1275 mm	Shear fracture in X direction of screws in Area A	110	124
Span 1500	1500 mm	Shear fracture in X direction of screws in Area A	97	117
Span 1800	1800 mm	Shear fracture in X direction of screws in Area A	90	132

* The screw areas (Areas A, B, C and D) as well as the global directions are indicated in Figure 27.

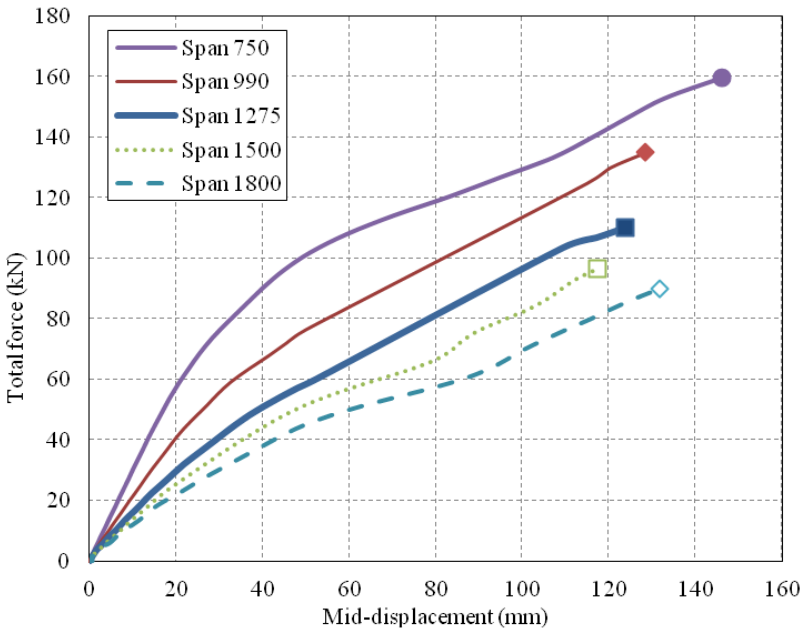

Figure 38: Influence of purlin span for cladding substructures under static loads

– Loading conditions

In order to study the effect of the loading condition on the substructures response five types of loading methods are applied on Specimen C-TR35-100. The setups are summarised in Table 23, while the force-mid-displacement as well as the failure mechanism are presented in Figure 44.

In the first two loading cases where Actuator 2 and 8 as well as Actuator 2, 5 and 8, respectively, are employed to transmit forces, the substructure exhibits lowest stiffness and capacity. The distribution of failure within the screws is different: failure occurred in the screws connected with the edge purlins (in Area C) in the former cases, whereas in the latter case the middle screws in the middle purlin (in Area D) fail due to the concentrated forces from the additional Actuator 5. It is also important to note that the total force-mid-displacement relationships of the studied cladding specimens are almost similar in both cases when the forces are applied in Actuator 1-3 and 7-9 as well as in Actuator 1-9. Moreover, the specimen in both loading conditions also exhibit similar failure mechanism, failing at a load of around 110 kN due to the shear fracture of the edge screws in the middle purlin. When the substructure is subjected to uniform pressure, the stiffness and capacity doubles as compared with the case when load is applied though Actuators 1-9.

Table 23: Summary of specimens accounting for the influence of loading methods and their failure mechanisms

Specimen	Force in Actuators	Screw Failure*	Force at Failure (kN)	Mid-displacement at Failure (mm)
Points 2 and 8	2, 8	Shear fracture in Z direction of screws in Area C	80	150
Points 2, 5 and 8	2, 5 and 8	Shear fracture in Z direction of screws in Area D	56	127
Points 1-3 and 7-9	1-3 and 7-9	Shear fracture in X direction of screws in Area A	110	124
Points 1-9	1-9	Shear fracture in X direction of screws in Area A	115	134
Uniform pressure	Uniform pressure	Shear fracture in X direction of screws in Area A	206	194

* The screw areas (Areas A, B, C and D) as well as the global directions are indicated in Figure 27.

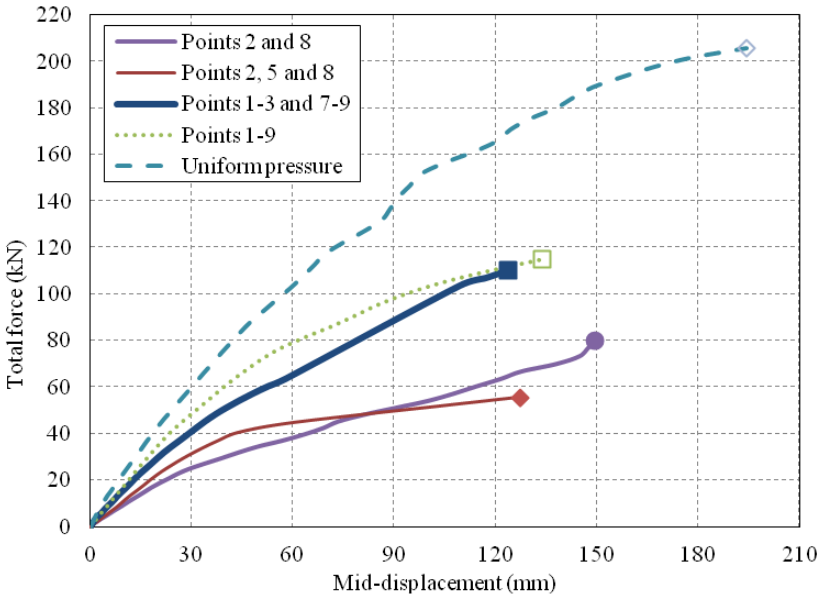

Figure 39: Influence of loading conditions for cladding substructures under static loads

3.3.6 Development of simplified models towards a new design approach

3.3.6.1 Introduction

Exceptional actions such as explosions load structures up to their ultimate resistance levels. Especially the members directly affected by the action undergo large plastic deformations that may lead locally to member failure and may affect the overall stability of the structure depending on its robustness. From this point of view, an accurate prediction of the dynamic response is decisive for a safe and robust design of the structure.

Due to the large amount of physical and geometrical nonlinearities, as well as the highly time dependent behavior present in explosive phenomena, the modelling and calculation of this processes is subjected to high computational requirements. The most exact and reliable method of predicting the structural response is achieved by the use of Finite Element Methods (FEM) with a transient explicit solver. Common Software packages used for the design of steel structures do not allow for this type of modelling and solving strategies. Hence the calculation of structures

undergoing explosive loads requires special expertise in FEM as well as very large computational power, with calculations taking several days to compute.

By means of defining an energetic equivalent system (also called dynamic equivalent systems) that shows the same deformational and energetic behaviour as the original system, the problem complexity can be dramatically reduced, and thus the solution time as well. For this reason simplified design methods based on energetic equivalent systems are still an important design tool that can be used by a wide spectrum of structural engineers.

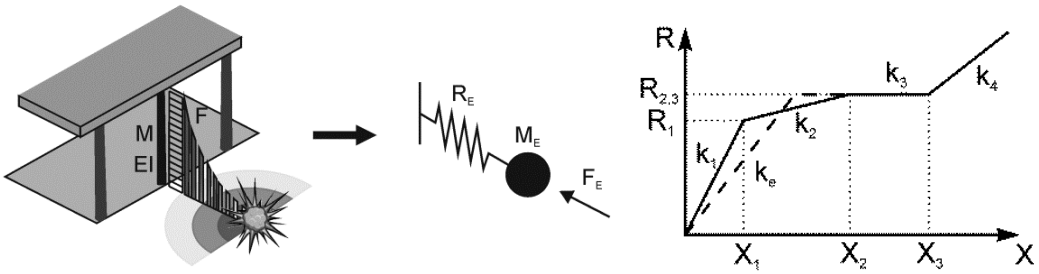

Figure 40: Conceptual system reduction of a column, exemplary nonlinear resistance curve

In a simplified design approach all structural nonlinearities are considered by a nonlinear definition of the force-displacement relation $R_E(x)$ of an equivalent spring (see Figure 40). While the first approaches from Norris et al [23] and Biggs [22], considered an elastic-perfectly plastic model, it was very soon observed, that this approach was too conservative, because it neglected the stiffening effect of membrane force activation. Different additions to the $R_E(x)$ curve have been proposed in modern codes ([9], [10], [11]), being the approach from the Fire and Blast Information Group [10] the most detailed one, proposing a 6-piece curve for $R_E(x)$.

Present existing simplified methods have found their way in codes yielding good results, but they present two main limitations:

- Lack of a generalized analytical solution under consideration of membrane forces. Here only the Biggs' approach (which does not account for membrane effects) can be solved analytically.
- Lack of integrability into a more complex structural model.

Within the scope of the project ADBLAST, a new approach to system reduction has been derived which overcomes these two limitations, thus giving an analytical solution to the blast response problem including membrane effects and opening the possibility to more complex studies of the structural behavior under blast loads.

3.3.6.2 New Simplified Model

Within the scope of the ADBLAST Project, a new approach to dynamic system reduction has been presented. This approach has allowed for the development of new analytical models in order to predict the dynamic response of structural members including arbitrary boundary conditions, including longitudinal connectors.

The proposed methodology reduces an axially and rotationally arbitrary supported beam to a 2DOF system consisting of a mass and 4 springs as presented in Figure 41.

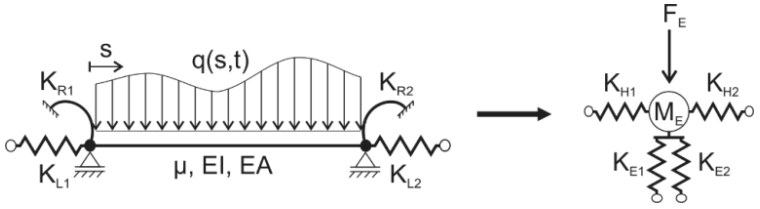

Figure 41: Member Reduction to a mass supported by four springs.

The new reduction concept is designed to explicitly address geometrical nonlinearities by means of two longitudinal springs with a nonlinear strain definition. This approach offers the possibility to explicitly model and calculate the connector forces in the system, which is a major advance in order to predict the dynamic response of structures by simplified models.

Extensive investigations ([20], [21]) show the very similar energetic behavior of the reduced and the original system, even in the elastic domain, where most classical approaches do not consider any membrane action.

Another great advantage offered by the presented methodology is the possibility to address arbitrary loading conditions in an arbitrary supported beam. Present simplification approaches could only deal with symmetrical uniformly distributed loading conditions.

A key aspect of the new methodology consisted in the fully decoupling of bending and membrane effects within the reduced model.

This means that the approach from Biggs, as well as the approaches from Norsok and Fabig (up to the fully development of plasticity in the beam) are fully compatible with the proposed approach. Therefore the characterization of the vertical nonlinear springs K_{E1} and K_{E2} is identical (see deliverable D.6/D.7 and [22] for further reference).

In order to keep the dynamic similarity, the horizontal springs K_{H1} and K_{H2} are designed to absorb the same amount of membrane strain energy as the original member undergoing a deformation $\Phi(s,t)$.

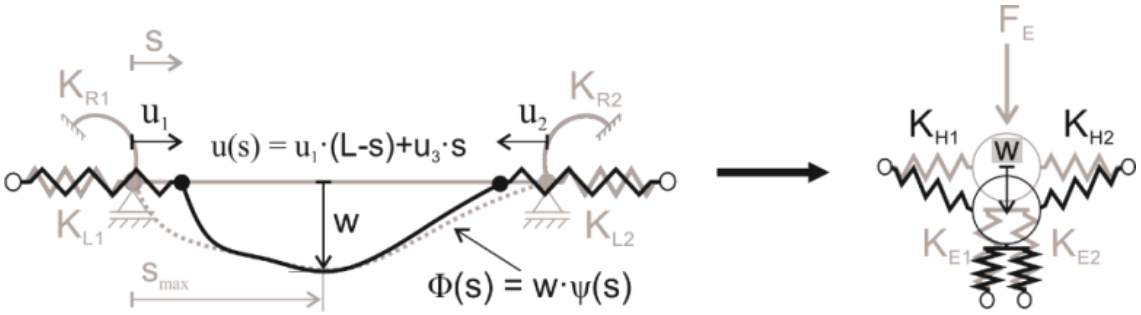

Figure 42: Deformation hypothesis in axial direction and equivalent model for the absorption of membrane strain energy.

In order to calculate the equivalent spring stiffnesses k_{H1} and k_{H2} of the springs K_{H1} and K_{H2}, the use of a nonlinear strain definition is needed. Assuming:

$$\varepsilon(s) = \frac{du(s)}{ds} + \frac{1}{2} \cdot \left(\frac{d\Phi(s)}{ds} \right)^2 \tag{9}$$

the membrane strain energy accumulated in the original system from Figure 42 can be calculated to:

$$E_{\varepsilon,S} = \frac{k_{L1}}{2} \cdot u_1^2 + \frac{k_{L2}}{2} \cdot u_2^2 + \frac{EA}{2} \cdot \int_0^L \varepsilon(s)^2 \cdot ds = \frac{k_{L1}}{2} \cdot u_1^2 + \frac{k_{L2}}{2} \cdot u_3^2 + \frac{EA}{2} \frac{(u_1 - u_2)^2}{L} + \\ + \frac{EA}{8} \int_0^L \left(\frac{d\psi(s)}{ds} \right)^4 ds \cdot w^4 - \frac{EA}{2} \frac{u_1 - u_2}{L} \int_0^L \left(\frac{d\psi(s)}{ds} \right)^2 ds \cdot w^2 \tag{10}$$

The values of the horizontal displacements at the supports u_1 and u_2 can be found at the points where eqn. (10) is minimised:

$$u_1 = \frac{1}{2} \cdot k_{1eq} \cdot \int_0^L \left(\frac{d\psi(s)}{ds} \right)^2 \cdot \mathrm{ds} \cdot \mathrm{w}^2 \tag{11}$$

with $k_{1eq} = \frac{k_{L2} \cdot k_S}{k_{L1} \cdot k_{L2} + k_{L1} \cdot k_S + k_{L2} \cdot k_S}$

$$u_2 = \frac{1}{2} \cdot k_{2eq} \cdot \int_0^L \left(\frac{d\psi(s)}{ds} \right)^2 \cdot \mathrm{ds} \cdot \mathrm{w}^2 \tag{12}$$

with $k_{2eq} = \frac{k_{L1} \cdot k_S}{k_{L1} \cdot k_{L2} + k_{L1} \cdot k_S + k_{L2} \cdot k_S}$

where k_{L1}, k_{L2} are the longitudinal stiffnesses of K_{L1} and K_{L2} and

k_S = EA/L is the axial beam stiffness.

From an energetical point of view, the left side of the beam behaves like a geometrically nonlinear spring, whose energy behaviour depends solely on w^4 as in

$$E_{\varepsilon,GNL} = \frac{k_{GNL}}{8} \cdot \frac{w^4}{s_{max}^2} \tag{13}$$

with

$$k_{GNL} = s_{max}^2 \left[L \cdot k_T \int_0^{s_{max}} \left(\frac{d\psi(s)}{ds} \right)^4 ds + \frac{s_{max}}{L} k_T \left(k_{1eq} + k_{2eq} \right)^2 \cdot \left(\int_0^L \psi(s)^2 ds \right)^2 - \quad 2k_T \left(k_{1eq} + k_{2eq} \right) \int_0^L \psi(s)^2 ds \int_0^{s_{max}} \psi(s)^2 ds \right] \tag{14}$$

After substituting the left side of the beam by a virtual spring K_{GNL} with the same energy dissipating properties, the last step consists of defining the equivalent spring K_{H1}, which groups both the connector and the beam spring in one element (see Figure 43).

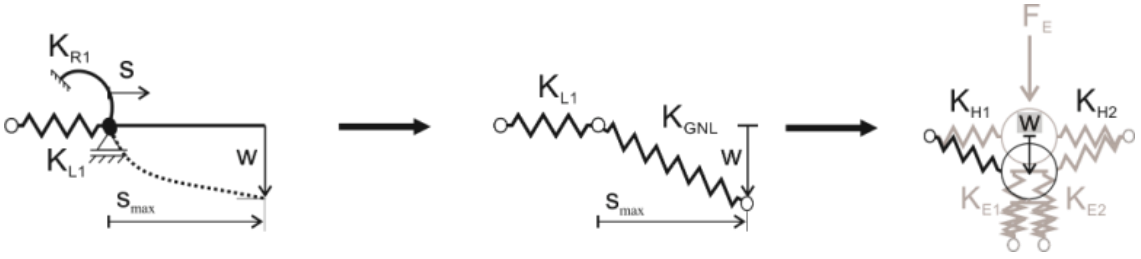

Figure 43: Reduction procedure in order to determine K_{H1}; a) original system; b) Connector + Equivalent Beam Model; c) Final Model.

Without further demonstration it can be shown that the spring K_{H1} is equivalent from an energetic point of view to the serial connection of both springs K_{L1} and K_{GNL}. Therefore the stiffness of the equivalent longitudinal spring K_{H1} can be calculated with the expression:

$$k_{H1} = \frac{1}{\frac{1}{k_{L1}} + \frac{1}{k_{GNL}}} \tag{15}$$

with k_{L1} longitudinal connector stiffness of spring K_{L1}

k_{NGL} equivalent beam stiffness from eqn. (16)

In a very similar manner, the equivalent spring stiffness of K_{H2} can be derived to:

$$k_{H2} = \frac{1}{\frac{1}{k_{L2}} + \frac{1}{k_{GNR}}} \tag{16}$$

where

$$k_{GNR} = (L - s_{max})^2 \left[L \cdot k_T \int_{s_{max}}^{L} \left(\frac{d\psi(s)}{ds}\right)^4 ds + \frac{(L-s_{max})}{L} k_T (k_{1eq} + k_{2eq})^2 \cdot \left(\int_0^L \psi(s)^2 ds\right)^2 - 2k_T (k_{1eq} + k_{2eq}) \int_0^L \psi(s)^2 ds \int_{s_{max}}^{L} \psi(s)^2 ds \right] \quad (17)$$

For practical purposes, new conversion diagrams have been generated to calculate the value of k_{GNL} and k_{GNR}. These diagrams are given exemplarily for the same cases as in [22] (see Figure 44) in the Deliverable D.6, here only for cases 1 and 2.

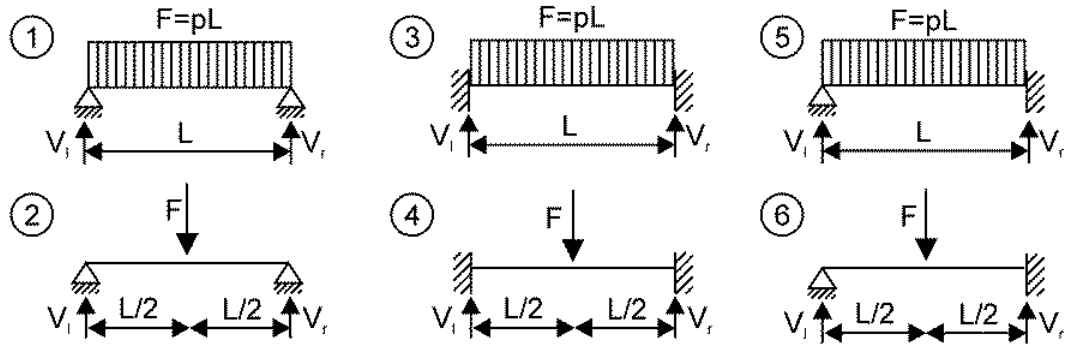

Figure 44: Investigated combinations of load and boundary conditions for the generation of dynamic conversion factors for the ADBLAST design approach.

Table 24: Transformation factors between connector stiffness and k_{H1} and k_{H2} for free-free supported beams, ADBLAST design

①	k_{H1}		k_{H2}	
El (i = 1) Pl (i = 3)	$\left(\frac{1}{k_{L1}} + \frac{1}{k_{GNL,i}}\right)^{-1}$	Figure 45 left	$\left(\frac{1}{k_{L1}} + \frac{1}{k_{GNR,i}}\right)^{-1}$	Figure 45 right
②	k_{H1}		k_{H2}	
El (i = 1) Pl (i = 3)	$\left(\frac{1}{k_{L1}} + \frac{1}{k_{GNL,i}}\right)^{-1}$	Figure 46 left	$\left(\frac{1}{k_{L1}} + \frac{1}{k_{GNR,i}}\right)^{-1}$	Figure 46 right

with k_{H1} stiffness of the equivalent longitudinal spring on the left

k_{H2} stiffness of the equivalent longitudinal spring on the right

k_{L1} stiffness of the left connector

k_{L2} stiffness of the right connector

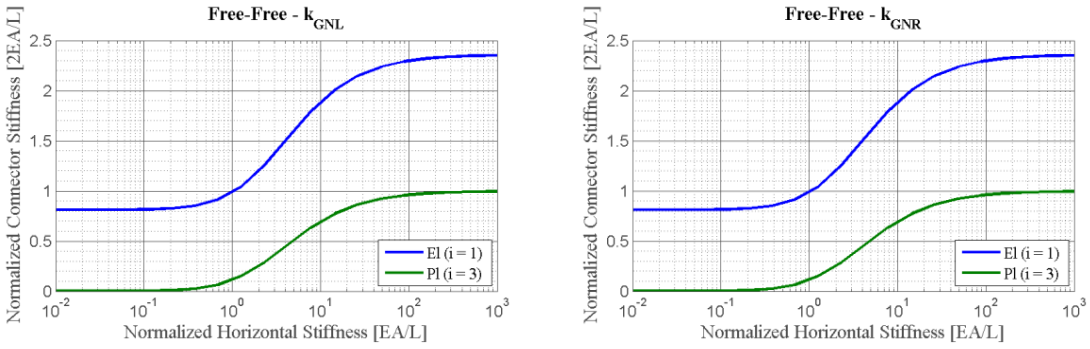

Figure 45: Conversion factors between k_{Li} (input on the x-axis) and $k_{GNL,i}$ (output on the y-axis), unif. distributed load, free-free supports

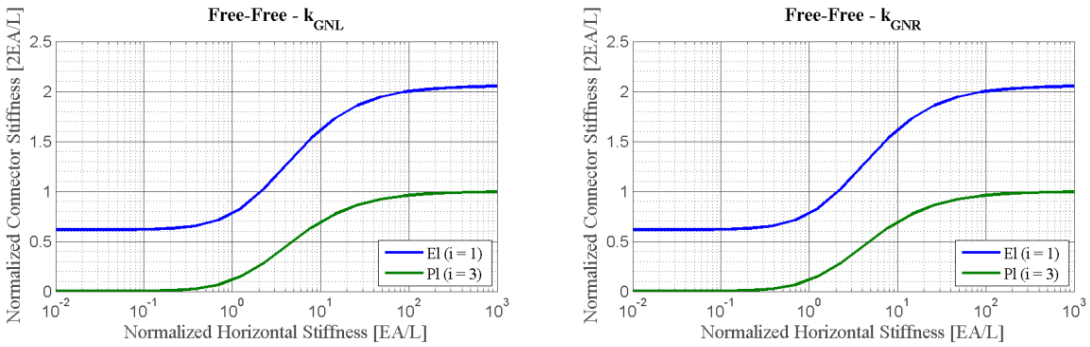

Figure 46: Normalized Stiffness for the longitudinal springs, concentrated load, free-free supports

3.3.6.3 Analytic Solution of the New Simplified Model

The energy dissipation mechanisms in the new model were investigated analytically. Special attention was paid to the use of normalised values, which led to a general valid formulation.

The analysis is divided into two stages. First, an analysis of the spring forces due to an arbitrary deformation *(u,w)* of the mass is being performed. Once the general expression for the vertical force depending on the deformation *F(u,w)* is known. The absorbed energy by the system can be analysed by solving the equation $\int^{w_{max}} F(w)dw$.

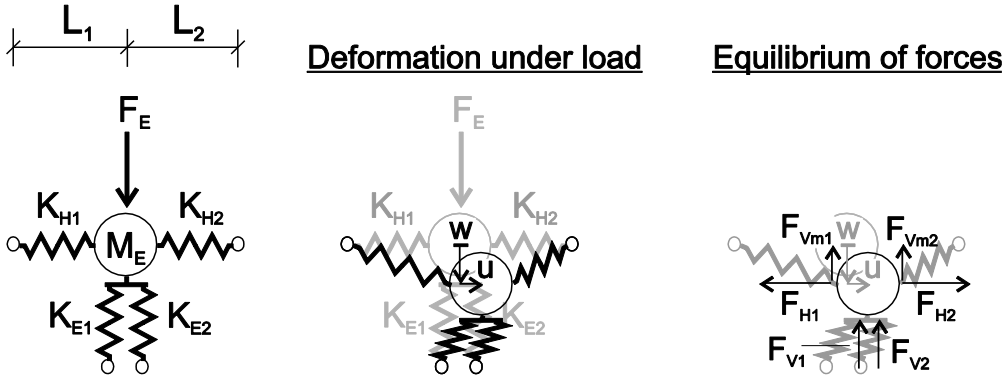

Figure 47: Deformation under vertical load of the new model, equilibrium of forces in a deformed state.

Assuming an arbitrary deformation state *(u,w)* the forces acting on each spring can be calculated by the expressions:

$$F_{V1} = k_{E1} \cdot w \; ; \; F_{V2} = k_{E2} \cdot w \; ; \tag{18}$$

$$F_{H1} = k_{H1} \cdot (u + \frac{w^2}{2L_1}) \; ; \; F_{H2} = k_{H2} \cdot \left(-u + \frac{w^2}{2L_2}\right) ; \tag{19}$$

$$F_{Vm1} = F_{H1} \cdot \frac{w}{L_1} \; ; \; F_{Vm2} = F_{H2} \cdot \frac{w}{L_2} \; ; \tag{20}$$

The equilibrium of horizontal forces yields to a unique solution of *u* for each deformation level *w*:

$$u = k_{HLon} \frac{w^2}{L} \tag{21}$$

where

$$\boldsymbol{k_{HLon}} = \frac{(k_{H2} \cdot L_1 - k_{H1} \cdot L_2) \cdot L}{2 \cdot (k_{H1} + k_{H2}) \cdot L_1 \cdot L_2} \tag{22}$$

is defined as the **adimensional longitudinal stiffness**, which relates horizontal deformation *u* to vertical deformation *w*.

Substituting equation (21) in (19), yields the expression for the membrane forces:

$$F_{\mathrm{H1}} = k_{Heq} \cdot \frac{w^2}{L} \; ; \; F_{H2} = -k_{Heq} \cdot \frac{w^2}{L} \; ; \tag{23}$$

where

$$\boldsymbol{k_{Heq}} = \frac{k_{H1} \cdot k_{H2}}{2 \cdot (k_{H1} + k_{H2})} \cdot \frac{L^2}{L_1 \cdot L_2} \tag{24}$$

is defined as the **equivalent membrane stiffness**.

In a similar manner, eq. (20) can be expressed as:

$$F_{Vm1} = k_{Heq} \cdot \frac{w^3}{L_1 \cdot L} \; ; \; F_{Vm2} = k_{Heq} \cdot \frac{w^3}{L_2 \cdot L} \; ; \tag{25}$$

Defining F_{Vm} as the sum of both F_{Vm1} and F_{Vm2}, it can be written:

$$F_{Vm} = k_{Heq} \cdot \frac{w^3}{L_1 \cdot L_2} \tag{26}$$

This force represents the total vertical resistance related to membrane action. Similar to that, the total vertical resistance due to bending action F_V can be expressed as:

$$F_V = k_{Veq} \cdot w \tag{27}$$

where

$$\boldsymbol{k_{Veq}} = k_{E1} + k_{E2} \tag{28}$$

is defined as the **equivalent bending stiffness**.

All springs in the new dynamic model have been defined as elastic-perfectly plastic springs. The deformation for which yielding occurs in any of the vertical or longitudinal springs is calculated by the expressions:

$$w_{elV} = \frac{R_V}{k_{Veq}} \tag{29}$$

$$w_{elH} = \sqrt{\frac{\min(R_{H1}, R_{H2}) \cdot L}{k_{Heq}}} \tag{30}$$

where R_V is defined as the yielding limit of the vertical springs (equivalent to the bending resistance of the beam) and $\min(R_{H1}, R_{H2})$ is the smallest resistance of the longitudinal connectors.

If $w_{elV} < w_{elH}$ yielding will occur first in the member before connector failure. In the contrary case, connector failure is expected to happen before member plastification, i.e. almost no membrane action is expected in the system.

In the following, focus will be given to energy dissipation mechanisms in systems with $w_{elV} < w_{elH}$, i.e. with strong membrane action.

For the further analysis, a normalization of all magnitudes is necessary in order to develop a general approach to the solution of the dissipated energy of the proposed model. Therefore, the use of following normalized values is proposed:

$$\lambda = \frac{F_{Vm}}{F_V} \qquad \mu = \frac{w}{w_{elV}} \qquad \eta = \frac{F_V + F_{Vm}}{R_V} \tag{31}$$

Where λ is defined as the membrane force ratio, which relates the vertical component of the force due to membrane action to the vertical component of the reaction force due to bending action, μ is the ductility ratio and η is the effective force ratio between the total acting vertical reaction force and the yielding limit of the vertical springs (yield load under pure bending). For a system with plasticity the relation between η and μ can be written as:

$$\eta(\mu) = \begin{cases} \big(1 + \lambda(\mu)\big) \cdot \mu & \text{if} \quad \mu \leq 1 \\ 1 + \lambda(\mu) & \text{if} \quad 1 < \mu \end{cases} \tag{32}$$

On the other hand, the relation between λ and μ can be calculated from eqs. (26) and (27) and yields:

$$\lambda(\mu) = \begin{cases} K_{Stif} \cdot \mu^2 & \text{if} \quad \mu \leq 1 \\ K_{Stif} \cdot \mu^3 & \text{if} \quad 1 < \mu \leq w_{elH}/w_{elV} \\ K_{Res} \cdot \mu & \text{if} \quad w_{elH}/w_{elV} \leq \mu \end{cases} \tag{33}$$

where two new dimensionless parameters have been introduced. The adimensional **stiffness ratio**

$$K_{Stif} = \frac{K_{Heq} \cdot w_{elV}^2}{K_{Veq} \cdot L_1 \cdot L_2} \tag{34}$$

and the adimensional **resistance ratio**

$$K_{Res} = \frac{\min(R_{H1}, R_{H2}) \cdot L \cdot w_{elV}}{R_V \cdot L_1 \cdot L_2} \tag{35}$$

which can be directly determined from the original spring characteristics.

The expression for the maximum energy absorption capacity of the system is given by the expression $\int_0^{w_{max}} F(w) \cdot \mathrm{d}w$, which can be expressed in adimensional form by:

$$\mathrm{E}^* = \int_0^{\mu_{max}} \eta(\mu) \cdot \mathrm{d}\mu \tag{36}$$

After susbtituting (32) and (33) in (36), one obtains the analytical expression of the normalized energy for the proposed dynamic model with arbitrary spring characteristics:

$$E^*(\mu) = \begin{cases} \frac{\mu^2}{2} + K_{Stif} \cdot \frac{\mu^3}{3} & \text{if} \quad \mu \leq 1 \\ \mu - \frac{1}{2} + K_{Stif} \cdot (\frac{1}{12} + \frac{\mu^4}{4}) & \text{if} \quad 1 < \mu \leq w_{elH}/w_{elV} \\ \mu - \frac{1}{2} + K_{Stif} \cdot \left(\frac{1}{12} + \frac{\left(\frac{w_{elH}}{w_{elV}}\right)^4}{4} \right) + \frac{K_{Res}}{2} \cdot (\mu^2 - \left(\frac{w_{elH}}{w_{elV}}\right)^2) & \text{if} \quad w_{elH}/w_{elV} \leq \mu \end{cases} \tag{37}$$

Through the explicit modelling of the longitudinal connectors, the achieved ductility can be calculated from the equation:

$$\mu_{Lat,1} = \left(\frac{k_{HLon}}{L} + \frac{1}{2L_1}\right) \cdot \frac{K_{H1}}{R_{H1}} \cdot w_{elV}^2 \cdot \mu^2 \tag{38}$$

$$\mu_{Lat,2} = \left(\frac{k_{HLon}}{L} + \frac{1}{2L_2}\right) \cdot \frac{K_{H2}}{R_{H2}} \cdot w_{elV}^2 \cdot \mu^2 \tag{39}$$

respectively for the left and right connectors.

3.3.6.4 Results

The design approach proposed within the ADBLAST project opens many new possibilities for an accurate design of steel structures under blast loading.

The approach is fully compatible with existing approaches as in ([22], [9], [10], [11]) and extends its validity (and applicability) to arbitrary axially restrained systems.

The new approach offers a fully analytic solution for the maximum achieved ductility, which includes explicitly the longitudinal connector stiffness and yielding limit. Thus it is possible to predict connector failure as well as member failure and foresee which is more likely to happen sooner.

The new simplified model can be solved numerically leading to general design aids, which extend the range of validity of former approaches that would consider membrane effects in a very limited manner.

An overview of the existing design methodologies is briefly presented in Figure 48 and more extensively presented in the Design Guide and the deliverable D.6/D.7. Each design approach offers different calculation methodologies. ADBLAST method is the most general applicable one (arbitrary longitudinal connectors, arbitrary rotational fixings, arbitrary loading conditions) and yet, its usage is as easy as any other approach.

	Analytical	Design Aids	Numerical
UFC / Biggs	μ, V	μ, V	μ(t), V(t)
Norsok		μ, V	μ(t), V(t)
Fabig			μ(t), V(t)
ADBLAST	μ, μ_L, V	μ, μ_L, V	μ(t), V(t), FEM

Figure 48: Overview of Design Methods and Calculation Methodologies, investigated in ADBLAST.

The ADBLAST methodology yields very accurate results for the design of members with an expected strong membrane action at high deformation levels. Different calculation methodologies (ranging from fully analytical to FEM integration) can be used with the new presented model, allowing for a more efficient assessment of the resistance of steel members under explosion. In this regards, different design methodologies with corresponding examples have been proposed in the design guide.

By means of the new model, the different cladding and substructure systems investigated in ADBLAST could be evaluated in parametric studies and the results were presented in normalised pressure-impulse (p^*-i^*) diagrams, see Example in Figure 49. For each investigated system, a dynamic reduction according to the principles presented in D.6/D.7 has been performed. The resulting reduced model has been solved then for different loading scenarios corresponding to the different risk classes. The response of the system both in transversal and longitudinal direction has been evaluated and the ductility requirements for each system have been determined.

Interpretation of diagram in Figure 49

Using the developed design approach within the Adblast project, the reference cladding systems (TS 35 and TS85) were evaluated against the different risk scenarios (CC1, CC2, CC3) by looking at the expected damage (or required ductility level) suffered by the cladding systems (including longitudinal connectors!) depending on the chosen span width of the cladding.

This diagram shall facilitate the choice of cladding type, span and connector type given a risk scenario. For instance, assuming a risk scenario of type SS CC2 and a trapezoidal sheet of type TS 85 1.0 mm spanning over a length of 4 m, we can expect a required ductility of the trapezoidal sheet of between 1.8 and 2.5 depending on the chosen connector type, which will presumably suffer low damage (region between LD and SD). The stronger the connector type is used, the less expected ductility and damage in the connectors can be expected.

Inversely, if a certain cladding type is given (here TS 85 0.75mm with longitudinal connectors 4x HILTI S-MP52S 6.3) and no damage in the cladding is required for a risk scenario of type SS CC2, then the maximum free span of the cladding must not exceed 3.7 m.

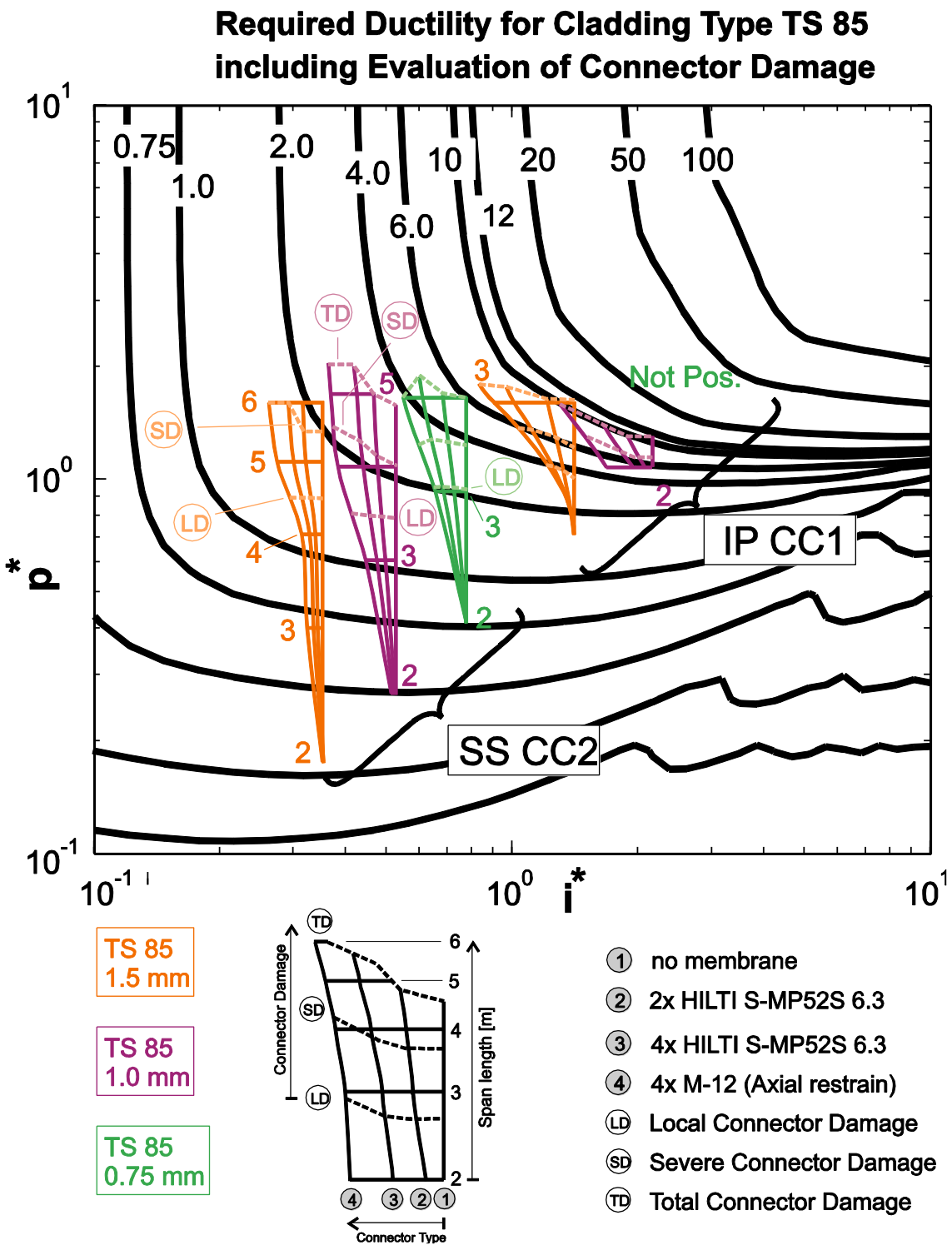

Figure 49: p^*-i^* diagram for Trapezoidal Claddings of Type TS 85, assuming Free-Free rotational support of the cladding (safe-side assumption), all ADBLAST longitudinal connectors considered, all Risk Scenarios considered.

3.3.7 P-I Assessment

3.3.7.1 Introduction

An *P-I*-Assessment was conducted exemplarily for a small hall. The basic procedure is shown hereafter.

The structure of the hall was simplified in several steps to a moderate size in the finite-element code, to allow for extensive calculations. This was followed by a parametric assessment, using

pressure-impulse representation, of the blast response of this form of structure alongside discussions of key behavioural characteristics.

3.3.7.2 Modelling

The sub-structure model for the selected industrial warehouse structure consists of three UPN 100 side rails and TR35/207 corrugated sheeting. As shown in Figure 50, the sub-structure is 5 m long and 4 m wide, with a spacing of 2 m between the side rails. The actual details for the angle connections were incorporated in the model. In addition, connector elements were included to capture the response of the self-tapping screws and the M10/M12 bolts. The whole assemblage was placed on six fully fixed rectangular plates which represented the flange of the primary columns.

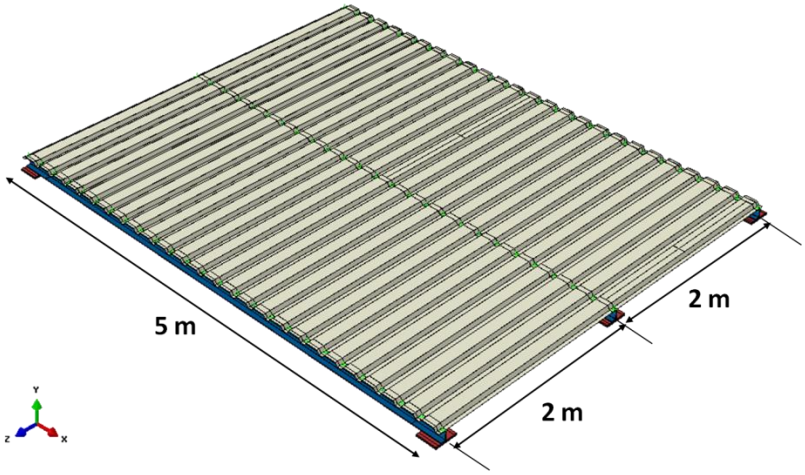

Figure 50: Sub-assemblage model representing the side wall of the warehouse

It was assumed for the purpose of the studies conducted in this section that the cladding system has two corrugated sheets with mineral wool infill as insulation. Only the single layer (the external sheet) was modelled here as it resists the external forces, but the mass of the infill and the internal sheeting was added to the external layer as non-structural mass to take into account the actual inertia of the whole cladding system. The finite element model only represents part of the whole wall structure. The supported mass of the cladding system on the neighbouring span were therefore also included as non-structural mass of the outer side rails of the FE model.

Since the numerical model only represents part of the wall structure, continuity should be maintained by imposing appropriate boundary conditions to side rails. The flanges of the outer side rails were subjected to translational restraints in the z-direction and rotational restraints about the x-axis, in such a way to represent the pulling action from the neighbouring sheets.

Figure 51 presents the numerical connector model for the self-tapping screw fastener. The connector model consists of two nodes, one is on the cladding and the other is on the flange of the side rail. Each node is assigned with an effective radius which is shown as green circles in Figure 51. The radius is equivalent to the radius of the head of the screw. All the finite element nodes within the radius are coupled with the two nodes of the connector in order to distribute the motion and load in a small area.

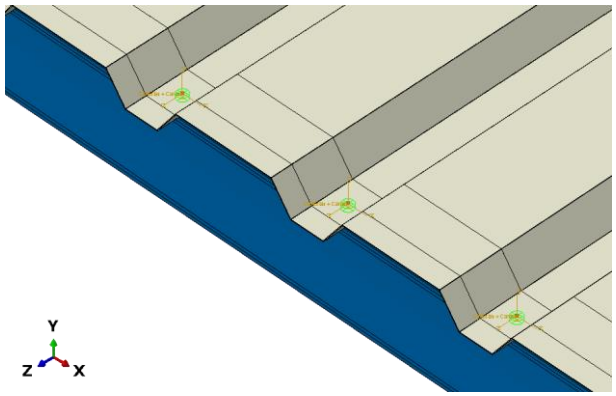

Figure 51: Self-tapping screw connector model

The detailed modelling of the connectors and their calibrated response is not further explained here, but the reader might refer to deliverable D6 for further information.

The dynamic response of the sub-structure model to blast loads was investigated through a parametric assessment. The blast overpressure was applied uniformly over the surface of the cladding sheets as shown in Figure 52(a), while the time profile of the blast loading is shown in Figure 52(b). This is a detonation type of load with peak overpressure of P and duration of t_d. The specific impulse (I), the area under the blast curve, is defined as: $\frac{1}{2}P \cdot t_d$.

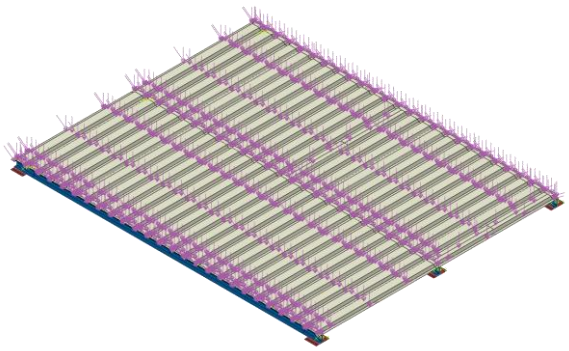

(a) Uniform pressure load

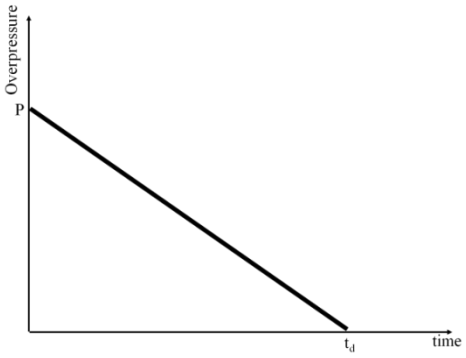

(b) Pressure – time history of the blast loading

Figure 52: Blast load application and profile

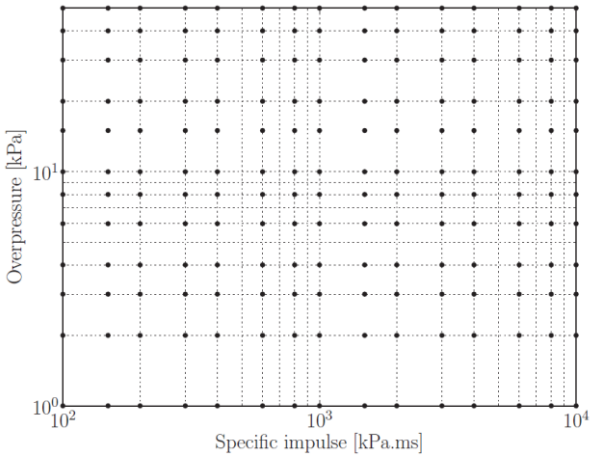

Figure 53: Loading scenarios: combination of overpressure (P) and specific impulse (I)

The finite element model of the sub-assemblage was then subjected to blast loading with a series of combinations of overpressure and duration in the parametric study. The combinations in the loading scenario are shown in Table 25. The overpressure range of the parametric study covers from 1 to 50 kPa and the impulse range covers from 100 kPa.ms to 10000 kPa.ms.

Table 25: Combination of overpressures and impulses with corresponding case number and duration

		Cases no.															
Overpressures (kPa)	**50**	166	167	168	169	170	171	172	173	174	175	176	177	178	179	180	**50**
	40	151	152	153	154	155	156	157	158	159	160	161	162	163	164	165	**40**
	30	136	137	138	139	140	141	142	143	144	145	146	147	148	149	150	**30**
	20	121	122	123	124	125	126	127	128	129	130	131	132	133	134	135	**20**
	15	106	107	108	109	110	111	112	113	114	115	116	117	118	119	120	**15**
	10	91	92	93	94	95	96	97	98	99	100	101	102	103	104	105	**10**
	8	76	77	78	79	80	81	82	83	84	85	86	87	88	89	90	**8**
	6	61	62	63	64	65	66	67	68	69	70	71	72	73	74	75	**6**
	4	46	47	48	49	50	51	52	53	54	55	56	57	58	59	60	**4**
	3	31	32	33	34	35	36	37	38	39	40	41	42	43	44	45	**3**
	2	16	17	18	19	20	21	22	23	24	25	26	27	28	29	30	**2**
	1	1	2	3	4	5	6	7	8	9	10	11	12	13	14	15	**1**
		100	**150**	**200**	**300**	**400**	**600**	**800**	**1000**	**1500**	**2000**	**3000**	**4000**	**6000**	**8000**	**10000**	
		Dutration (ms)															
Overpressures (kPa)	**50**	4.0	6.0	8.0	12.0	16.0	24.0	32.0	40.0	60.0	80.0	120.0	160.0	240.0	320.0	400.0	**50**
	40	5.0	7.5	10.0	15.0	20.0	30.0	40.0	50.0	75.0	100.0	150.0	200.0	300.0	400.0	500.0	**40**
	30	6.7	10.0	13.3	20.0	26.7	40.0	53.3	66.7	100.0	133.3	200.0	266.7	400.0	533.3	666.7	**30**
	20	10.0	15.0	20.0	30.0	40.0	60.0	80.0	100.0	150.0	200.0	300.0	400.0	600.0	800.0	1000.0	**20**
	15	13.3	20.0	26.7	40.0	53.3	80.0	106.7	133.3	200.0	266.7	400.0	533.3	800.0	1066.7	1333.3	**15**
	10	20.0	30.0	40.0	60.0	80.0	120.0	160.0	200.0	300.0	400.0	600.0	800.0	1200.0	1600.0	2000.0	**10**
	8	25.0	37.5	50.0	75.0	100.0	150.0	200.0	250.0	375.0	500.0	750.0	1000.0	1500.0	2000.0	2500.0	**8**
	6	33.3	50.0	66.7	100.0	133.3	200.0	266.7	333.3	500.0	666.7	1000.0	1333.3	2000.0	2666.7	3333.3	**6**
	4	50.0	75.0	100.0	150.0	200.0	300.0	400.0	500.0	750.0	1000.0	1500.0	2000.0	3000.0	4000.0	5000.0	**4**
	3	66.7	100.0	133.3	200.0	266.7	400.0	533.3	666.7	1000.0	1333.3	2000.0	2666.7	4000.0	5333.3	6666.7	**3**
	2	100.0	150.0	200.0	300.0	400.0	600.0	800.0	1000.0	1500.0	2000.0	3000.0	4000.0	6000.0	8000.0	10000.0	**2**
	1	200.0	300.0	400.0	600.0	800.0	1200.0	1600.0	2000.0	3000.0	4000.0	6000.0	8000.0	12000.0	16000.0	20000.0	**1**
		100	**150**	**200**	**300**	**400**	**600**	**800**	**1000**	**1500**	**2000**	**3000**	**4000**	**6000**	**8000**	**10000**	
		Specific impulse (kPa.ms)															

In total 180 loading cases were analysed and the results are presented in subsequent sections. Table 25 presents the case number and duration corresponding to the defined load combinations. It is worth noting that the analysis is conducted on a high performance platform (HPC, 12 Xeon 2.2 GHz CPU and 12 GB Ram). It requires about 5 hours for each case for 300 ms simulation time.

3.3.7.3 Response measurement and damage levels

One of the key advantages of the sub-assemblage model is that it combines reasonably efficient computational demand with the ability to provide relatively detailed information on the behaviour of key components of the structure. The details of the adopted sub-assemblage model is depicted in Figure 54.

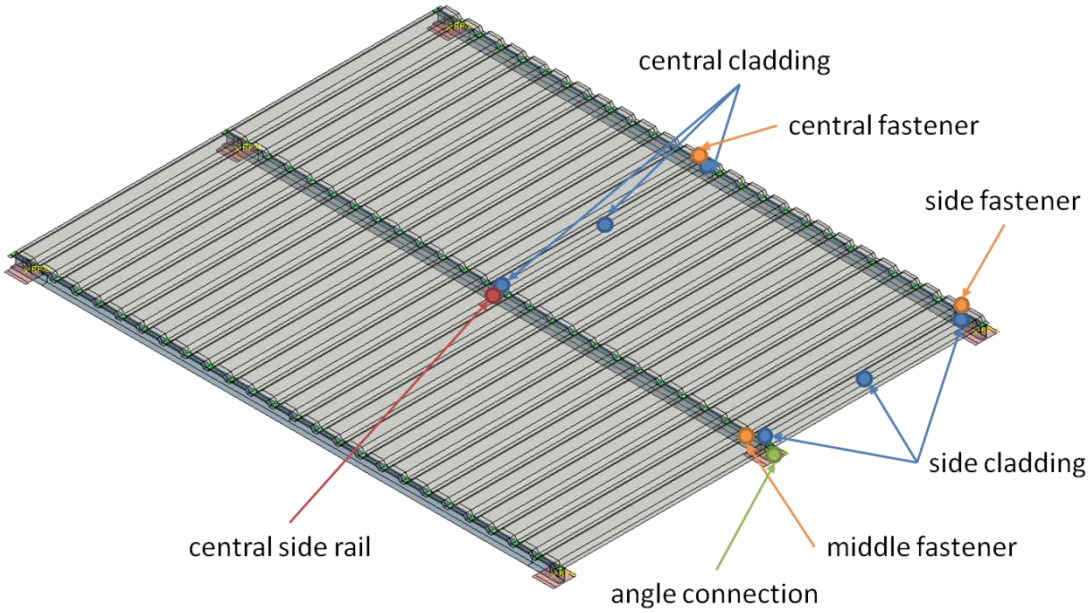

Figure 54: Details of the sub-assemblage model

The primary output of the model is the displacement history at mid span of the central side rail. Selected typical deflections of the cladding panels are also recorded. At mid-span, the deflections of the central cladding are registered by three gauges from edge to centre: upper, middle and lower. Similarly, deflections of side cladding to the edge of the model are also recorded by three gauges. Two connectors labelled as central and side fasteners were chosen to be analysed and their locations are shown in Figure 54. One more connector was also chosen near the support of the central side rail (labelled as the middle fastener). The last connector (labelled as angle connection) was chosen to study the response of the connection between the central side rail and the primary column.

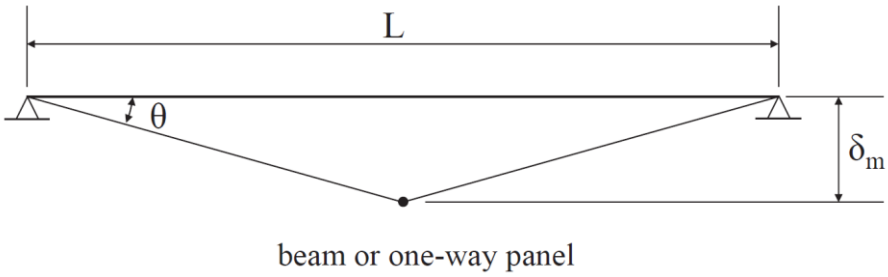

Figure 55: Mid-span deflection and end rotation of a structural component

In order to restrict the damage to a structure or element which is subjected to incidental dynamic loading, limiting values must be assigned to appropriate response quantities. These response limits define the performance criteria of the structural components under blast loading. Deformation limits can be defined corresponding to different damage levels. The relationship between the component damage and the response limit are briefly presented below (USACE, 2008b) and (ASCE, 1997).

Deformation limits are defined in terms of the ductility ratio and support rotation for individual structural components. The ductility ratio indicates the component ability to absorb energy and is defined as the ratio of the maximum mid-span displacement to the displacement at yielding. The support rotation is defined as the tangent of the maximum mid-span deflection over the component half length. The two response parameters are illustrated in Figure 55.

The ductility ratio μ is defined as $\mu = \delta_m/\delta_e$ where δ_m is the maximum component displacement and δ_e is the deflection at yielding. The support rotation is then defined as $\theta = tan^{-1}(2\delta_m/L)$, where L is the length of the component.

Damage levels of components to a dynamic load are usually defined by reference to a range of ductility and support rotation values to provide upper and lower limits for each damage level. Guidance on response limits for structural components are presented in a number of references (ASCE, 1997), (USACE, 2008b) and (USDOD, 2008). Typical values for cold formed thin wall members are presented in Table 26.

Table 26: Response limits for cold formed structural steel members

Damage level:		moderate		heavy		Hazardous	
		μ	θ	μ	θ	μ	θ
Side rail and purlin	No catenary action	-	3^0	-	10^0	-	20^0
	With catenary action	-	4^0	-	12^0	-	20^0
Corrugated panel	Full tensile membrane capacity	3	3^0	6	6^0	10	12^0
	Some tensile membrane capacity	-	1^0	-	4^0	-	8^0
	No tensile membrane capacity	1.8	1.3^0	3	2^0	6	4^0

Applying the response limiting values to the components in the sub-assemblage, the limiting values of deflection at mid-span of the side rail and cladding panel are shown in Table 27, where $\delta_m = \frac{1}{2}Ltan(\theta)$ (L = 2000 mm for cladding and L = 5000 mm for side rail). Therefore, the damage levels and limiting respons are now based on maximum mid-span deflections.

Table 27: Response limits for side rail and cladding panel

Damage level	Side rail		Cladding panel	
	θ	δ_m (mm)	θ	δ_m (mm)
Moderate	4^0	147	1^0	17
Heavy	12^0	531	4^0	70
Hazardous	20^0	909	8^0	141

In addition to conventional criteria, the sub-assemblage model can produce two more response parameters: side rail axial displacement and the failure of fasteners. The rotation of the side rail at the support was neglected since the maximum deflection at mid-span is used. For the axial displacement (damage to the side rail – column connection), two limiting values were used: 10mm (connection heavy damage) and 100 mm (connection loss of component). When the deformation within the M10 bolts reaches 10mm it is assumed that heavy damage level is reached while when the connection deforms by 100mm the side rail will be pulled out of the connection, then the component is lost.

The ultimate behaviour was also modelled for the self-tapping screw fasteners. During the blast loading, some or all of them would fail at different times due to the structural response and the nature of the loading. The percentage of the fastener failures was defined as the ratio of the number of failed fasteners over the total number of fasteners in the sub-assemblage. This was used as an additional damage criterion in the current investigation.

3.3.7.4 Pressure – impulse diagrams

After a detailed study of connector failure behaviour to predict the failure mode, this information is used to construct pressure - impulse diagrams of the sub-assemblage. The damage criteria used here are: transverse displacement of side rail, axial displacement of side rail and percentage of total fastener failure. A series of iso-curves for TNT charges were also constructed for ease of identifying the explosion source and safe siting of structures.

The pressure - impulse diagrams have the same range of overpressure and impulse as discussed before. Three damage criteria were used: maximum transverse displacement of side rail,

maximum axial displacement of side rail and the maximum percentage of total fastener failure. All 180 cases defined before were used. The maximum value of the time history in each case was extracted and populated over the full range of the pressure - impulse diagram. The iso-damage curves were then determined by interpolating between the points within the grid.

3.3.7.4.1 Side rail transverse displacement

The pressure – impulse diagrams of maximum dynamic transverse displacement of the central side rail of the sub-structure (corresponding to detonation blast scenarios defined in Table 25) are shown in Figure 56. The damage levels are defined in Table 27. These three iso-damage curves were based on the displacement criteria. The limiting values for the damage levels are summarised and discussed in subsequent sections.

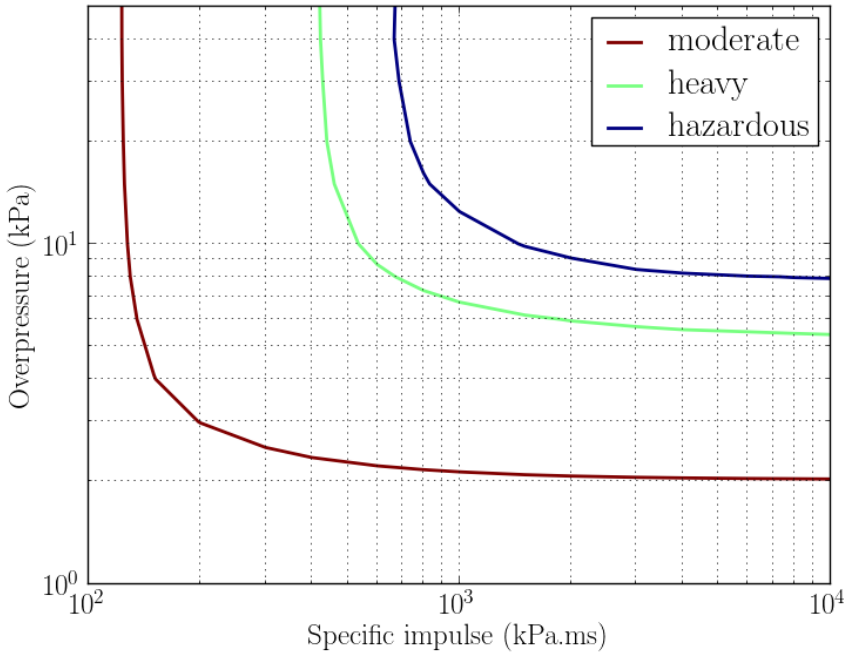

Figure 56: Pressure – impulse diagram: maximum side rail displacement

3.3.7.4.2 Side rail connection response

The pressure – impulse diagrams of maximum bolt shear displacement of the middle angle connection of the sub-assemblage structure corresponding to the various detonation loading scenarios is shown in Figure 57. Two iso-damage curves are used to represent two damage levels in terms of bolt shear deformation. The heavy damage corresponds to shear displacement of 10 mm (diameter of the bolt) while the failure curve corresponds to 100 mm (pull-out). Beyond this failure iso curve, the side rail would be pulled out of the connection and the component would be ineffective. The limiting values for the damage levels are summarised and discussed in subsequent sections.

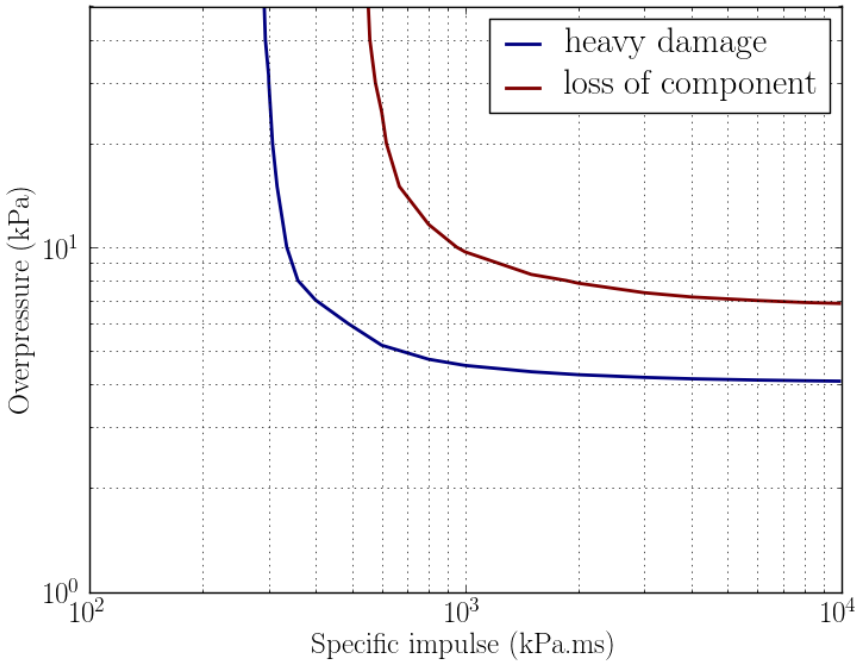

Figure 57: Pressure – impulse diagram: side rail connection damage

3.3.7.4.3 Percentage of total fastener failure

The pressure – impulse diagrams of total fastener failure of the sub-assemblage structure are shown in Figure 58. The failure of fasteners was used in addition to the displacement of cladding as an alternative damage criterion. These iso-damage curves were proposed to enable a more direct assessment of structural damage.

Five damage levels were used here: 5%, 25%, 50%, 75% and 99%. It can be seen that the iso curves are not as smooth as for other damage criteria but the levels of damage are still very clear. Above 25% damage level, in the quasi-static region, the range between iso-damage curves is smaller than the range in the impulsive region. This suggests that the failure of fasteners is more sensitive to the peak overpressure when the damage level is greater than 25%. Also, the failure is less sensitive to impulse loading and can be interpolated very well over the damage range. In the quasi-static region, the blast loading was applied over a long period. Accordingly, once the failure of fasteners started to occur, the neighbouring fasteners would become prone to fail due to the continuously applied load. In the impulsive range, the load could reduce before the failure of connector occurs hence the neighbouring fasteners would not be affected. The limiting values for the damage levels are summarised and discussed in subsequent sections.

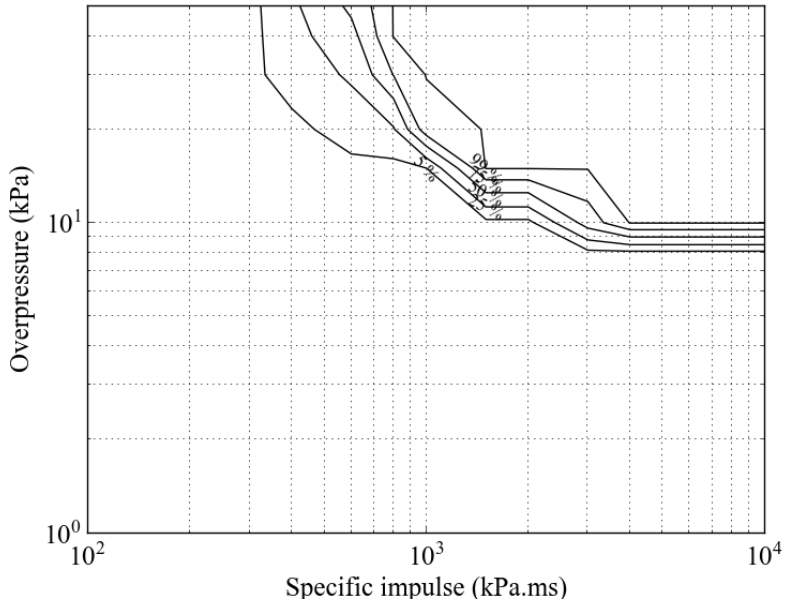

Figure 58: Pressure – impulse diagram: total percentage of fastener failure

3.3.7.4.4 Iso-curves for TNT explosive charges

Overpressure and impulse of the blast wave generated by TNT high explosives can be determined by established relationships in the literature. Iso-distance and iso-charge weight curves can also be constructed. The iso-distance curves can be created by keeping the distance R constant at 200, 400, 1000, 6000 and 30000 m while varying the weight of TNT charge W. Similarly, the iso-charge weight curves can be plotted by keeping the weight of TNT charge W constant at 1, 7.5, 150, 2000, and 25000 m while varying the stand-off distances R. The overpressure and impulse presented in the illustrative Figure 59 are reflected values.

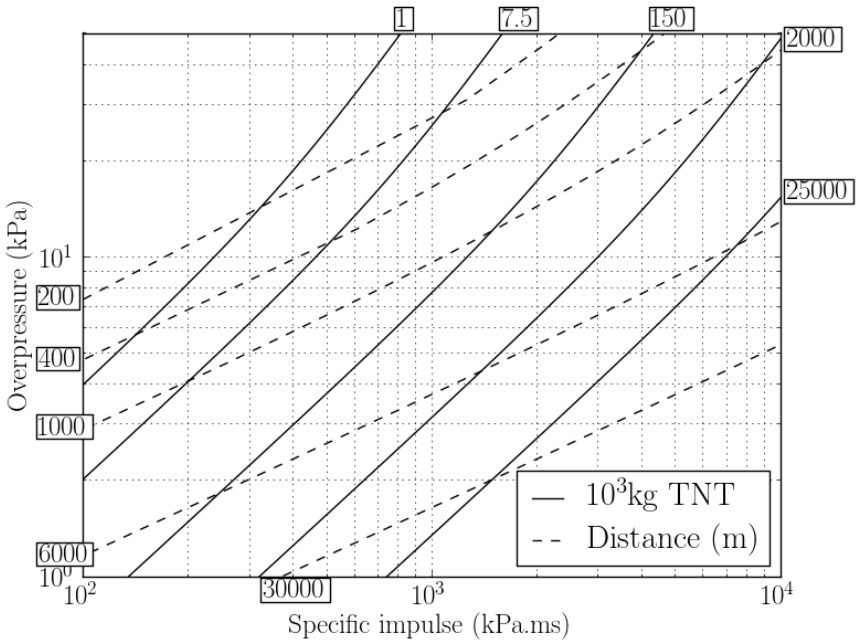

Figure 59: ISO curves for TNT explosive charge

As an example, the intersection of the curve of 1 kg with the curve of 200 m would give the reflected overpressure and impulse of a 1 kg TNT charge at a stand-off distance of 200 m. Interpolating and extrapolating between the iso-curves would define the detonation blast loading for TNT charge sizes from 1 to 25000 kg at stand-off distances from 200 to 30000 m. Combing these iso-curves of TNT charges to the pressure - impulse diagrams of the structure would make the estimation of the expected damage or safe distance more straightforward.

3.3.7.4.5 Combined pressure – impulse diagrams

The previously discussed three pressure-impulse diagram plots are combined into one graph as shown in Figure 60. The iso-curves of TNT charges are also superimposed. These combined pressure – impulse diagrams can be used to identify the most critical component or parameter which controls the response of the sub-structure. Table 28 summarises the limiting pressure and impulse values for the three damage criteria. For better interpretation, three damage levels were selected for fastener failures: 5% (moderate), 50% (heavy) and 99%(hazardous). For the side rail connection response, the heavy damage and loss of component criteria were classified as heavy and hazardous levels.

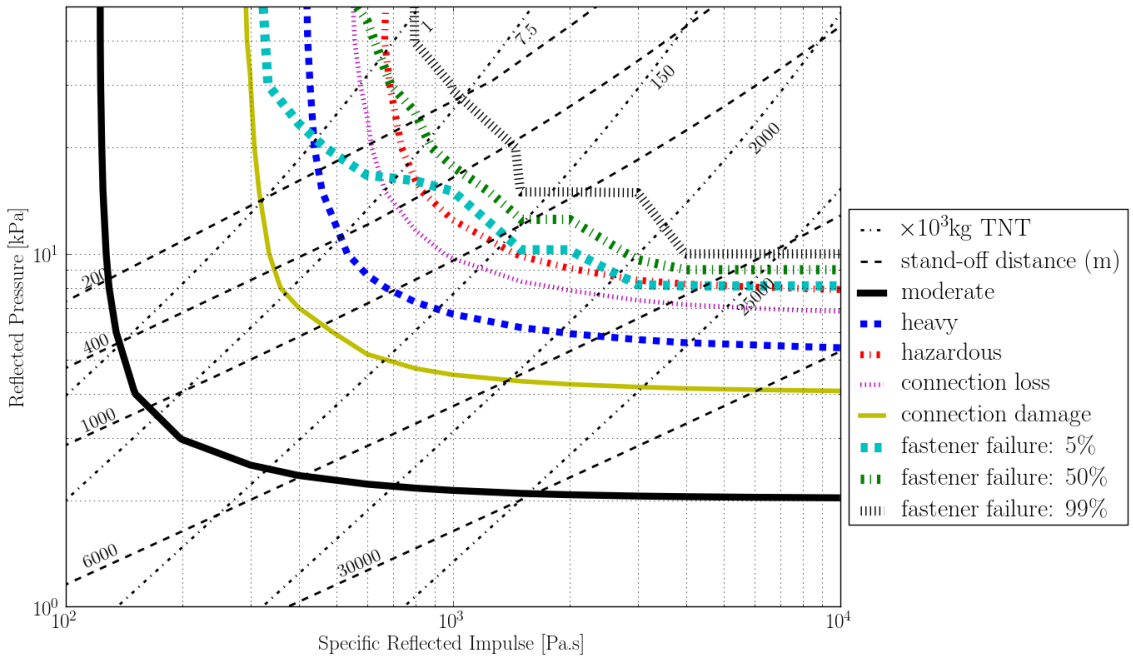

Figure 60: Combined pressure – impulse diagrams

The minimum overpressure values for moderate, heavy and hazardous damage levels for the transverse displacement of the side rail are 2, 5.4 and 8 kPa, respectively. The corresponding values for fastener failure are 8, 9 and 10 kPa. Only two damage levels are available for the connection response of the side rail. The minimum overpressure values in this case for the heavy and hazardous damage levels are 4 and 7 kPa, respectively. Therefore, the connection side rail transverse deformation or the connection damage are the most critical parameter in the response of the sub assemblage in both the impulsive and quasi-static regions. It is worth noting that the design wind pressure for the wall can be as low as 0.5 – 0.6 kPa for this type of structure. The damage of the connection would occur at nearly 7 times the wind pressure. The side rail supporting the cladding system would only sustain 12 times the wind pressure before the hazardous damage level is reached (pull-out failure and loss of components).

Table 28: Limiting values of overpressure and impulse for various damage criteria

P - kPa	Moderate damage		Heavy damage		Hazardous damage	
I - kPa.ms	Impulse	Pressure	Impulse	Pressure	Impulse	Pressure
Side rail	121	2	413	5.4	662	8
Angle connection	-	-	289	4	547	7
Fastener failure (%)	325	8	594	9	800	10

The combined pressure – impulse diagram suggests that for the selected design of warehouse in the current study, the most critical component in the structure is the connection between the side rails and columns, based on the fact that the moderate damage of the side rail transverse deformation is minor. The margin of safety around 12 times the wind pressure. Moreover, the derived iso-damage curves of the overall fastener failure could be fitted and interpolated as necessary for the design and assessment of such structures. The damage levels corresponding to percentage of fastener failure can be change according to design requirements. Most importantly, the study provided in this section provides an in-depth insight into the interaction between the various failure conditions of a representative sub-structure, and the methodology can be applied to similar structures with a wider range of geometries and properties. On this basis, the various failure criteria can be adapted to suit a performance that is consistent with the design objectives of the structure under consideration.

3.3.8 Transfer of seismic design rules to blast resistance

From a general point of view, blast and seismic actions are both dynamic phenomena that induced structural engineers to adapt their seismic knowledge to blast-resistant analysis and/or design scenario, but an adequate seismic design does not necessarily imply adequacy from a blast-resistant design perspective [12] [13].

Aside from the dynamic nature of both types of loads, earthquake ground motion characteristics are markedly different from those of a blast-induced overpressure history: in fact the duration of an unconfined blast pulse from a high-explosive detonation is generally on the order of microseconds to milliseconds with one overpressure peak followed by rapid decay till negative pressure, whereas the strong motion duration of a typical earthquake record is generally on the order of several seconds and can last over a minute with acceleration cycles and multiple peaks.

Furthermore earthquake demand input is kinematic in nature that affects the entire lateral force resisting system by inertial forces accelerating the masses and inducing relative displacements between structural components. On the contrary blast demand input is force-based in nature because an explosion produces shock wave that impinges upon exposed surfaces of nearby structural components, not affecting contemporarily the lateral force resisting system but with time shift and variable magnitude.

One of the main differences between blast and seismic loading from a system response perspective is the area over which the load is distributed: because seismic loads are a secondary effect of base excitation, they effectively engage the entire structure and require system response to resist the forces. The primary effects of external blast are typically localized, affecting isolated areas along the façade and often creating less overall demand than earthquakes.

Other relevant differences between blast and seismic design are the objectives. The main goal for seismic-resistant design is to mitigate overall structural damage and prevent global collapse by limiting inter-story drifts and allowing for controlled and distributed plastic deformations. The key structural variables in seismic design are mass and stiffness distributions. In contrast, blast design focuses on protecting building occupants and critical assets from localized hazards by mitigating primary and secondary debris, preventing failure of various components of the building envelope, and providing continuity between structural elements to prevent disproportionate collapse due to

extreme damage to a localized area of a structure. Exterior building envelope hardening and structural redundancy are generally key variables in blast design.

There are many unique aspects of component-level response that pertain specifically to seismic or blast applications. For instance, strain rates in blast-loaded components can be orders of magnitude higher than those generated during a seismic event. It has been shown through experimental testing, that common construction materials, such as concrete and steel, experience strain-rate-dependent dynamic strength increases beyond certain threshold limits. In practice, these apparent strength increases are typically captured through the use of dynamic increase factors (DIF) applied to nominal yield and/or ultimate material strengths. In general, strain-rate effects tend to increase yield and ultimate strengths while reducing material-level ductility. Stiffness remains largely unaffected by strain-rate effects.

Structural components respond to seismic excitation in a cyclic manner. A properly designed and detailed component will undergo numerous cycles of response without a major reduction in load carrying capacity. For structural components designed specifically for controlled plastic deformation, this sustained fidelity is of utmost importance from both, an energy dissipation and a system-level structural integrity point of view. Because the entire structural system plays a major role in resisting seismic forces, horizontal elements such as diaphragms, collectors, and their connections are just important as of the entire lateral force resisting system and vertical elements.

Blast-loaded structural components undergo a complex response evolution involving early-time local material response followed by "global" component response. These early-time wave propagation effects can lead to material damage such as spall and breach, which can cause locally reduced section capacity and hazardous secondary blast-borne fragments before the entire component is even set in motion. If a blast-loaded component survives the early-time wave propagation effects and is properly designed to resist direct shear forces, it will respond in flexure. Unlike structural response to seismic loads, where cyclic behaviour is expected, response to blast loads typically involves a single, high-demand inbound incursion – rebound can also be important for scenarios involving stiff components, interior detonations, or blast pulses with a significant negative phase – followed by numerous cycles of relatively benign free vibration response. The peak deflection during initial inbound response can be very large depending on the desired performance objective, particularly if flexural hinging and perhaps even membrane response are permitted.

On the other hand, there are also common features: the three primary areas where synergies exist are capacity design, ductile detailing, and design for continuity – all of which are somewhat related in regard to plasticity requirements.

The capacity design methodology focuses on designing connections to allow for structural components to reach their full capacity and deform in a ductile manner up to failure. This precludes connection failure and undesirable component failure modes such as shear or failed elements, thus maintaining structural and local buckling. For example capacity design ensures connections are stronger than their connected structural members by considering for the calculated loads an overstrength factor to ensure indirectly that the elements are connected to develop their full capacity.

In blast-resistant design, efficiently designed members will exceed their elastic capacity during response. Therefore, their connections are commonly designed for the full member capacity and/or the peak calculated reaction.

Ductile detailing, which is intimately related to capacity design, is achieved by designing members to exhibit "ductile" modes of response involving plastic deformations that occur prior to failure and away from connections. This is accomplished through adequate confinement, bracing/stiffening, and overall system connectivity. These are all recommended detailing practices for both seismic and blast design. By designing and detailing for ductility, members and systems

can dissipate energy in a predictable and controlled manner without a premature loss in load carrying capacity.

Adequate connectivity of critical members is also required for most blast-resistant and seismic-resistant design applications. In progressive collapse design (strictly related to blast-resistant design even though thread-independent) a basic concept is to ensure continuity of load- path-critical framing members and floor slabs to allow the structure to bridge over removed or failed elements, thus maintaining structural integrity and preventing collapse of the structure.

From a structural point of view, modern seismic design approaches are based on performance based engineering philosophy as in several international standards [14][15]. They tend to promote global collapse mechanisms and to avoid the formation of local collapse mechanisms by imposing a collapse and resistance hierarchy between brittle and ductile members and mechanisms. In this step the local failure is avoided providing a sufficient resistance capacity, herein intended as both displacement and force.

Blast loads on building structures produce fundamentally different component responses than earthquake shaking [16]: they usually hit only subparts of the building structure such as a façade, some columns, etc, requiring high local resistances that can be sustained also by plastic deformation of members if they have sufficient local ductility. Further, blast loads are mostly characterized in a deterministic way using scenario events, rather than in a probabilistic framework.

3.4 Design Guidance

Throughout the progress of the project it became apparent that it's not possible to have one general guideline for blast resistant that cover all types of blast and structures.

Within the project overview of steel structures and their topology has been performed in WP1. In WP2 detailed analysis of blast scenarios and risk assessment was investigated. Based on the results it became evident that not all blast scenarios can be considered due to the scale of the damage and economy of the possible solution. Also not all structures can be taken into consideration due to their specific cladding system (sandwich panels). Therefore panel such as sandwich are not considered in the project. Finally the complexity of the global model showed that for engineering use the design guide derived from this project has to be based on the most simplified models.

The final deliverable – Design Guide with Examples – shows an overview of existing criteria and models for blast analysis, simplified risk analysis and load assumption, modification of material properties for dynamic load, simplified models to analyse individual components of the structure and their connections. The application of the ADBLAST method is illustrated by an example.

The design guide – which can be used separately – is included as annex to this document.

3.4.1 Design Procedure

Design of the structure consists of different steps. Different parties are involved in each of them specifying requirements for the building shape and behaviour on one hand and responding to them through the adequate design on the other hand.

Figure 61 represents schematically the calculation process of blast loaded structures.

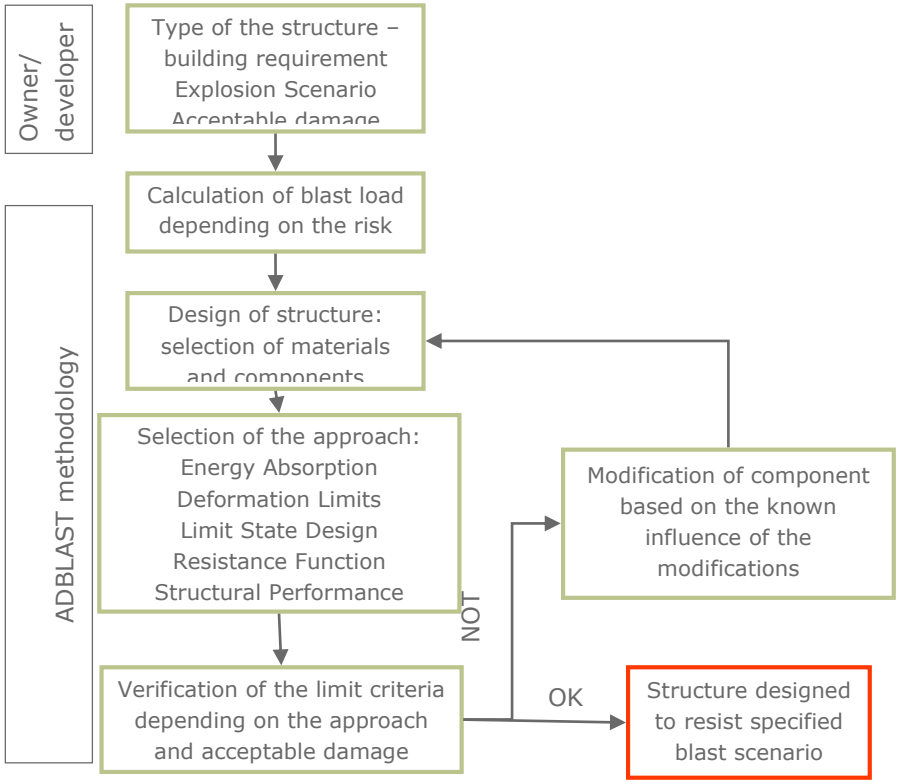

Figure 61: Iterative modification of structure to achieve acceptable load on main structure through modification of secondary elements and failure mode

The main step of concern within ADBLASTADBLAST is the structural analysis of the chosen system.

3.4.2 ADBLAST approach

Design Guide presents three possibilities to predict the dynamic response of members exposed to blast loading:

- Full Analytic Approach
- Semi-Analytic Approach with Design Aids
- Numerical Approach

The first two methodologies are very similar and yield conservative results on the estimation of the maximum required ductility's both for the member and the longitudinal connectors. While the full analytic approach gives more insight on the theoretical background of the new reduced model, the designer can achieve the same results using the semi-analytic approach with design aids.

Only in the case that the designer requires to comprehend the dynamic behaviour over time of the member, then numerical methods are required.

Following the next steps, it is possible to design any structural member against blast. More detailed information on the methodologies and different approaches can be found in the design guide, which is attached to this document.

3.5 Conclusions

Typical industrial facilities and buildings identified with typical structural components (e.g. span length, façade-systems, roof decking configurations, fastening systems etc.). Safety and performance requirements were classified and could be used as benchmark examples for designers.

A framework for an explosion risk analysis could be given, and relevant statistical data for various explosion scenarios were gathered and made available.

Pressure-impulse scenarios were derived in dependence of risk/consequence class and blast source. The respective calculations and values can be used by designers in a general approach.

During different experimental test campaigns, the mechanical behaviour of typical steel façade components such as trapezoidal cladding, cassettes and purlins were investigated under different loading conditions.

First investigations focused on the rotational/deformational capacity of claddings and connectors, as well as in the failure mechanisms of these elements under static loading. After a separate assessment of the local resistance/ductility capabilities of each component, tests followed in substructure assembly. At the same time, explosive tests of a very similar set-up were performed in Brussels in order to investigate a possible transferability between static and dynamic tests.

The comparison of static and explosive tests yielded results which are not easily comparable. It was observed that the failure mechanisms were substantially different between a quasi-static and an impulsive loading situation in the blast tests; this concerned the order of appearance and the localisation of damage in the cladding.

In an impulsive loading situation, the behaviour of the substructure assembly is dominated by both the stiffness and mass ratios of the components (cladding and purlin), whereas in the quasi-static loading situation only the stiffness ratio of the components influence the response. Commonly, the mass and stiffness properties of the cladding and the purlins are in a similar range, so that complex dynamic interaction occurs between cladding and purlin.

The structural response in an impulsive situation is characterised by the kinetic energy input into the system, which accelerates both the cladding and the substructure element in such a manner, that very strong detachment forces in the connectors between cladding and substructure element appear. These forces do not appear in a quasi-static loading situation. Additionally, the energy dissipation mechanisms in the case of an impulsive load are different than in the quasi-static loading situation. It could be observed that a considerable amount of the explosive energy applied to the system is rapidly dissipated by a generalised formation of local buckles in the trapezoidal cladding. This local dissipation phenomenon is to be seen positively with regard to the performance characteristics of the claddings but can hardly be taken into account by quasi-static approaches.

Additionally to the experimental investigations, analytical models and a simplified design approach were developed for the design with steel components, which are characterised by their high ductility compared to high-mass solutions. Special focus for the development of the simplified model was put on the consideration of membrane load bearing behaviour, which is of decisive influence when admitting large ductility levels (as it can be assumed with steel components) and on the consideration of longitudinal connector resistance (as a limiting magnitude for the development of membrane forces).

This simplified model was used for the development of a design concept which includes both membrane effects and connector failure. According to this design concept, diagram aids were generated for the derived pressure-impulse scenarios according to the different risk classes and evaluated for common cladding systems chosen at the first stage of the project.

The results let to a design guide which allow designers to use the developed methods and examples for practical use.

3.6 Exploitation and impact of the research results

3.6.1 Applications and technical potential use of results

A framework for risk assessment of industrial buildings in certain scenarios was introduced and allows for an insight in derivation of safety and performance requirements.

The design procedure developed within ADBLASTADBLAST allows structural engineers to design blast loaded steel structures in a comprehensive, economical and safe-sided way.

3.6.2 Publications

Elghazouli, A.Y., Malaga-Chuquitaype, C., Liu, Y. and Eder, M. "Ultimate behaviour of cladding assemblages in industrial buildings." Eurosteel 2014, Naples.

Colomer Segura, C.; Feldmann, Markus (2014): A New Model Reduction Technique to Predict the Effects of Blast Loading on Structures. In: EURODYN'2014 - 9th European Conference on Structural Dynamics. EURODYN 2014. Lisbon.

Colomer Segura, C.; Feldmann, Markus (2014): A New Simplified Design Method for Steel Structures under Impulsive Loading. In: WIT-Press (Hg.): WIT Transactions on the Built Environment, Bd. 141. Wessex. Wessex Institute.

Colomer Segura, C.; Feldmann, Markus (2013): Modelling Nonlinear Material Behaviour for arbitrary Cross-Section Geometries with a two dimensional Geometrically Exact Beam Model. In: International Conference on Vibration Problems. Lisbon, Portugal, 9 - 12 September 2013.

Castiglioni, CA, Nardini L, Salvatore W. 2011. *Protezione dalle esplosioni di edifici industriali in acciaio: il progetto di ricerca 'ADBLAST'*. Atti del XXIII Congresso C.T.A. Giornate Italiane della Costruzione in Acciaio, Ischia - Napoli, 9-12 ottobre 2011 (in Italian)

3.6.3 Dissemination of results

The results and the achieved simplified design approach is published within the ADBLAST final report, which makes it possible for the community to download the final report via bookshop.eu.

4 List of abbreviations

Chapter 3.3.2:

λ	occurrence rate [1/a]
λ_H	occurrence rate of an explosion
P	probability
$P(F)$	annual failure probability
$P(H)$	actual failure probability
D	damage given an event that has occurred
C	related costs
C_o	initial costs
r	real annual discount ratio
i	year
$Risk_i$	risk related to year i
CC	consequence class
N_d	number of fatalities
p_d	design pressure
p	free air overpressure [kPa]

Chapter 3.3.5:

t_c	critical time

Chapter 3.3.6:

$R_E(x)$	force-displacement relation of an equivalent spring
K_R	rotational spring
K_L	longitudinal spring
K_E	vertical spring
K_H	horizontal spring
K_{GNL}	virtual spring
K_{Stif}	stiffness ratio
K_{res}	resistance ratio
$\Phi(s,t)$	deformation
w	vertical deflection
u	horizontal deflection

p_{peak}	peak overpressure
p_{free}	calculated free air pressure [kPa]
p_{fac}	maximum pressure on the façade
E	energy [GJ]
E_{eff}	effective energy [GJ]
R	distance [m]
I	impulse [Pas]
I_{free}	computed impulse by the computer program ConWep
I_{fac}	total impulse
t	time [ms]
Δt	duration [ms, s]
V	coefficient of variation
$f_R(r)$	probability of R
β	target reliability index

Chapter 3.3.4:

HS	high speed
MS	medium speed
SS	slow speed
TS	trapezoidal sheet
BS	blank sheet
ST	self-tapping screw
LL	Load line
SL	Sensors line
FL	Fixing line
R	Rib
V	Valley
σ	tension
θy	"yielding point"
θu	"ultimate (lower)" load value

w_{el}	deformation for which yielding occurs
L	length
$E_{\varepsilon,S}$	membrane strain energy
k_s	axial beam stiffness
k_L	longitudinal stiffness
k_H	membrane stiffness
k_V	bending stiffness
$k_{GNL,R}$	equivalent beam stiffness left, right, respectively
$_{eq}$	equivalent
k_{HLon}	adimensional longitudinal stiffness
F_H	membrane force
F_V	vertical Force
F_{Vm}	total vertical resistance related to membrane action
λ	membrane force ratio
μ	ductility ratio
$\mu_{Lat,1,2}$	achieved ductility for the left, right connectors, respectively
η	effective force ratio
E^*	maximum energy absorption capacity
LD	local connector damage
SD	severe connector damage
TD	total connector damage

Chapter 3.3.7:

P	peak overpressure
t_d	duration
I	specific impulse
L	Length of the component
δ	vertical deflection
δ_m	deflection at mid-span
δ_e	deflection at yielding
θ	end rotational angle
μ	ductility ratio

5 List of figures

6 List of tables

7 References

[1] Eurocode EN 1991-1-7 on Accidental design situations.

[2] Eurocode EN 1990 Basis of Design

[3] P.A.M. Uijt de Haag, B.J.M. Ale, Guidelines for quantitative risk assessment, PGS3, "Purple Book", The Hague 1999

[4] C.J.H. van den Bosch, R.A.P.M. Weterings, Methods for the calculation of physical effects – due to releases of hazardous materials (liquids and gases), PGS2, "Yellow Book", The Hague 1996

[5] P.D. Smith and J.G. Hetherington, Blast and Ballistic Loading of Structures, CRC Press, 1994

[6] Soroushian, P. and Choi, K. (1987) Steel mechanical properties at different strain rates. Journal of Structural Engineering, ASCE, 113(4) 663-673.

[7] CEB (1988), Structures under impact and impulsive loading, Bulletin d'Information No 187, Comite Euro-International de Beton, CEB

[8] Bodner, S.R. and Symonds, P.S. (1960) Plastic deformations in impact and impulsive loading of beams. Proceedings of the Second Symposium on Naval Structural Mechanics, Rhode Island, USA, 488-500.

[9] United States of America, Department of Defense, UFC 3-340-02: United Facilities Criteria: Structures to Resist the Effects of Accidental Explosions, 2008

[10] Fire and Blast Information Group (FABIG), *Simplified methods for analysis of* response to dynamic loading, Ascot: Steel Construction Institute, 2002.

[11] Norsok, N-004: Design of Steel Structures, Oslo, 2013

[12] Sanmarco, EL, Jones, CA, Williamson, EB, Sprague, HO: Design for Blast and Seismic. Structure magazine, March 2014.

[13] Hinman, E. 2011. Blast Safety of the Building Envelope. Whole Building Design Guide, http://www.wbdg.org/resources/env_blast.php.

[14] CEN, European Committee for Standardization. 2005. EN 1998-1. Eurocode 8: Design of structures for earthquake resistance. Part 1: General rules, seismic actions and rules for buildings. European Community, Brussels, Belgium.

[15] Federal Emergency Management Agency (FEMA), 2003. NEHRP Recommended Provisions and Commentary for Seismic Regulations for New Buildings and Other Structures. FEMA Report 450.

[16] Mays, G.C., Smith, P.D. 1995. Blast effects on buildings. Thomas Teldford, London.

[17] ABAQUS. ABAQUS Theory Manual, Version 6.7, Hibbit, Karlson and Soresen Inc., 2003

[18] MATLAB 7.3 Getting Started Guide, The MatchWorks Inc. USA, 2006

[19] Colomer Segura, C.; Feldmann, Markus (2013): Modelling Nonlinear Material Behaviour for arbitrary Cross-Section Geometries with a two dimensional Geometrically Exact Beam Model. In: International Conference on Vibration Problems. Lisbon, Portugal, 9 - 12 September 2013.

[20] Colomer Segura, C.; Feldmann, Markus (2014): A New Simplified Design Method for Steel Structures under Impulsive Loading. In: WIT-Press (Hg.): WIT Transactions on the Built Environment, Bd. 141. Wessex. Wessex Institute.

[21] Colomer Segura, C.; Feldmann, Markus (2014): A New Model Reduction Technique to Predict the Effects of Blast Loading on Structures. In: EURODYN'2014 - 9th European Conference on Structural Dynamics. EURODYN 2014. Lisbon.

[22] J. M. Biggs, Introduction to structural dynamics, New York: McGraw-Hill, 1964

[23] C. H. Norris, R. J. Hansen, M. J. Holley, J. M. Biggs, S. Namyet und J. K. Minami, Structural Design for Dynamic Loads, New York: McGraw-Hill, 1959.

Research Fund for Coal & Steel

RFCS Project ADBLAST
RFSR-CT-2010-00030

Design Guide

Advanced Design Methods for Blast Loaded Structures

UNIVERSITÀ DI PISA

ArcelorMittal

Photo: Nigel Cox

This page is intentionally left blank

Contents

1 Summary

Steel structures and components can provide ideal systems for blast resistance, yet this potential has not been adequately utilised due to lack of appropriate investigations. The work performed in this project involved realistic blast tests on key non-structural and structural assemblages, coupled with complementary dynamic material characterisation, nonlinear analyses and comparative quasi-static tests. Findings from the experimental and numerical studies used in conjunction with appropriately assessed loading scenarios and carefully selected structural configurations are exploited to define reliable performance based design procedures.

This project aim was to develop fundamental design guidance for blast resistant steel structures, with emphasis on procedures suitable for typical industrial buildings. Overview of steel structures and their topology has been performed and detailed analysis of blast scenarios and risk assessment was investigated. Background information about these topics can be found in the deliverables to the project ADBLAST.

Throughout the progress of the project it became apparent that it’s not possible to have one general guideline for blast resistant that cover all types of blast and structures.

Based on the results it became evident that not all blast scenarios can be considered due to the scale of the damage and economy of the possible solution. Also not all structures can be taken into consideration due to their specific cladding system (sandwich panels).

2 Risk Assessment and Load scenarios

Based on the considered blast scenario, safety requirements are defined either by owner or by authority. Furthermore, performance requirements are specified describing how a blast affected building or facility has to perform in order to fulfil the safety requirements. The Table A 1 below summarizes typical safety and performance requirements collected from past projects.

Table A 1: Safety requirements for explosion scenarios

Explosion Scenario	Safety Requirement	Performance Requirement	Typical Structure	ADBLAST
1 Internal Explosion	A No collapse of the building Prevention of secondary explosions No domino effects No damages outside the building Investment protection	Structural stability of the structure Moderate damage of the structure **Ventilation through failure of defined area in roof or cladding** (or assembly of special products like pressure release openings)	Standard steel structures and cladding / roofing systems	Partly Considered
	B See A Prevention of pollution release	Integrity of structure and cladding	Concrete structures	Not considered
2 External Explosion	A No collapse of the building No domino effects Investment protection	Structural stability of the structure Moderate damage of the structure Pressure reduction through defined failure of cladding	Standard steel structures and cladding / roofing systems	Considered
	B See A Prevention of pollution release Protection of humans Protection of process control systems	Integrity of structure and cladding Moderate damage of structure and cladding	Small Blast Wave Standard steel structures and cladding / roofing systems	Considered
			Large Blast Wave Concrete Structure Double-wall system	Not considered

In general, regardless of whether an internal or external blast scenario is considered, the classification of performance requirements should be dependent on the defined safety requirement and the probability of occurrence.

A scenario refers to a set of site related physical main characteristics and corresponding events like the type and amount of possible explosive material, the release process, ignition, the resulting pressure waves and temperatures, etcetera. All aspects of such a scenario involve a degree of scatter and uncertainty, starting from the probability that in the period under consideration an exposure occurs at all. But in general also items like the amount (mass) of explosive material, time and location of the explosion, the turbulence inside a vapour cloud or the resistance of the structure will remain unknown to the designer. The best thing one can do is to estimate likelihood's

and make best guesses, depending on the specific circumstances. Given those models one may strive for an optimal design where costs of mitigating measures are in balance with risk reduction.

The main elements for a Quantitative Risk Assessment (QRA) are given by:

- The available type and amount of possible explosive material;
- The possible release and ignition processes;
- The development of the explosion;
- The location of the source in relation to the building;
- The resulting pressures on the structure
- The structural response analysis
- The estimation of the damage and casualties

For the design purpose it is convenient to translate the (free) pressure diagram to a triangle having a **peak load value p** and **duration** Δ, as indicated in Figure A 1. Alternatively, the pressure and impulse values may be presented. In the case of a triangle it is simply:

$$I = 0.5 \cdot p \cdot \Delta \; [Pa \cdot s] \tag{1}$$

This representation will be later referred to as ***PI*** (pressure/impulse values).

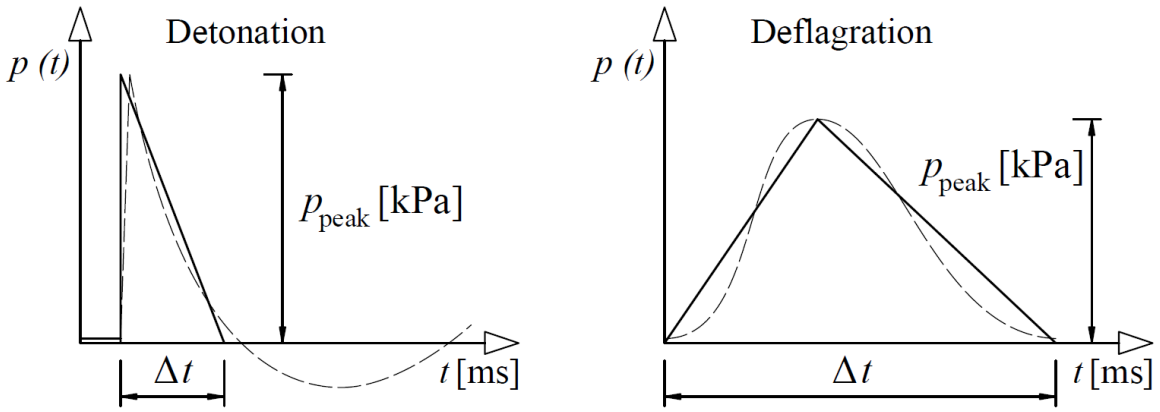

Figure A 1: Triangular pressure-time models

Elaborating all possible scenarios for a specific building – including relevant parameters like the distance to roads, pipelines and other buildings on the plant – may be time-consuming and is not practical for many low-risk industrial buildings. The suggestion is to provide more general and more detailed models and information, depending on the probability of explosion and the consequences of the explosion as shown in Table A 2.

Table A 2: Example of general models depending on consequence class (cc) and type of activity

Probability of explosion	CC1	CC2	CC3
-single source	Design pressure	Design pressure	Model to determine the pressure
-industrial area	Design pressure	Design pressure	Risk Analysis

For different types of explosives and distance to the building different PI values have been obtained. Depending on the risk category of the buildings different PI values have been defined for design of the building to resist blast as shown in Table A 3.

Table A 3: The design pressure for different categories of risk

		Single source			Industrial plants		
	Unit	CC1	CC2	CC3	CC1	CC2	CC3
p_d	[kPa]	0	5	To be calculated	20	50	Risk Analysis
I_d	[Pas]	0	160		600	1600	
Δt_d	[ms]	0	64		64	64	

The consequences classes CC1, CC2 and CC3 refer to low, medium and high consequences as defined in the Eurocode EN 1990 Basis of Design (or EN 1991-1-7, Accidental actions) and further described in the corresponding National Annexes for every individual country. Consequences may refer to both economic damage as well as to possible casualties. For some buildings the consequences may be confined to the building itself, for other structures the loss of function may have more consequences.

For the various cased we have the following conclusions:

CC1 structures, single explosion source:

From Table A 3 is can be concluded that in the case of very low consequences due to failure (that is CC1) and only a single explosion load in the neighbourhood, no specific design verification is required.

CC2 and CC1 structures on plant

For CC2, and also for CC1 in the case of a set of sources or plant (see Figure A 2) , the Table A 3 gives design values for the pressure (in kPa) and the duration (in ms). For calculations based on pressure and impuls the corresponding design value for the impulse (in Pa·s) is given, according to formula (1). These values can be used in the calculation method in Chapter 6 as follows:

Figure A 2: Example of industrial plant (Pernis, The Netherlands, source: Google Earth)

CC3 structures

For CC3 Table A 3 suggests a more refined approach, both for the single source as for the industrial plant. For the single source no specific analysis of the consequences is recommended. It is sufficient to base the design pressure on the standard annual reliability target β=5.2 as

defined in the Eurocode. For the plant case, on the other hand, it is recommended to make an estimate of the consequences and derive a target reliability thereof. If human safety is the dominant issue, a minimum reliability should follow from a maximal accepted individual risk of say 10^{-6} per year. This criterion, however, may be different per country. Other criteria like Social Risk or Economic Optimum may give rise to stronger requirements, where relevant.

We will confine the discussion here to the case where the prescribed Eurocode reliability index β_t = 5.2 is considered as sufficient and show how to arrive at design values for pressure and duration. Note that the procedure summarised here has been used to derive the other design values in the Table A 3 and can be used for the CC3/plant case as soon as the target has been set.

According to the Eurocode EN 1990, the design value for a random load or pressure can be formulated as:

$$p_d = \mu(p) + \alpha \cdot \beta_t \cdot \sigma(p) \qquad (2)$$

This formula holds for normally distributed variables; $\mu(p)$ stands for the mean, $\sigma(p)$ for the standard deviation, βt for the target beta and α for the influence coefficient. In this case α=1 as an explosion load is very dominant. Note further that the explosion load is believed to be lognormal distributed rather than normal. So in actual application this formula becomes more complicated, as can be seen in the WP2 report.

The target reliability, β_t may be less than the 5.2 value specified above, as we may correct for the fact that an accidental load has a limited probability of occurrence. The probability of occurrence for a number of examples have been derived in the WP2-report using event tree analysis and numerical values based on Dutch data. An example of such a tree is presented in Figure A 3. The probability of an accidental explosion somewhere will depend on the plant area A and the type of activities. In the Netherlands there is a major explosion about once per 10 years. Assuming about 100 relevant industrial areas this leads to λ = 0.001/a for an industry park. If we assume on average about 100 installations in one industrial area this leads to λ = 1E-5/a for an installation. This is in the order of magnitude of most cases in Table A 4. We will use 3E-6/a for an installation and 3E-4/a for a plant.

Table A 4: Explosion parameters (selected examples)

1	2	3	4	5	6	7	8	9	10
	E_{eff} [kg TNT]	E_{eff} [GJ]	R [m]	p_{free} [kPa]	Δt [ms]	I_{free} [Pas]	p_{fac} [kPa]	I_{fac} [Pas]	λ [1/a]
underground LPG tank	160	0.8	10	340	11	800	1364	786	2E-6
	160	0.8	100	6,7	32	90	13.8	170	
	160	0.8	200	2,4	39	40	4.9	76	
road tanker pumping	12700	63.5	10	6000	6	4000	52500	69900	5E-7
	12700	63.5	100	60	80	1600	139	3500	
	12700	63.5	500	6	140	340	11	620	
ethanol vessel with protective outer shell	260	1.3	10	500	13	1100	2200	3100	4E-5
	260	1.3	100	8	35	130	17	234	
	260	1.3	250	2	45	50	4.8	89	
propane vessel	200	1	10	400	12	900	1670	2500	1 E-6
	200	1	100	7	33	100	15	195	
	200	1	200	2,4	41	46	4.8	81	
	3000	15	10	2400	10	2600	16900	17000	3E-7
	3000	15	100	20	60	550	49	1080	
	3000	15	500	2	90	110	5.2	200	

Finally, the façade pressure *p* [kPa] itself depends on the amount of available energy E [GJ] at the explosion and the distance R [m] from source to building. Available calculation models are the Multi Energy, CFD or TNT equivalent. In this project the latter has been used via the computer program ConWep. Given estimated means and other statistics for the variables *E*, *R* and a model uncertainty θ, we may derive the mean and standard deviation of *p* using a Monte Carlo Simulation.

In a similar way design values for the impulse I and the duration Δ have been derived.

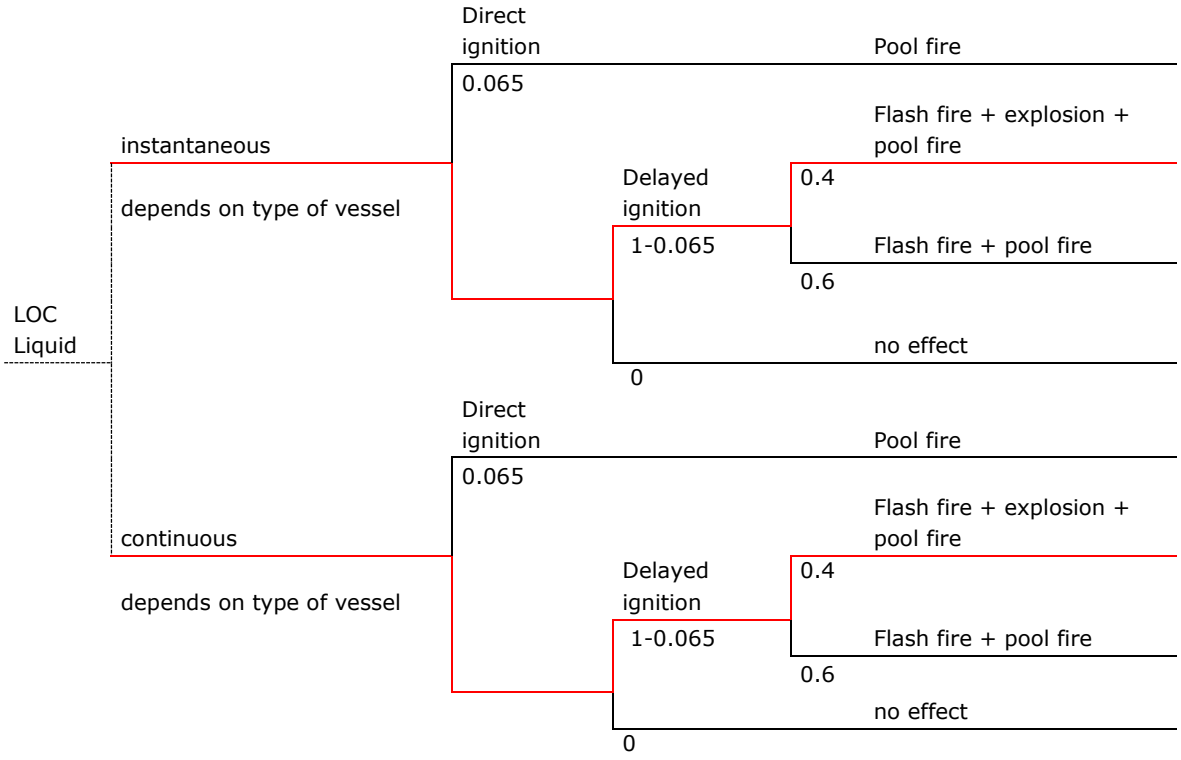

Event tree 4 – LOC from atmospheric flammable fluid tank

Figure A 3: Failure trees for a chemical plant with stationary atmospheric vessels containing solvents, e.g. ethanol. The LOC (Loss of Containment, initial event) probability for an instantaneous release of a single containment tank is 5 10 $^{-6}$ per year

3 Material Properties under dynamic loading

Under high-speed dynamic conditions such as blast loading, the material experiences high rates of strain increments that may have notable effects on the corresponding stress-strain relationships. These effects include a significant increase in the material yield strength and a less pronounced increase in the ultimate strength. On the other hand, the modulus of elasticity of steel is remains largely insensitive to the loading rate, and the same typically applies to its elongation at failure.

The factor by which the dynamic stress increases in comparison with its static value is conventionally referred to as the Dynamic Increase Factor (DIF). Figure A 4 below shows the DIF obtained as part of the ADBLAST project for the yield strength and maximum strength on typical cladding profiles (i.e. TR35 and TR84 shown in Figure A 5 and Figure A 6 respectively). Figure A 4 also depicts three of the commonly used models which are employed to characterise the influence of strain-rate effects on the material properties [7-9]. On the basis of this comparison, the CEB [7] model appears to be the most appropriate for obtaining an estimate of the DIF under blast loading situations.

The formulation of the CEB [7] model is expressed in terms of the material Dynamic Over-strength (O) in MPa as follows:

$$O = c \cdot \ln(\dot{\varepsilon}/\varepsilon_S) \tag{3}$$

Where $\dot{\varepsilon}$ and ε_S are the strain rate and static strain, respectively. The value of the constant c is recommended as 6. It is important to note that this level of dynamic-increase relates to the actual material stress level and any difference between the nominal and actual strength should be accounted for by means of static over-strength factors such as those defined by seismic design codes (e.g. γ_{ov}).

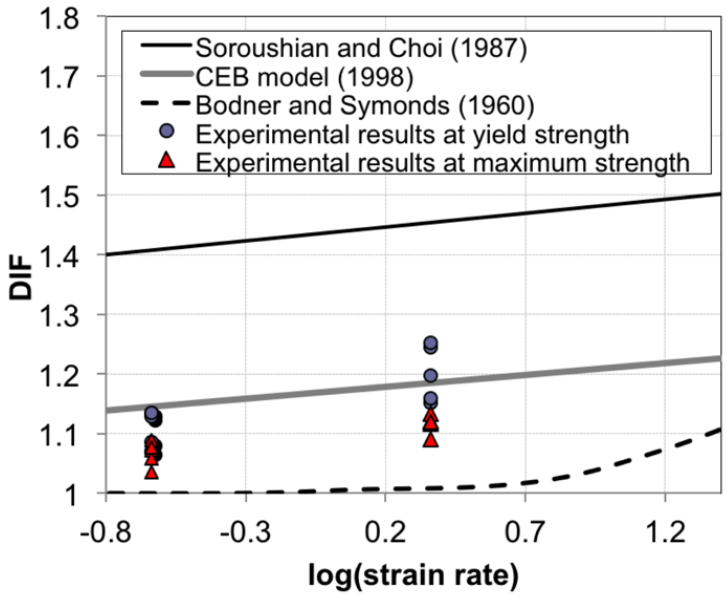

Figure A 4: Dynamic Increase Factor from tests conducted on TR35 and TR84 cladding

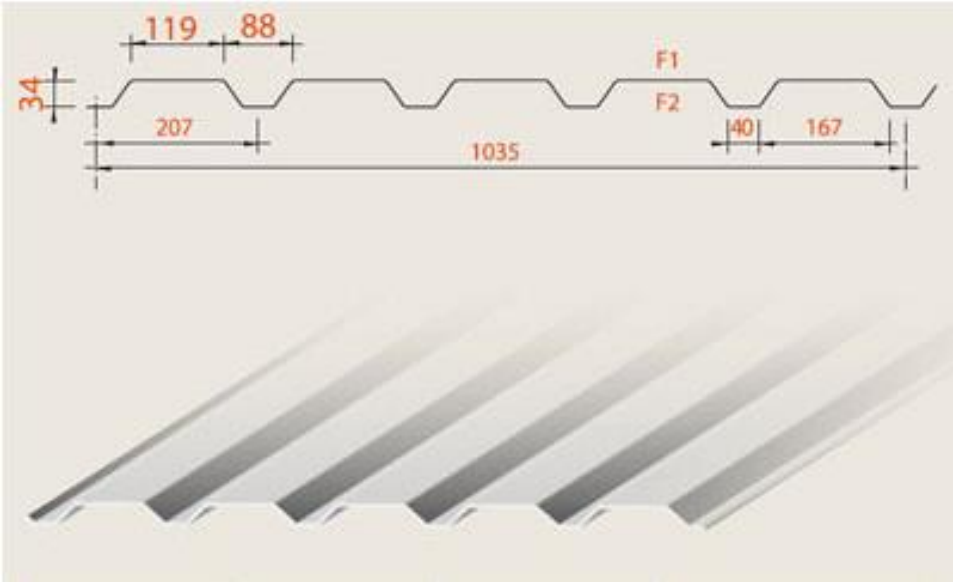

Figure A 5: Façade trapezoidal cladding Hacierba 35/207 (TR35)

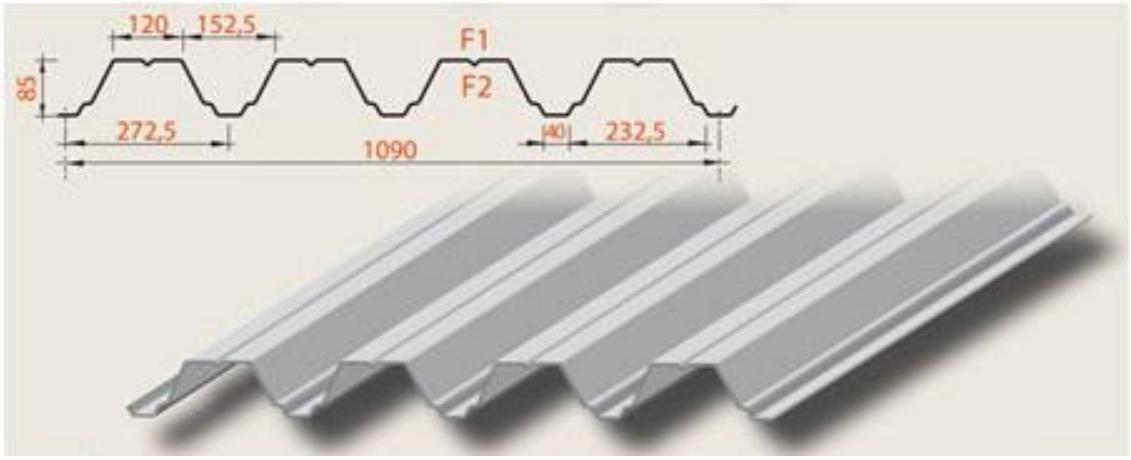

Figure A 6: Roof trapezoidal cladding Hacierco 84/273 (TR84)

4 Deformation criteria

4.1 Rotational Capacity

Due to the high loadings provided by the explosion loads, usually plastic resistance is assumed to verify the structural integrity. However, if plastic hinges are to be exploited the connections between cladding to substructure and substructure to main structure have to be checked in regard to their strength and rotational capacity.

4.1.1 EN 1993-1-8

Welded connections

For column to beam connections, where the web of the column is stiffened in compression but not in tension, the rotation capacity φ_{Cd} may be assumed to be not less then:

$$\varphi_{Cd} = 0.025 \cdot {}^{h_c}/_{h_b} \quad (4)$$

where:

- h_b is the depth of the beam;
- h_c is the depth of the column.

(provided its design moment resistance is not governed by the design shear resistance of the column web panel).

An un-stiffened welded beam-to-column joint designed in conformity with the code may be assumed to have a rotation capacity φ_{Cd} of at least 0,015 radians.

Bolted connections

Sufficient rotation capacity is assumed for connections with either a bolted end-plate or an angle flange cleat connection, if two conditions are fulfilled:

1. the design moment resistance of the joint is governed by the design resistance of either:
    a. the column flange in bending or
    b. the beam end-plate or tension flange cleat in bending.

2. the thickness t of either the column flange or the beam end-plate or tension flange cleat (not necessarily the same basic component as in (a)) satisfies:
   $t \leq 0.36 \cdot d \cdot \sqrt{f_{ub}/f_y}$
   where f_y is the yield strength of the relevant basic component.

A beam-to-column joint in which the design moment resistance of the joint $M_{j,Rd}$ is governed by the design resistance of the column web panel in shear, may be assumed to have adequate rotation capacity for plastic global analysis, provided that $d/t_w \leq 69\varepsilon$.

A joint with a bolted connection in which the design moment resistance $M_{j,Rd}$ is governed by the design resistance of its bolts in shear, should not be assumed to have sufficient rotation capacity for plastic global analysis.

4.1.2 Norsok Standard (2004)

The Norsok standard refers to recognised codes for calculating the capacity of connections.

If the axial strength of the connection is exceeded, the connection shall be assumed to be disconnected. Post-collapse strength may be taken into account, if data is available.

No limits for rotational capacity are defined.

4.1.3 UFC (2008)

UFC gives recommendations for deformation criteria to comply with (Table A 5):

Table A 5: Deformation criteria acc. UFC

Element	Level of Protection	Additional Specifications	Maximum Rotation
Beams, purlins	1		2°
	2		12°
Frame Member	1		2°
Cold-formed steel floor and wall panels	1	Without membrane action	1.25°
		With membrane action	4°

4.1.4 ADBLAST

On the basis of cladding-purlin-column sub-structure tests performed as part of the ADBLAST project, a maximum rotational capacity of around Θ=5° can be adopted for the purlin-to-column connection before failure.

Tests performed within the ADBLAST project suggest that for the cold-formed sub-structure panels a minimum rotational capacity approaching Θ=6° under consideration of membrane action is possible, if the failure of the fasteners can be excluded.

4.2 Ductility Limits

With ductility limits the maximum allowable deformation in a beam or column is defined. It is usually specified with the ductility ratio μ, where

$$\mu = w_{max}/w_{el} \quad (5)$$

w_{max}: maximum deformation

w_{el}: elastic deformation

4.2.1 Norsok Standard (2004)

In the Norsok standard the ductility limits are given in dependence of the boundary conditions, the applied load distribution and the cross-section classification of the member.

Table A 6: Ductility ratios μ values – beams with no axial restraint acc. to NORSOK standard N-004 – Table A.6-3

Boundary conditions	Load	Cross-section category		
		Class 1	Class 2	Class 3
Cantilevered	Concentrated	6	4	2
	Distributed	7	5	2
Pinned	Concentrated	6	4	2
	Distributed	12	8	3
Fixed	Concentrated	6	4	2
	Distributed	4	3	2

4.2.2 UFC (2008)

UFC distinguishes the requirements depending on the member function.

Table A 7: μ-values acc. to UFC

Element	Level of Protection	Additional Specifications	Maximum Deflection
Beams, purlins	1		10
	2		20
Frame Member	1	Relative side way deflection between stories	H/25
Cold-formed steel floor and wall panels	1	Without membrane action	1.75
		With membrane action	6

4.2.3 ADBLAST

On the basis of cladding-purlin-column sub-structure tests performed as part of the ADBLAST project, a value of μ=2.5 is suggested as an estimate of ductility for systems employing channel section purlins and TR35 or TR84 steel sheeting if the failure of the cold-formed panels controls the ultimate response. Alternatively, if ductile purlin-to-column connection governs the ultimate response of the system a value of μ=3.3 can be adopted. It should be noted however that the above values of ductility adopt an effective yield level definition based on a bilinear representation of the load-deformation response. If, alternatively, the ductility ratio is based on first structural yield, then values exceeding μ=6 could be employed as suggested in the UFC recommendations.

5 Design Procedure

Design of the structure to resist blast load according to the defined risk class, consists of different steps. Different persons are involved in each of them specifying requirements for the building shape and behaviour on one hand and responding to them through the adequate design on the other hand.

Figure A 7 represents graphically calculation process of blast loaded structures.

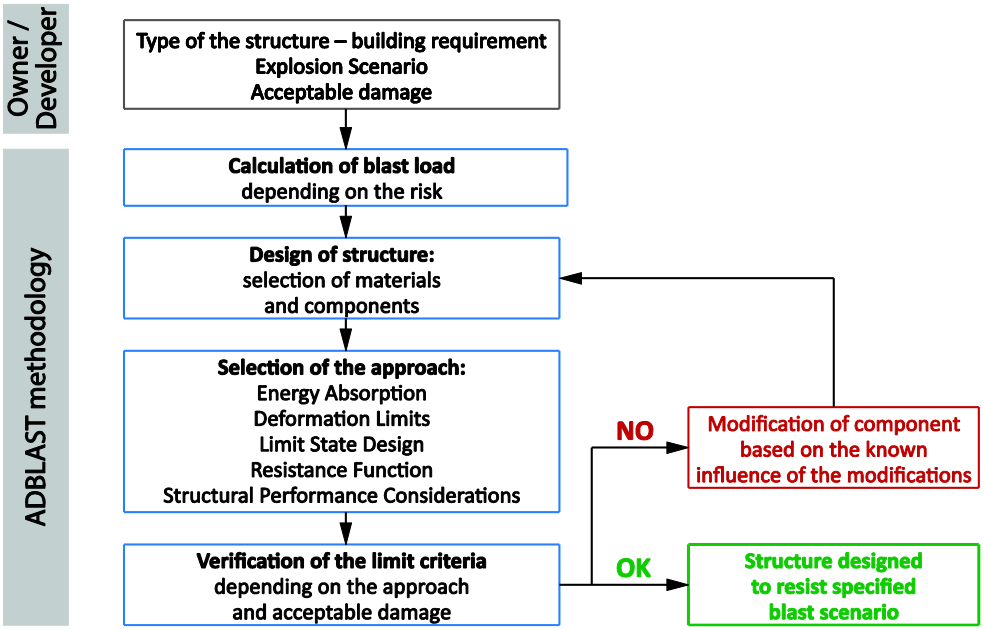

Figure A 7: Iterative modification of structure to achieve acceptable load on main structure through modification of secondary elements and failure mode

The main step of concern within ADBLAST is the structural analysis of the chosen system. In the following chapter, an overview is given about possible approaches.

5.1 Approaches for Structural Analysis

5.1.1 Energy Absorption

The requirement for a remaining structural capacity leads to a high strength, but ductile structure. The ductile behaviour or the ability to undergo very large deformations and rotations can be quantified by an energy absorption approach.

The absorbed strain energy, characterised by the area under a load-deflection diagram, depends on the structural dimensions, material and stiffness of the member and the connections.

This approach is suitable to characterise the overall behaviour of a structure in a very general way.

Equating the maximum possible work to the strain energy to obtain quasi-static asymptote, equating the kinetic energy to the strain energy to obtain the impulsive loading realm asymptote:

1. Assumption of deformed shape
2. Differentiation of the deformed shape to obtain strains
3. Substitution of strains into appropriate relationship for energy per unit volume
4. Integration of strain energy per unit volume over volume of structural element to obtain the total strain energy
5. Computation of kinetic energy by substituting into $I^2/(2m)$
6. Computing the maximum possible work by integrating over the loaded area for the pressure times the deflections
7. Obtaining the deformation in the impulsive loading realm by equating kinetic energy to strain energy
8. Obtain the deformation in the impulsive loading realm by work to strain energy
9. Substitution of deformation into strain equation to obtain strains

5.1.2 Deformation limits

This approach is related to the energy absorption approach: strain energy demands are compared with the strain energy absorption capacity of the structure. The deformation values allow here for a quantification of possible energy absorption. Large deformations, including high strains are desirable for a ductile structural resistance.

The Limits depend on the type of structure, material, surrounding and the desired safety level. The allowable response of a frame component is less than for an individual member. This is to avoid progressive collapse. However, the integrity of connections has to be secured in order to achieve member deformations.

5.1.3 Limit State Design

Allow for prediction of failure mechanisms and structural capacities.

"Each of the limit state design specifications contains special provisions for high seismic conditions, which are commonly used for blast resistant design. These provisions are intended to protect against non-ductile failure modes, such as buckling or premature crushing of brittle materials, through use of special detailing and design requirements."

5.1.4 Resistance Functions

To derive resistance functions, the plastic capacity of a structure needs to be identified. This is done by calculating the plastic moment or shear capacity in virtual hinges. Following up a possible collapse mechanism, the maximum collapse load can be calculated. This approach is similar to the static plastic hinge method.

5.1.5 Structural Performance Considerations

In this approach limit values for deflections, storey drifts and damage tolerances are defined.

6 Design Process ADBLAST

6.1 Introduction

Within the scope of the ADBLAST Project, a new approach to dynamic system reduction has been presented. The proposed methodology reduces an axially and rotationally arbitrary supported beam to a 2DOF system consisting of a mass and 4 springs as presented in Figure A 8.

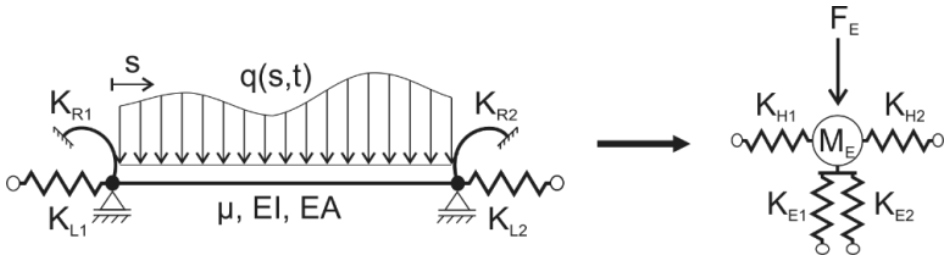

Figure A 8: Member Reduction to a mass supported by four springs

The new reduction concept is designed to explicitly address geometrical nonlinearities by means of two longitudinal springs with a nonlinear strain definition. This approach offers the possibility to explicitly model and calculate the connector forces in the system, which is a major advance in order to predict the dynamic response of structures by simplified models (Figure A 9)

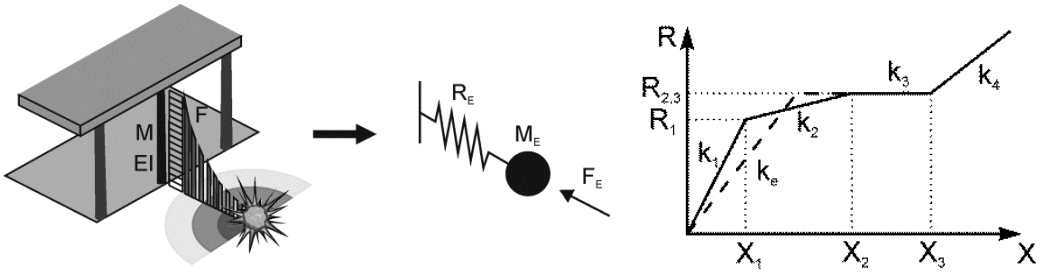

Figure A 9: Conceptual system reduction of a column, example of a non-linear resistance curve

Extensive investigations show the very similar energetic behavior of the reduced and the original system, even in the elastic domain, where most classical approaches do not consider any membrane action.

Another great advantage offered by the presented methodology is the possibility to address arbitrary loading conditions in an arbitrary supported beam. Present simplification approaches could only deal with symmetrical uniformly distributed loading conditions.

Classical approaches become more and more complex when trying to deal with geometrical non-linearities. The definition of complex load-deformation spring characteristics is interesting only if a numerical solution is searched. In general, this segmented load-deformation curves have two great disadvantages:

- They do not allow for an analytical solution of the problem. The integral expression of the dissipated energy $\int_0^{x(t_{\dot{x}=0})} R(x) \cdot dx$ becomes more and more complex and needs to be evaluated numerically.
- They do not allow for the creation of normalized response diagrams.

The new ADBLAST approach overcomes these two disadvantages and even opens a new way for the Finite Element analysis of complex structures.

In the calculation of the response of blast loaded structures, there is a large separation between complex FE calculations and the use of simplified models. The main disadvantage of classical reduction techniques is the fact that they cannot be integrated to more complex FE systems, so that the analysis remains for one isolated member. This limitation is mainly due to the fact that they would only offer one connection node to the rest of the FE system, thus not being able to separate membrane effects from bending effects or asymmetrical support action. The new approach overcomes this limitation by offering 4 connection nodes that separately consider the effects of bending and membrane action for both for the left and right support. An implementation of an "equivalent beam" element in a FE system is possible and is opened for the design engineer with deeper computational knowledge.

6.2 Dynamic Reduction: ADBLAST approach

A key aspect of the new methodology consisted in the fully decoupling of bending and membrane effects within the reduced model.

This means that the approach from Biggs [6], as well as the approaches from Norsok [8] and FABIG [9] (up to the fully development of plasticity in the beam) are fully compatible with the proposed approach.

For practical purposes it suffices to use existing dynamic conversion factor tables for the bending components. For the longitudinal springs, new conversion diagrams have been generated. These diagrams are given exemplarily for the same cases as in [6] (see Figure A 10).

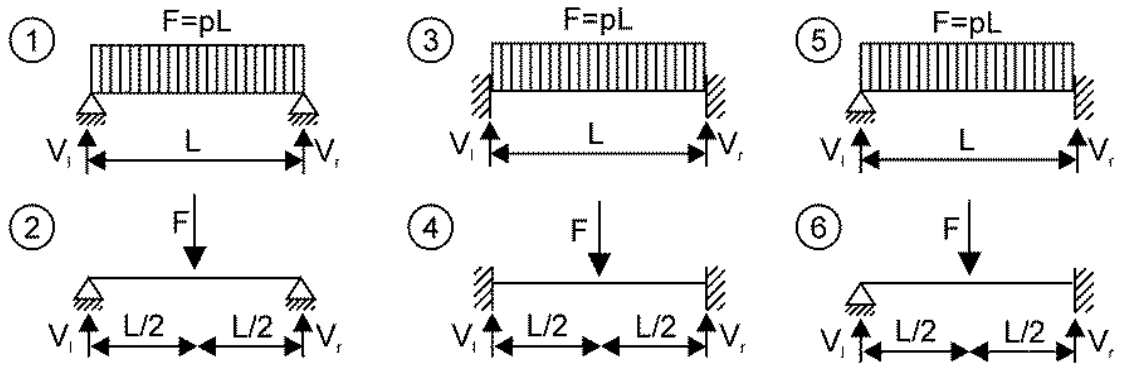

Figure A 10: Investigated combinations of load and boundary conditions for the generation of dynamic conversion factors for the ADBLAST design approach

*Summary of Biggs approach [6] for practical use

Table A 8: Transformation factors for free-free supported beams, acc. to [5]

①	K_L	K_{LM}	k_i	R_i	X_i	V_l	V_r
EI (i = 1)	0,64	0,78	$\frac{384EI}{5L^3}$	$\frac{8M_p}{L}$	$\frac{5M_pL^2}{48EI}$	$0{,}39R + 0{,}11F$	$0{,}39R + 0{,}11F$
PI (i = 3)	0,50	0,66	0	$\frac{8M_p}{L}$	$\frac{2M_p}{N_p}$	$0{,}38R_1 + 0{,}12F$	$0{,}38R_1 + 0{,}12F$
②	K_L	K_{LM}	k_i	R_i	X_i	V_l	V_r
EI (i = 1)	1,0	0,49	$\frac{48EI}{L^3}$	$\frac{4M_p}{L}$	$\frac{M_pL^2}{12EI}$	$0{,}78R - 0{,}28F$	$0{,}78R - 0{,}28F$
PI (i = 3)	1,0	0,33	0	$\frac{4M_p}{L}$	$\frac{M_p}{N_p}$	$0{,}75R_1 - 0{,}25F$	$0{,}75R_1 - 0{,}25F$

with k_i stiffness of segment *i* of the load-deformation curve in Figure A 11.

R_i yielding load of segment *i* of the load-deformation curve

X_i yielding deformation of segment *i* of the load-deformation curve

V_l Dyn. force in left support

V_r Dyn. force in right support

M_p plastic bending resistance of the member

EI bending stiffness of the member

Table A 9: Transformation factors for fixed-fixed supported beams, acc. to [5]

③	K_L	K_{LM}	k_i		R_i	X_i	V_l	V_r
EI (i = 1)	0,53	0,77	$\frac{384EI}{L^3}$	k_e	$\frac{12M_{ps}}{L}$	$\frac{M_{ps}L^2}{32EI}$	$0{,}36R + 0{,}14F$	$0{,}36R + 0{,}14F$
EP (i = 2)	0,64	0,78	$\frac{384EI}{5L^3}$		$\frac{8(M_{ps}+M_p)}{L}$	$\frac{(5M_p - M_{ps})L^2}{48EI}$	$0{,}39R + 0{,}11F$	$0{,}39R + 0{,}11F$
Pl (i = 3)	0,50	0,66	0		$\frac{8(M_{ps}+M_p)}{L}$	$\frac{2(M_{ps}+M_p)}{N_p}$	$0{,}38R_2 + 0{,}12F$	$0{,}38R_2 + 0{,}12F$
④	K_L	K_{LM}	k_i		R_i	X_i	V_l	V_r
EI (i = 1)	1,0	0,37	$\frac{192EI}{L^3}$		$\frac{4(M_{ps}+M_p)}{L}$	$\frac{(M_{ps}+M_p)L^2}{48EI}$	$0{,}71R - 0{,}21F$	$0{,}71R - 0{,}21F$
Pl (i = 3)	1,0	0,33	0		$\frac{4(M_{ps}+M_p)}{L}$	$\frac{(M_{ps}+M_p)}{N_p}$	$0{,}75R_1 - 0{,}25F$	$0{,}75R_1 - 0{,}25F$

with $k_e = 307 \cdot \frac{EI}{L^3}\left(\frac{1{,}5M_{ps}}{M_{ps}+2M_p} + 0{,}25\right)$

M_{ps} plastic moment resistance of the support

Table A 10: Transformation factors for fixed-free supported beams, acc. to [5]

⑤	K_L	K_{LM}	k_i		R_i	X_i	V_l	V_r
EI (i = 1)	0,58	0,78	$\frac{185EI}{L^3}$	k_{e1}	$\frac{8M_{ps}}{L}$	$\frac{8M_{ps}L^2}{185EI}$	$0{,}26R + 0{,}12F$	$0{,}43R + 0{,}19F$
EP (i = 2)	0,64	0,78	$\frac{384EI}{5L^3}$		$\frac{4(M_{ps}+2M_p)}{L}$	$\frac{5(2M_p - M_{ps})L^2}{96EI} + \frac{8M_{ps}L^2}{185EI}$	$0{,}39R + 0{,}11F - \frac{M_{ps}}{L}$	$0{,}39R + 0{,}11F + \frac{M_{ps}}{L}$
Pl (i = 3)	0,50	0,66	0		$\frac{4(M_{ps}+2M_p)}{L}$	$\frac{M_{ps}+2M_p}{N_p}$	$0{,}38R_2 + 0{,}12F - \frac{M_{ps}}{L}$	$0{,}38R_2 + 0{,}12F + \frac{M_{ps}}{L}$
⑥	K_L	K_{LM}	k_i		R_i	X_i	V_l	V_r
EI (i = 1)	1,0	0,43	$\frac{107EI}{L^3}$	k_{e2}	$\frac{16M_{ps}}{3L}$	$\frac{16M_{ps}L^2}{321EI}$	$0{,}25R + 0{,}07F$	$0{,}54R + 0{,}14F$
EP (i = 2)	1,0	0,49	$\frac{48EI}{L^3}$		$\frac{2(M_{ps}+2M_p)}{L}$	$\frac{(6M_p - 5M_{ps})L^2}{72EI} + \frac{16M_{ps}L^2}{321EI}$	$0{,}78R - 0{,}28F - \frac{M_{ps}}{L}$	$0{,}78R - 0{,}28F + \frac{M_{ps}}{L}$
Pl (i = 3)	1,0	0,33	0		$\frac{2(M_{ps}+2M_p)}{L}$	$\frac{M_{ps}+2M_p}{2N_p}$	$0{,}75R_2 - 0{,}25F - \frac{M_{ps}}{L}$	$0{,}75R_2 - 0{,}25F + \frac{M_{ps}}{L}$

with $k_{e1} = 160 \cdot m_2$ $k_{e2} = 106 \cdot m_2$

$$m_2 = \frac{EI}{L^3}\left(\frac{1{,}5M_{ps}}{M_{ps}+2M_p} + 0{,}5\right)$$

The ADBLAST approach adds two longitudinal springs to the Biggs' model. Since the longitudinal springs are calculated from the deformation shape, its shape will be determined by a bilinear or trilinear curve with changes at the same deformation points X_i than the bending springs.

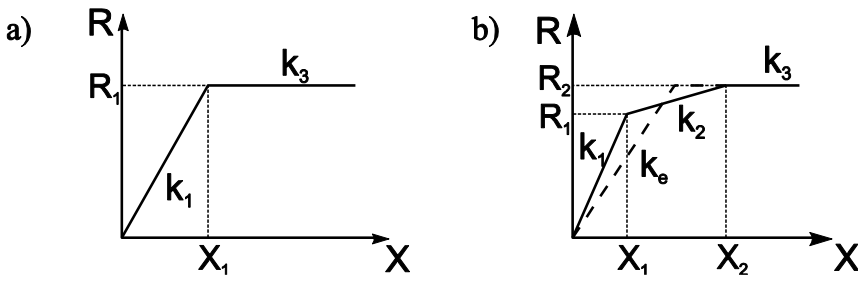

Figure A 11: Load-deformation curves for the longitudinal springs, bilinear (a), trilinear (b)

Table A 11: Transformation factors for free-free supported beams, ADBLAST design, additional parameters to complete Table A 8

①	k_{H1}		k_{H2}	
El (i = 1) Pl (i = 3)	$\left(\frac{1}{k_{L1}}+\frac{1}{k_{GNL,i}}\right)^{-1}$	Figure A 12 **left**	$\left(\frac{1}{k_{L1}}+\frac{1}{k_{GNR,i}}\right)^{-1}$	Figure A 12 **right**
②	k_{H1}		k_{H2}	
El (i = 1) Pl (i = 3)	$\left(\frac{1}{k_{L1}}+\frac{1}{k_{GNL,i}}\right)^{-1}$	Figure A 13 **left**	$\left(\frac{1}{k_{L1}}+\frac{1}{k_{GNR,i}}\right)^{-1}$	Figure A 13 **right**

with k_{H1} stiffness of the equivalent longitudinal spring on the left

k_{H2} stiffness of the equivalent longitudinal spring on the right

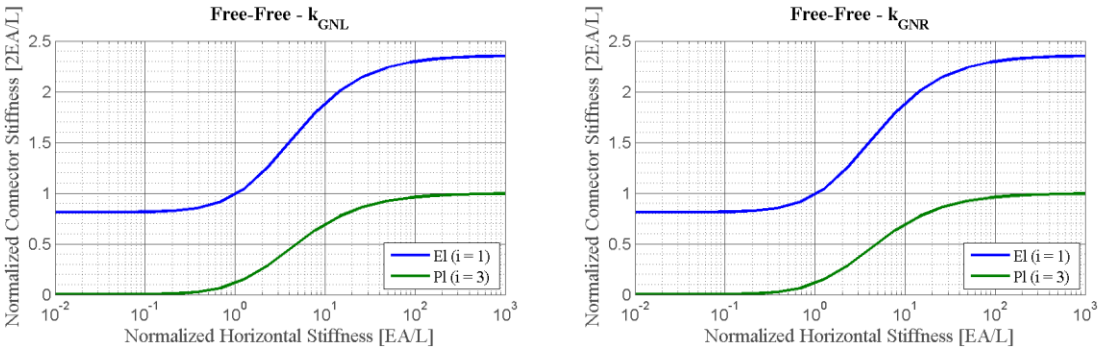

Figure A 12: Normalized Stiffness for the longitudinal springs, unif. distributed load, free-free supports

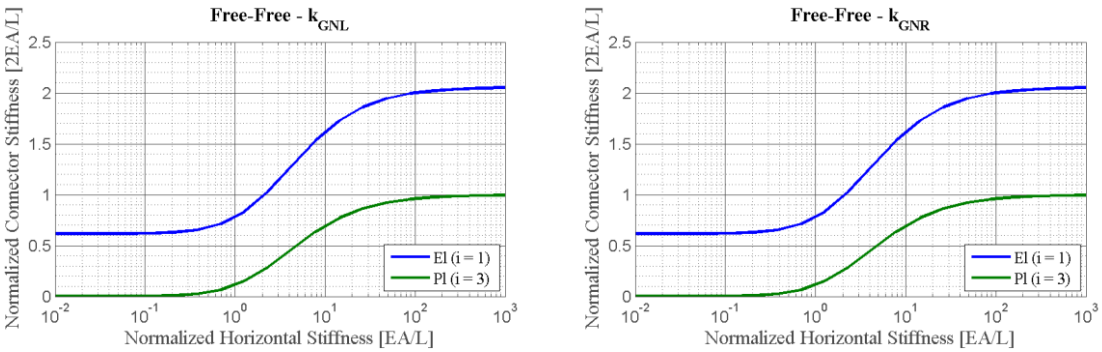

Figure A 13: Normalized Stiffness for the longitudinal springs, concentrated load, free-free supports

Table A 12: Transformation factors for fixed-fixed supported beams, ADBLAST design, additional parameters to complete Table A 9

③	k_{H1}		k_{H2}	
El (i = 1)	$\left(\frac{1}{k_{L1}}+\frac{1}{k_{GNL,i}}\right)^{-1}$	Figure A 14 **left**	$\left(\frac{1}{k_{L1}}+\frac{1}{k_{GNR,i}}\right)^{-1}$	Figure A 14 **right**
E-P (i=2)				
Pl (i = 3)				
④	k_{H1}		k_{H2}	
El (i = 1)	$\left(\frac{1}{k_{L1}}+\frac{1}{k_{GNL,i}}\right)^{-1}$	Figure A 15 **left**	$\left(\frac{1}{k_{L1}}+\frac{1}{k_{GNR,i}}\right)^{-1}$	Figure A 15 **right**
E-P (i=2)				
Pl (i = 3)				

with k_{H1} stiffness of the equivalent longitudinal spring on the left

k_{H2} stiffness of the equivalent longitudinal spring on the right

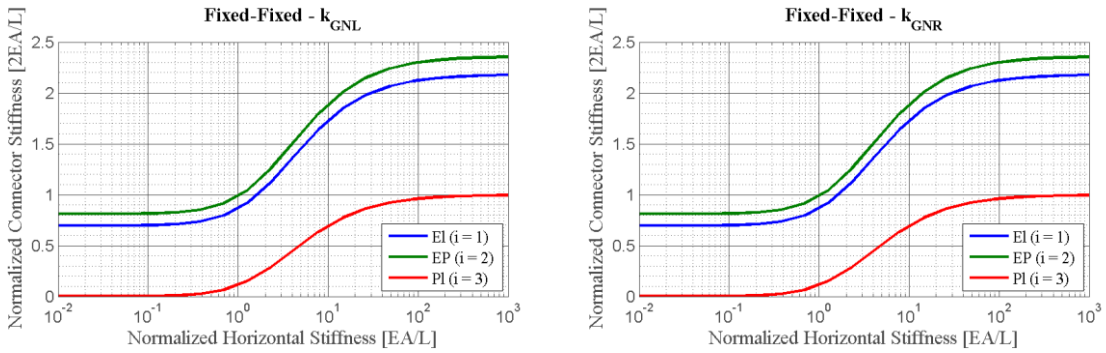

Figure A 14: Normalized Stiffness for the longitudinal springs, unif. distributed load, fixed-fixed supports

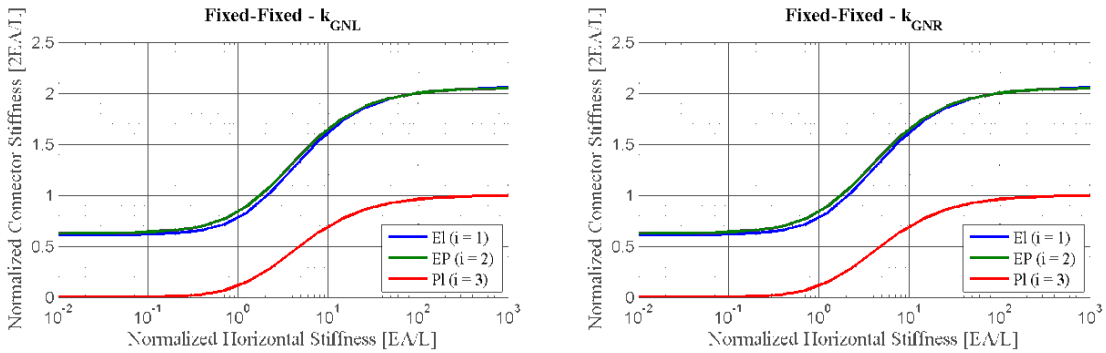

Figure A 15: Normalized Stiffness for the longitudinal springs, concentrated load, fixed-fixed supports

Table A 13: Transformation factors for free-fixed supported beams, ADBLAST design, additional parameters to complete Table A 10

⑤	k_{H1}		k_{H2}	
El (i = 1)	$\left(\frac{1}{k_{L1}}+\frac{1}{k_{GNL,i}}\right)^{-1}$	Figure A 16 **left**	$\left(\frac{1}{k_{L1}}+\frac{1}{k_{GNR,i}}\right)^{-1}$	Figure A 16 **right**
E-P (i=2)				
Pl (i = 3)				
⑥	k_{H1}		k_{H2}	
El (i = 1)	$\left(\frac{1}{k_{L1}}+\frac{1}{k_{GNL,i}}\right)^{-1}$	Figure A 17 **left**	$\left(\frac{1}{k_{L1}}+\frac{1}{k_{GNR,i}}\right)^{-1}$	Figure A 17 **right**
E-P (i=2)				
Pl (i = 3)				

with k_{H1} stiffness of the equivalent longitudinal spring on the left

k_{H2} stiffness of the equivalent longitudinal spring on the right

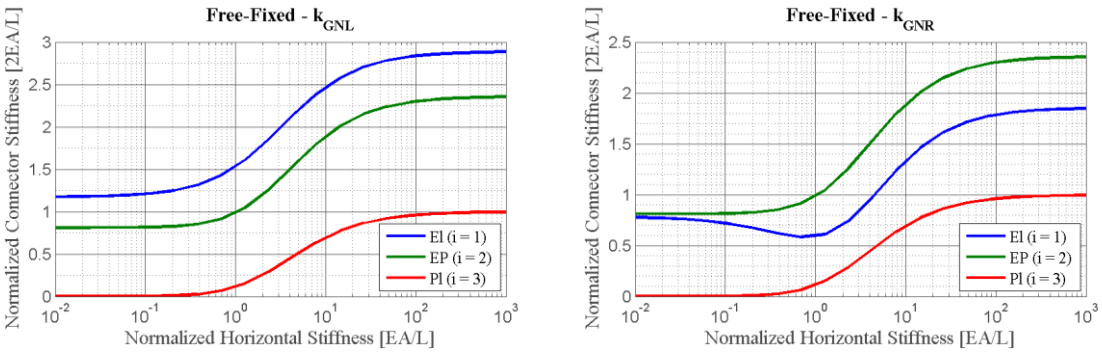

Figure A 16: Normalized Stiffness for the longitudinal springs, unif. distributed load, free-fixed supports

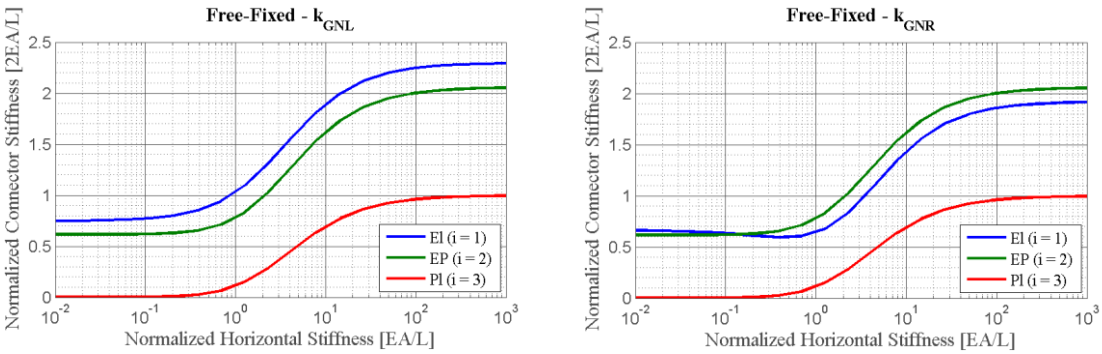

Figure A 17: Normalized Stiffness for the longitudinal springs, concentrated load, free-fixed supports

6.3 Calculation of the dynamic response

To allow for a fast and effective estimation of the expected deformations in the structure, the new ADBLAST approach offers different possibilities. In contrast to the presented existing approaches, it is the first one to offer a full analytical solution of the impulsive problem including a detailed membrane model and connector failure.

The ADBLAST approach offers as well an empirical method based on normalized response diagrams, which leads to the same results as the analytical approach.

The numerical approach is somewhat more complex than in the present approaches, mainly due to the existence of 4 springs instead of one single spring and the need for consideration of geometrical nonlinearities. On the other hand, the model allows for the integration in existing Finite Element Software, i.e. in combination with beam and shell elements for modelling a whole structural entity.

6.3.1 Analytic approach

Within the scope of work, the energy dissipation mechanisms of the ADBLAST model were derived. There a general solution for the normalized energy absorption could be found for an arbitrary system.

Given a certain amount of normalized energy, the maximum expected deflection in the system can be obtained with eq. (6).

$$E^*(\mu) = \begin{cases} \frac{\mu^2}{2} + K_{Stif} \cdot \frac{\mu^3}{3} & \text{if} \quad \mu \leq 1 \\ \mu - \frac{1}{2} + K_{Stif} \cdot (\frac{1}{12} + \frac{\mu^4}{4}) & \text{if} \quad 1 < \mu \leq w_{elH}/w_{elV} \\ \mu - \frac{1}{2} + K_{Stif} \cdot \left(\frac{1}{12} + \frac{\left(\frac{w_{elH}}{w_{elV}}\right)^4}{4} \right) + \frac{K_{Res}}{2} \cdot (\mu^2 - \left(\frac{w_{elH}}{w_{elV}}\right)^2) & \text{if} \quad w_{elH}/w_{elV} \leq \mu \end{cases} \tag{6}$$

The normalized energy that is input into the system until the time *t* is defined as:

$$\Delta E^*_{0\to t} = \int_0^{\mu(t)} \bar{f}^*(t) \cdot d\mu \tag{7}$$

with $\bar{f}^*(t) = f(t)/R_V$ as the normalised applied force

$\Delta E^*_{0\to t}$ offers a reference value at a purely impulsive load situation, where $\Delta E^*_{0\to t}$ does not depend on anything (shape of the load-time function, mechanical properties of the structure) but the applied normalized impulse:

$$i^* = \frac{i}{R_V \cdot T} \tag{8}$$

Hence, the normalized energy input in a purely impulsive case is given by the expression:

$$\Delta E^*_{imp} = 2 \cdot \pi^2 \cdot i^{*2} \tag{9}$$

In [5], Norris et al define the work done ratio as the relation between the actual work done (input) into a structure by a given load and the work done in an impulsive situation. In the same manner, the normalized work done ratio can be defined as:

$$C^*_W = \frac{\Delta E^*}{\Delta E^*_{imp}} \tag{10}$$

Within the scope of works of ADBLAST, a diagram for the calculation of the normalized work done ratio for different normalized blast durations was obtained.

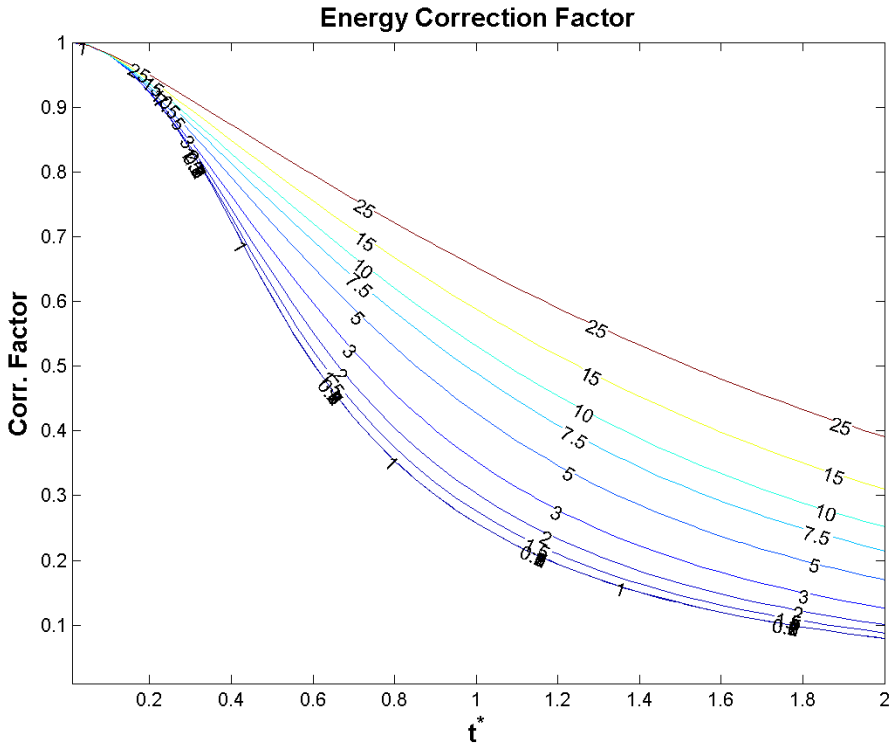

Figure A 18: Normalized Work done ratio, depending on the normalized blast duration and the achieved maximum ductility

After the calculation of the normalized energy input from $\Delta E^* = C_w^* \cdot \Delta E_{imp}^*$, the maximum achieved ductility can be obtained from eq. (6).

Through the explicit modelling of the longitudinal connectors, the achieved ductility can be calculated from the equation:

$$\mu_{Lat,1} = \left(\frac{k_{HLon}}{L} + \frac{1}{2L_1}\right) \cdot \frac{K_{H1}}{R_{H1}} \cdot w_{elV}^2 \cdot \mu^2 \tag{11}$$

$$\mu_{Lat,2} = \left(\frac{k_{HLon}}{L} + \frac{1}{2L_2}\right) \cdot \frac{K_{H2}}{R_{H2}} \cdot w_{elV}^2 \cdot \mu^2 \tag{12}$$

respectively for the left and right connectors.

6.3.2 Semi-Analytic Approach with Design Aids

The presented ADBLAST approach to dynamic reduction is fully compatible with the existing approach from Biggs [6] and UFC [10]. In the case of no axial restraint of the beam, the results are identical. In Figure A 19 and Figure A 20 a comparison of normalized response diagrams according to UFC and using the new ADBLAST reduction approach are shown.

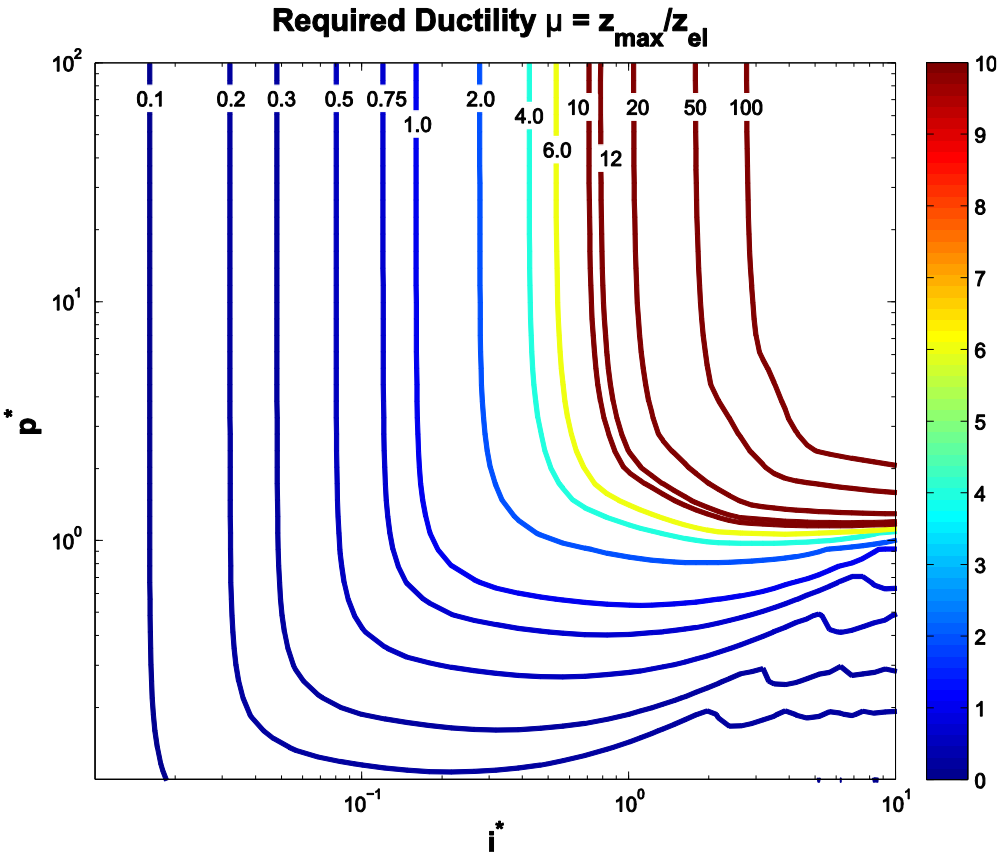

Figure A 19: p-i* diagram for general use, ADBLAST approach*

Both results are identical, so that the use of UFC's normalized response diagrams for the estimation of the maximum achieved ductility is acceptable.

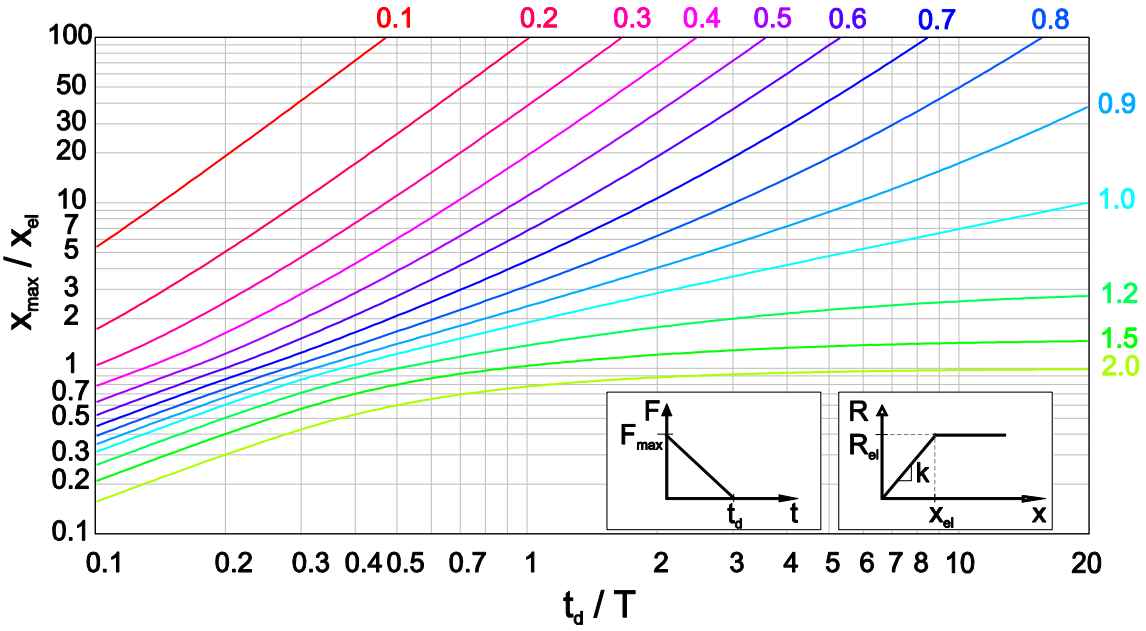

Figure A 20: Normalised response diagram as in [10]

In order to overcome the lack of consideration of membrane action in classic response diagrams, additional diagrams have been generated that relate the truly dissipated energy (including

membrane action) to the theoretical dissipated energy (without membrane action) as calculated fromFigure A 20.

Once the maximum achieved ductility in a system without membrane action μ_0 has been calculated with UFC's diagrams. The true maximum achieved ductility μ can be calculated by multiplication with the correction factor obtained from Figure A 21. This only depends on the parameters K_{Stif} and K_{Res} as defined in the Background Document D.7:

$$K_{Stif} = \frac{K_{Heq} \cdot w_{elV}^2}{K_{Veq} \cdot L_1 \cdot L_2} \tag{13}$$

$$K_{Res} = \frac{\min(R_{H1}, R_{H2}) \cdot L \cdot w_{elV}}{R_V \cdot L_1 \cdot L_2} \tag{14}$$

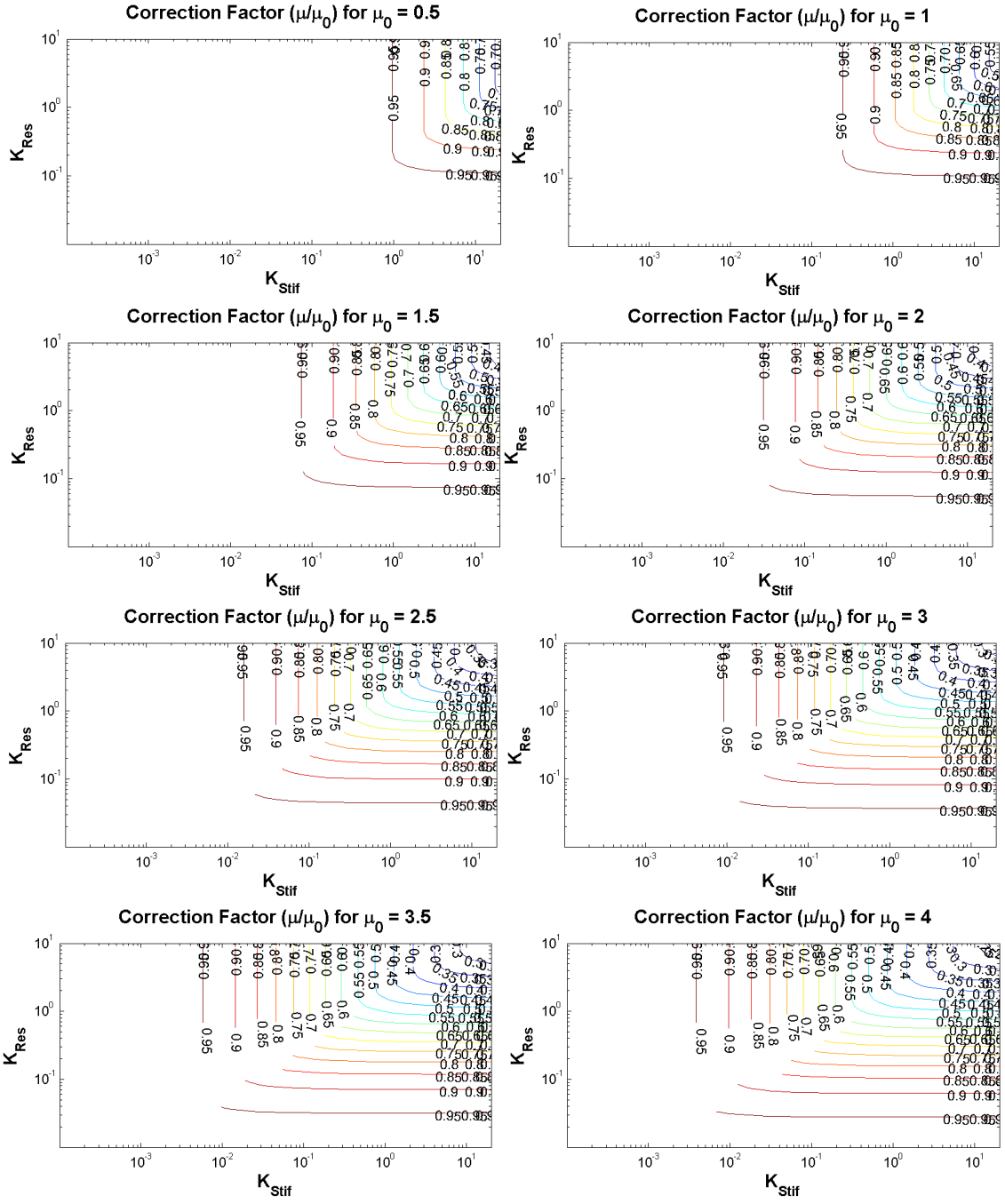

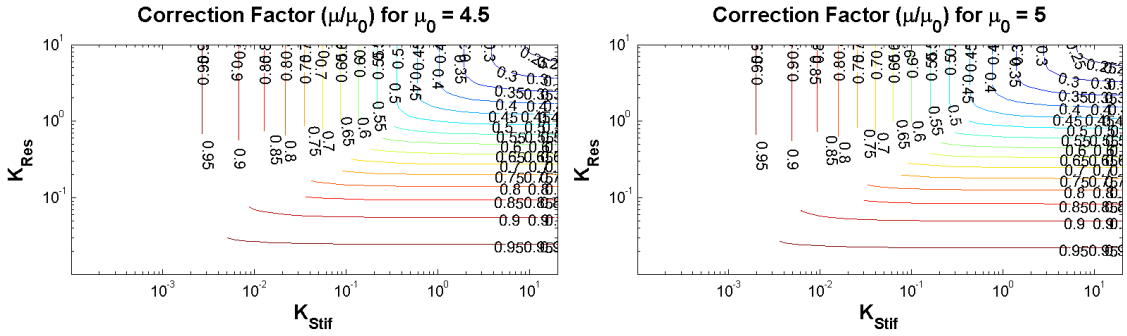
Correction Factor (μ/μ0) for μ0 = 4.5
KRes
KStif

Correction Factor (μ/μ0) for μ0 = 5
KRes
KStif

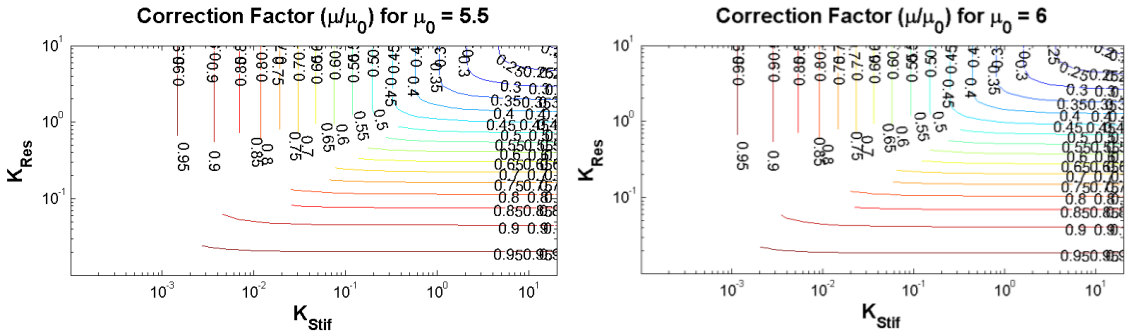
Correction Factor (μ/μ0) for μ0 = 5.5
KRes
KStif

Correction Factor (μ/μ0) for μ0 = 6
KRes
KStif

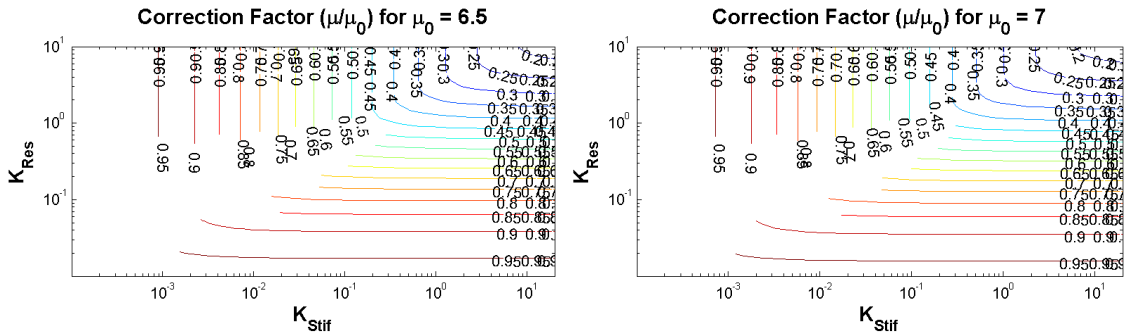
Correction Factor (μ/μ0) for μ0 = 6.5
KRes
KStif

Correction Factor (μ/μ0) for μ0 = 7
KRes
KStif

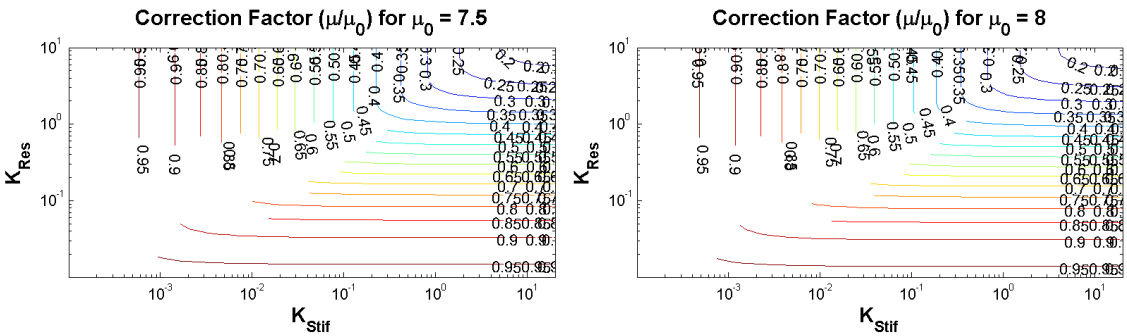
Correction Factor (μ/μ0) for μ0 = 7.5
KRes
KStif

Correction Factor (μ/μ0) for μ0 = 8
KRes
KStif

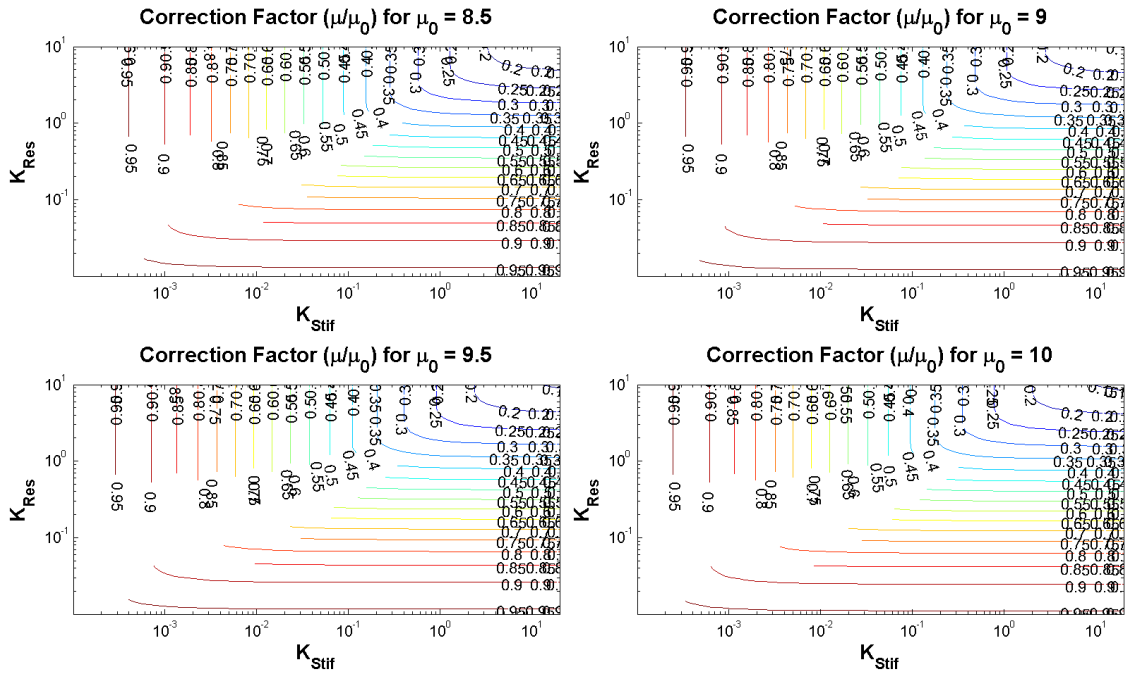

Figure A 21: Correction factor to consider membrane action using ADBLAST approach to dynamic reduction

The maximum achieved connector ductility can be obtained from eqs. (11) and (12).

6.3.3 Numerical approach

In comparison the existing design approaches, a numerical solution of the ADBLAST dynamic equivalent model is not as easy to implement due to the existence of geometrical nonlinear springs.

On the other hand, the model can be easily implemented in a Finite Element environment, where interaction with surrounding structural elements can be explicitly considered. It is a very interesting result, which opens the possibility of more complex dynamic structural calculations with very low computational requirements, but still modelling the bending and membrane response characteristic of the modelled member.

Such a numerical implementation has been successfully tested in an own Finite Element code in Matlab and yielded very successful results, see Example in Chapter 7 of this design guide.

6.4 Design Recommendation ADBLAST

Chapter 6.3 presents three possibilities to predict the dynamic response of members exposed to blast loading:

- Full Analytic Approach
- Semi-Analytic Approach with Design Aids
- Numerical Approach

The first two methodologies are very similar and yield conservative results on the estimation of the maximum required ductilities both for the member and the longitudinal connectors. While the full analytic approach gives more insight on the theoretical background of the new reduced model, the designer can achieve the same results using the semi-analytic approach with design aids.

Only in the case that the designer requires to comprehend the dynamic behaviour over time of the member, then numerical methods are required.

Following the next steps, it is possible to design any structural member against blast. Here, different methodologies can be used, depending on the level of detail required:

6.4.1 Methodology 1: Semi-analytical without membrane effects

1. *Perform Dynamic Reduction without considering Membrane Effects:*

   Knowing the stiffness (*EI*), distributed mass (*m*) and resistance (R_{max}) properties of the system, it is possible to perform a dynamic reduction as exposed in Chapter 6.2 (see Deliverable 6/7 for more detail).

   In case of using the analytical or semi-analytical approach, it is sufficient to calculate the period *T*.

2. *Use Design Aid from Figure A 19 or Figure A 20:*

   By using the normalized variables

   $$i^* = \frac{i}{R_{max} \cdot T}$$

   $$p^* = \frac{F_{max}}{R_{max}}$$

   $$t^* = \frac{t_d}{T}$$

   we can read directly the required ductility of the member to withstand this load.

3. *Comparison with ductility criteria from Chapter 4:*

   The calculated ductility must be compatible with the ductility capacity of the member. In case this condition is not fulfilled, an analysis according to methodology 2 is recommended.

Comments:

This methodology does not take into account any positive membrane effects and therefore gives a safe-side assumption on the maximum achieved ductility.

On the other hand, it does not evaluate the effects on the longitudinal connectors. Specially for large deformation levels on comparably slender members (cladding and substructure), connector failure can be expected before member failure. In this cases, Methodology 2 is recommended.

6.4.2 Methodology 2: Semi-analytical with membrane effects

1. *Perform Dynamic Reduction considering Membrane Effects:*

   Knowing the stiffness (*EI*), distributed mass (*m*) and resistance (R_{max}) properties of the system, and the stiffness and resistance of the longitudinal connectors (K_{H1}, K_{H2} and R_{H1}, R_{H2}) it is possible to perform a dynamic reduction as exposed in Chapter 6.2 (see Deliverable 6/7 for more detail) including the contribution of the connectors to the global resistance.

2. *Use Design Aid from Figure A 19 or Figure A 20:*

   By using the normalized variables

   $$i^* = \frac{i}{R_{max} \cdot T}$$

   $$p^* = \frac{F_{max}}{R_{max}}$$

   $$t^* = \frac{t_d}{T}$$

   we can read directly the required ductility of the member to withstand this load.

3. *Apply Correction Factor for consideration of Membrane Action:*

After calculating the normalized stiffness ratio K_{Stif} and resistance ratio K_{Res}, a correction factor can be determined (see Figure A 21) which allows for the calculation of the required ductility including membrane action.

4. *Determined required Connector Ductility:*

   From Equations (11) and (12), it is possible to relate the vertical ductility requirements to the longitudinal ductility requirements for the connectors.

5. *Comparison with ductility criteria from Chapter 4:*

   The calculated ductility must be compatible with the ductility capacity of the member

Comments:

This methodology does take into account positive membrane effects and therefore gives a more accurate estimation of the real ductility requirements.

This methodology is based on the full-analytical approach, which is not recommended for manual use, but can be implemented for an assessment without the use of design aids.

6.4.3 Methodology 3: Numerical

1. *Perform Dynamic Reduction considering Membrane Effects:*

   Knowing the stiffness (EI), distributed mass (m) and resistance (R_{max}) properties of the system, and the stiffness and resistance of the longitudinal connectors (K_{H1}, K_{H2} and R_{H1}, R_{H2}) it is possible to perform a dynamic reduction as exposed in Chapter 6.2 (see Deliverable 6/7 for more detail – available on request) including the contribution of the connectors to the global resistance.

   Here the full nonlinear spring curve must be determined.

2. *Implementation of a nonlinear dynamic solver:*

   See Deliverable D.6 /D.7 for an exemplary implementation. In the case of the new ADBLAST model, the implementation is not trivial but can be integrated in any nonlinear FEM code.

3. *Solution:*

   The response of the nonlinear SDOF-system is calculated in the domain.

4. *Comparison with ductility criteria from Chapter 4:*

   The calculated ductility must be compatible with the ductility capacity of the member at each time step.

Comments:

This methodology requires advanced programming skills and yields very similar results to the methodology 2. Its use is recommended for validation purposes or for the consideration of additional boundary conditions in a Finite Element environment.

6.4.4 Fast Design Aids

By means of parametric studies, the different cladding systems investigated in ADBLAST are evaluated within the presented normalised p^*- i^* diagram.

The investigated systems correspond to relevant structural cladding types including different connector types.

For each investigated system, a dynamic reduction according to the principles presented in Chapter 6.2 has been performed. The resulting reduced model has been solved then for different loading scenarios corresponding to the different risk classes. The response of the system both in transversal and longitudinal direction has been evaluated and the ductility requirements for each system have been determined.

The following case combinations were investigated:

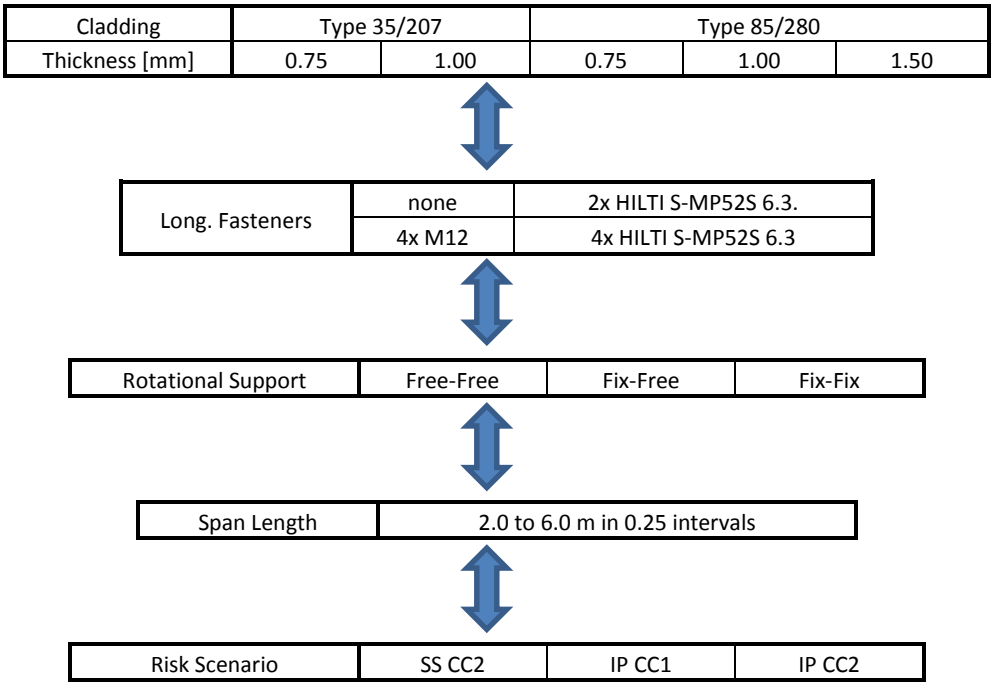

Figure A 22: Investigated combinations for parametrical studies

This leads to a total of 5 x 4 x 3 x 17 x 3 = 3060 investigated situations, for which the following diagrams were generated (Figure A 23, Figure A 24). In order to help the understanding of the designer, the results are grouped by cladding type (different colours) containing 4 different types of longitudinal connection (numbers 1 to 4) for all investigated span lengths (in vertical direction).

These diagrams allow for a fast assessment of the behaviour of a given cladding system under a given risk scenario. The required ductility can then be compared to the criteria in [10] and other codes.

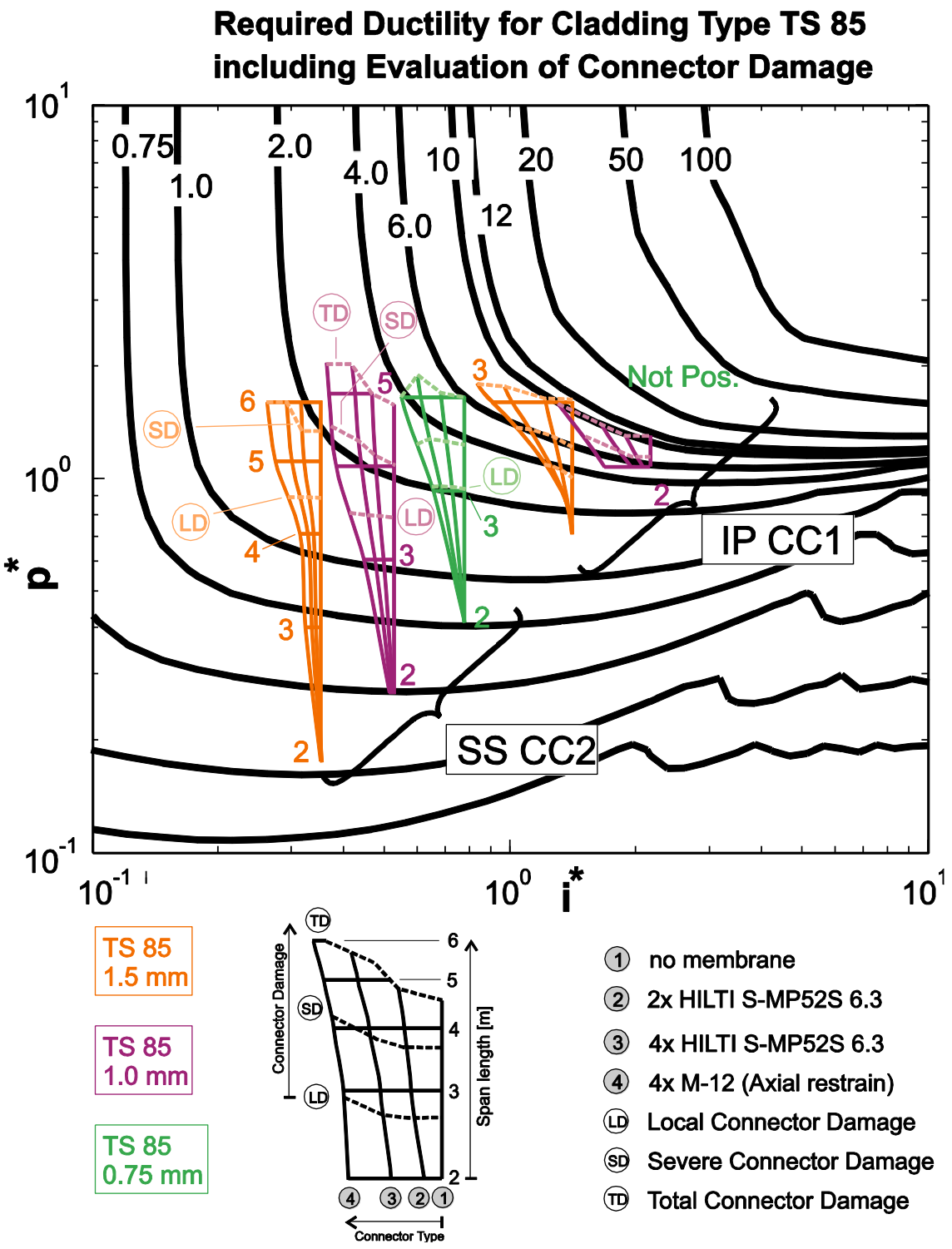

Figure A 23: p^*-i^* diagram for Trapezoidal Claddings of Type TS 85, assuming Free-Free rotational support of the cladding (safe-side assumption), all ADBLAST longitudinal connectors considered, all Risk Scenarios considered

In case of known system ductility, the designer can read the maximum span length allowable for the system to withstand the explosive load according to the chosen risk scenario.

These diagrams are based on conservative assumptions: free-free rotational supports and no additional mass on the cladding. In order to consider other boundary conditions, the designer is advised to use the methodology 2 for less conservative results.

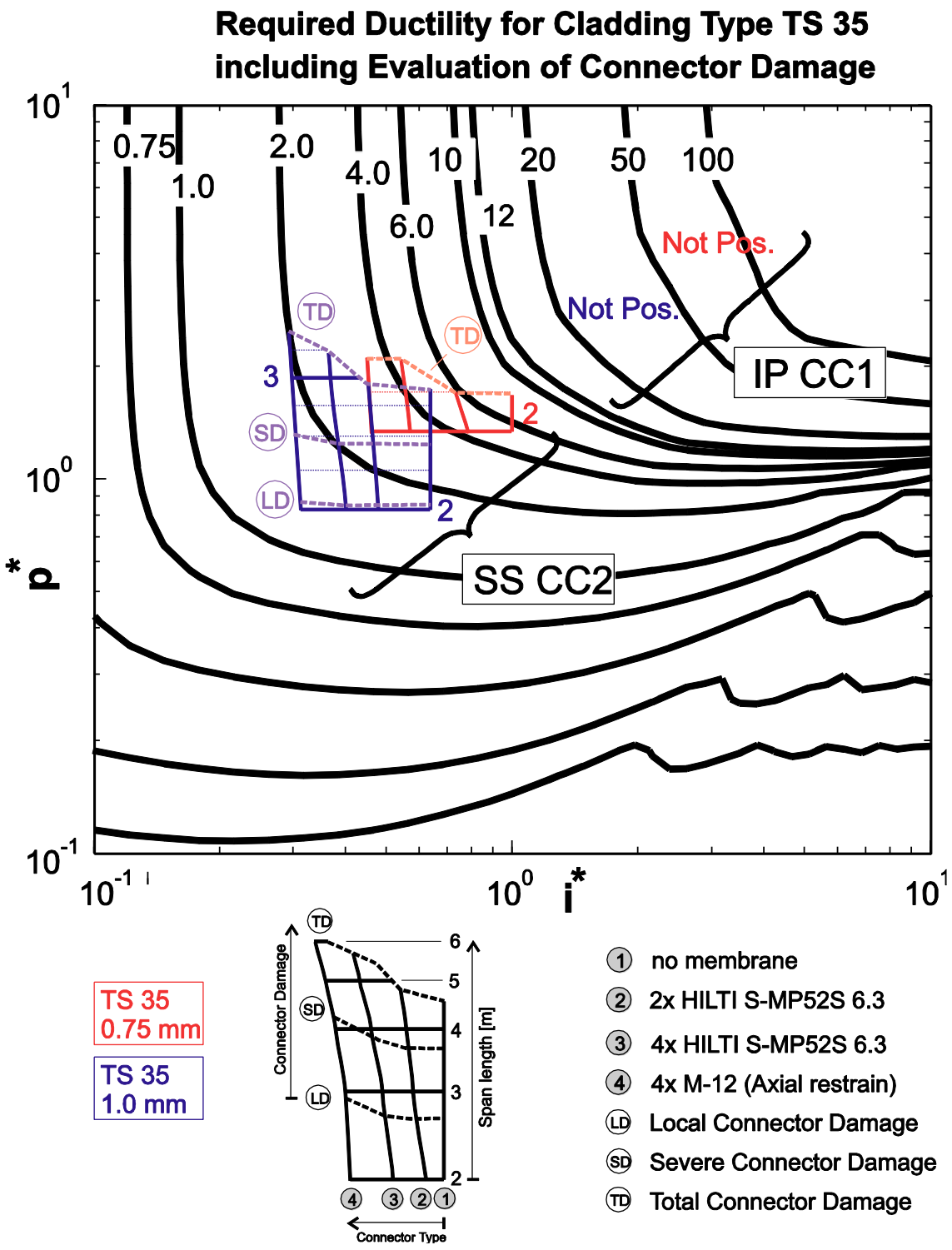

Figure A 24: p^*-i^* diagram for Trapezoidal Claddings of Type TS 35, assuming Free-Free rotational support of the cladding (safe-side assumption), all ADBLAST longitudinal connectors considered, all Risk Scenarios considered

7 Examples

7.1 Basic Steps

To perform a design procedure for a building, several crucial steps have to be undertaken:

1. Risk analysis: estimation of possible damage and allowable loss
2. Determination of Load Scenario
3. Determination of dynamic response of the structure
4. Design Checks

The following examples will show the procedure according to the Norsok Standard, the UCF recommendations and the developed recommendations from the ADBLAST project. The used models are based on a Single-Degree-of-Freedom analysis.

However, this model is only valid, if the eigenperiods of the system can be sufficiently separated from each other to allow for the evaluation of single members or combination of several members. If the member or component with the smallest eigenperiod enters the elastic-plastic domain, the period of the system would be increased and the calculation has to be adjusted.

7.2 Example

7.2.1 Structure and Utilization of the Building

Utilization of building: Production hall in chemical facility

Structural system: Fixed columns and truss structure.

Cladding and roofing: Double-skin cladding and roofing with insulation

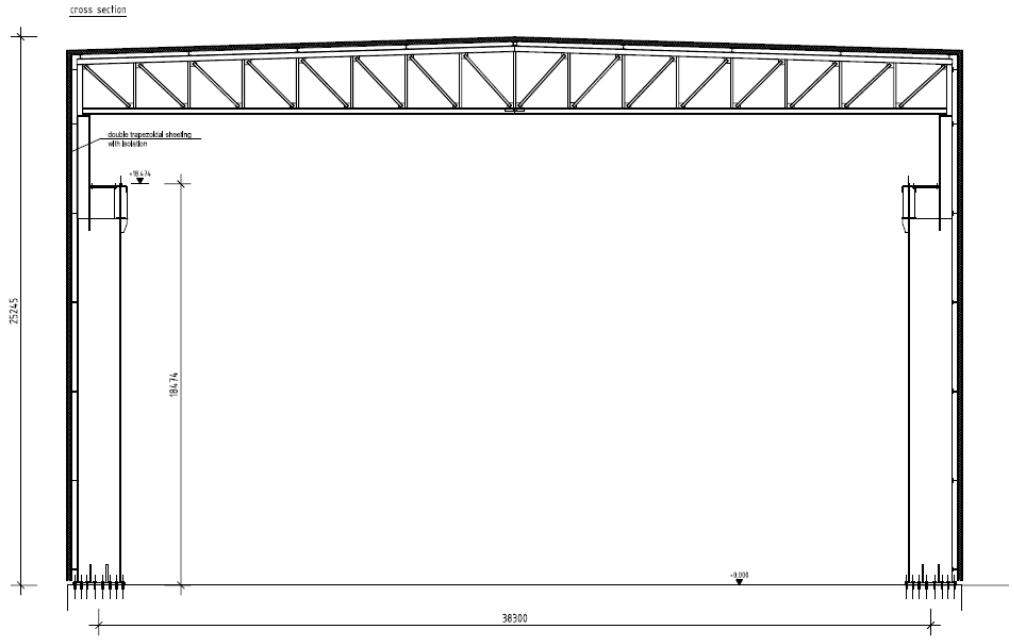

Figure A 25: Transverse Frame with truss roof girder

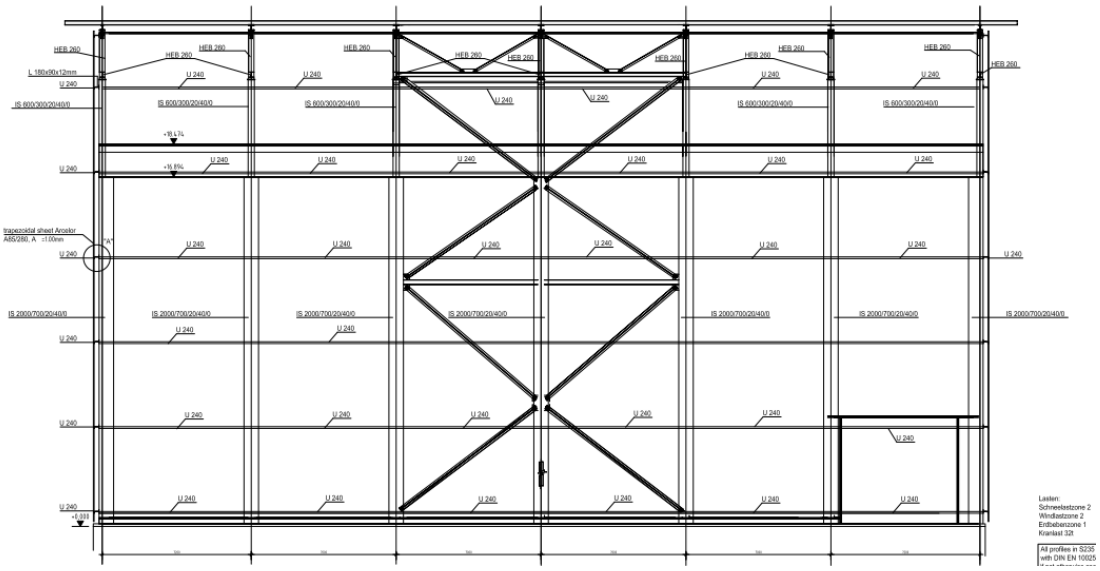

Figure A 26: Side view of the main structural system

Considered load cases for initial design:

Wind zone 2

Snow zone 2

Earthquake zone 1

Crane with capacity of 32 t

Investigated members under blast load:

Trapezoidal Sheet/ Cladding

Substructure/ Purlin

Results of initial Design

Wall Cladding:	T85/280, t_N= 0.75mm
	Connectors to Purlin: HILTI S-MP52S 6.3.
Purlins:	U240, S235JR
Windpost:	U260, S235JR
Column Cross-Section:	IS2000/700/20/40

7.2.2 Risk Assessment and Loading

Blast scenario: External explosion

Safety performance: Human protection and investment protection

Performance requirements:

- Structural stability of the building
- Small damage of the main structure, for example formation of small plastic zones and small remaining deflections
- Integrity of cladding and roofing and of the substructure is required

According to the risk assessment, the structure needs to be designed for an impulsive load according to the Risk Scenario SS CC2 (see Table A 3):

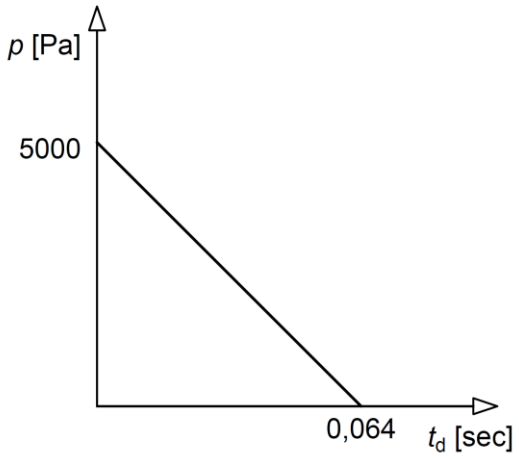

Figure A 27: Applied pressure-time function

7.2.3 Design of the Cladding

The claddings consist of trapezoidal sheets spanning over three purlins with a total length of 8.2 m. For the design, a single span of the trapezoidal sheet is extracted for consideration. Assuming a more or less constant distribution of the blast wave over the surface, it suffices to perform the analysis on a single stripe with 1m width.

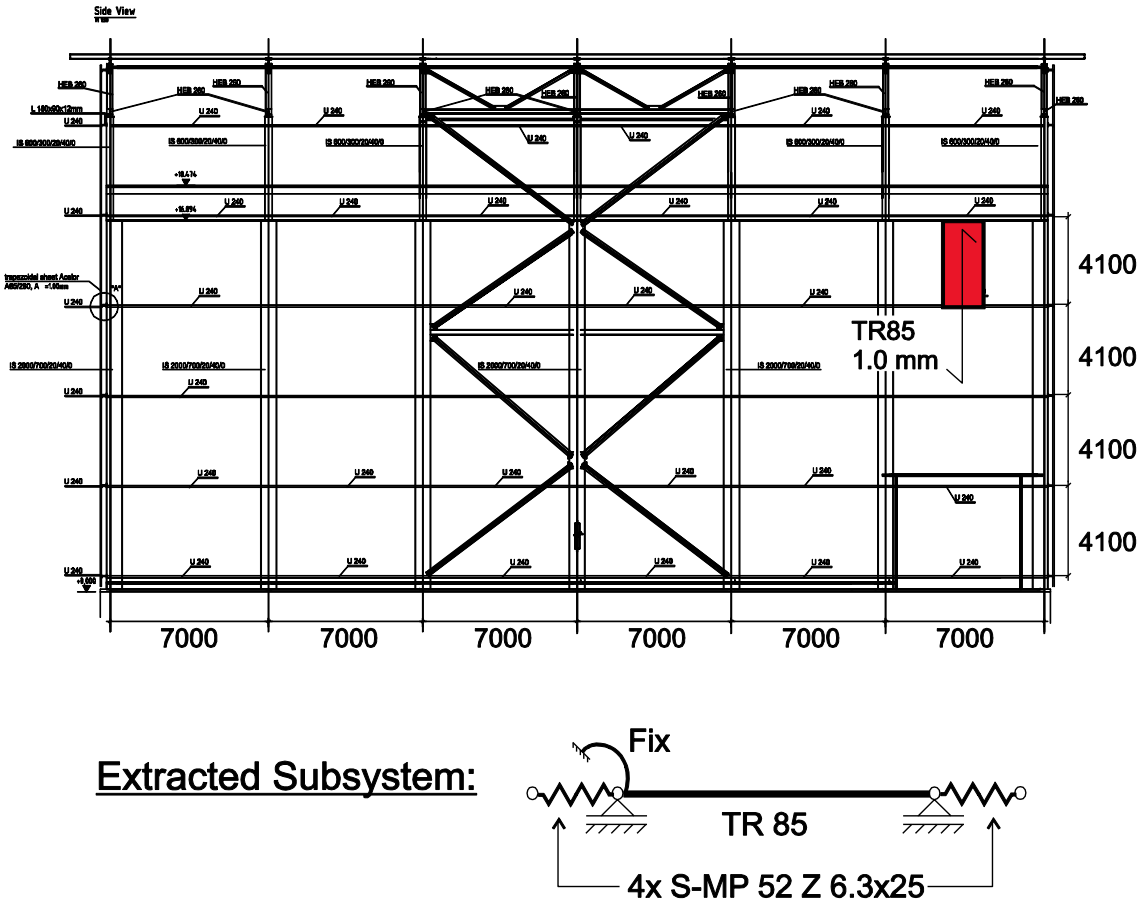

Figure A 28: Overview of the high-rise hall and extracted static subsystem for the analysis of the trapezoidal sheet by simplified methods

7.2.3.1 Subsystem Properties

Cladding Type 85/280				
Structure	Length	L =	4.10	m
	Mass	m =	10.91	kg/m²
Material	S320	E =	210000	N/mm²
		f_y =	320	N/mm²
		f_{dy} =	454.1	N/mm²
Section	Type 85/280	A =	12.67	cm²
		I =	123.91	cm⁴
		M_{pl} =	9230	Nm
Rotational Connectors				
Left:	Fixed	k =	∞	Nm/m
		M_{pl} =	∞	Nm
Right:	Free	k =	0	Nm/m
		M_{pl} =	0	Nm
Longitudinal Connectors				
Left:	4x S-MP 52 Z 6.3x25	k =	2.64E+06	N/m
		N_{pl} =	7700	N
Right:	4x S-MP 52 Z 6.3x25	k =	2.64E+06	N/m
		N_{pl} =	7700	N

7.2.3.2 Reduction to a dynamically equivalent system

System reduction Norsok

	K_L	K_{LM}	k_i	R_i	X_i
El (i = 1)	0,58	0,78	6,93E+05	1,80E+04	0,026
EP (i = 2)	0,64	0,78	2,88E+05	2,70E+04	0,057
Pl (i = 3)	0,50	0,66	0	2,70E+04	0,899
M (i = 4)	0,50	0,66	3,01E+04	-	-

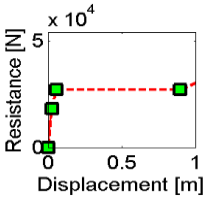

System reduction Fabig

	K_L	K_{LM}	k_i	R_i	X_i
El (i = 1)	0,60	0,80	7,18E+05	1,80E+04	0,025
El-Pl (i = 2)	0,64	0,79	2,88E+05	2,70E+04	0,056
El-Pl (i = 3)	0,50	0,67	0	2,70E+04	0,248
Pl (i = 4)	0,50	0,67	0	2,70E+04	0,248
M (i = 5)	0,50	0,67	1,80E+05	3,39E+04	0,286
M Pl (i = 6)	0,50	0,67	6,01E+04	-	-

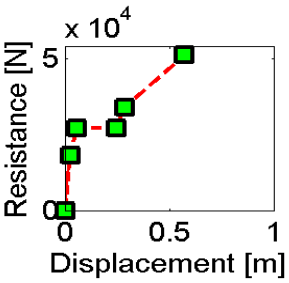

System Reduction ADBLAST

	K_L	K_{LM}	k_i	R_i	X_i	k_{GNR} *2	k_{GNL} *2
El (i = 1)	0,58	0,77	6,92E+05	1,80E+04	0,026	1,08E+08	1,69E+08
EP (i = 2)	0,64	0,79	2,88E+05	2,60E+04	0,054	1,20E+08	1,20E+08
Pl (i = 3)	0,50	0,67	0	-	-	9,77E+06	9,76E+06
Equivalent *1	0,60	0,78	590300	2,61E+04	0,044	9,19E+07	1,59E+08

*1: Equivalent system properties are obtained by forcing a elastic-perfectly plastic with equivalent energy dissipation properties.

$$\int_0^{X_2} R(x) \cdot dx = \int_0^{X_2} R_{eq}(x) \cdot dx$$

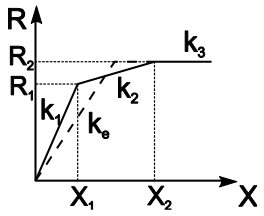

*2: Calculation of k_{H1} and k_{H2}:

Normalized Connector Stiffness: 2.64E6 · *L* / *EA* = 0.04

Looking up in tables for the new ADBLAST Reduction Concept

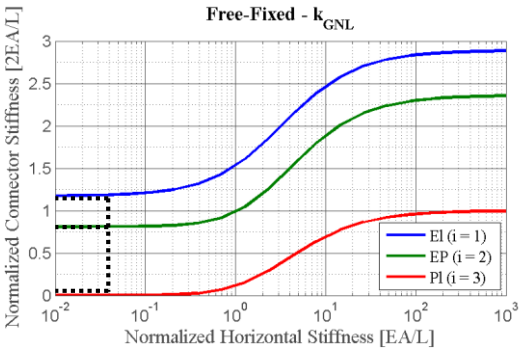

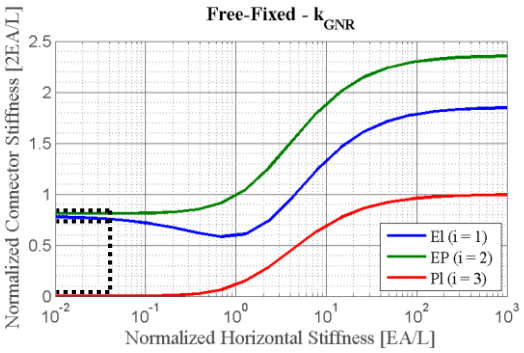

	El (*i*=1)	*EP* (*i* = 2)	*Pl* (*i* = 3)
k_{GNL} [·2*EA*/*L*]	1.31	0.93	0.008
k_{GNR} [·2*EA*/*L*]	0.84	0.93	0.008

The values of k_{H1} and k_{H2} for the equivalent model are:

$$k_{H1} = \left(\frac{1}{k_{L1}} + \frac{1}{k_{GNR,eq}}\right)^{-1} \cdot \frac{1}{K_L} = \left(\frac{1}{4x2.64E6} + \frac{1}{9.19E7}\right)^{-1} \cdot \frac{1}{0.6} = 1.58E7\ N/m$$

$$k_{H2} = \left(\frac{1}{k_{L2}} + \frac{1}{k_{GNL,eq}}\right)^{-1} \cdot \frac{1}{K_L} = \left(\frac{1}{4x2.64E6} + \frac{1}{1.59E8}\right)^{-1} \cdot \frac{1}{0.6} = 1.65E7\ N/m$$

7.2.3.3 Prediction of the response by analytical methods

The eigenperiod of the investigated member can be calculated to:

$$T = 2\pi \cdot \sqrt{K_{LM} \cdot M/K} == 2\pi \cdot \sqrt{0{,}78 \cdot 4.1 \cdot 10.91/590300} = 0.0483\ s$$

The duration of the load is 64 ms, therefore an analytical solution is only possible by means of the ADBLAST energetic approach.

The normalized energy input in a purely impulsive case is given by the expression:

$$\Delta E^*_{imp} = 2 \cdot \pi^2 \cdot i^{*^2}$$

In this case:

$$\Delta E^*_{imp} = 2 \cdot \pi^2 \cdot \left(\frac{5000 \cdot 4.1 \cdot 1.0 \; x \; 0.064}{2x2.61E4 \cdot 0.0483}\right)^2 = 5.345$$

The relation between the actual work done (input) into a structure by a given load and the work done in an impulsive situation ΔE^*_{imp} is characterized by the normalized work done ratio:

$$\Delta E^* = C^*_W \cdot \Delta E^*_{imp}$$

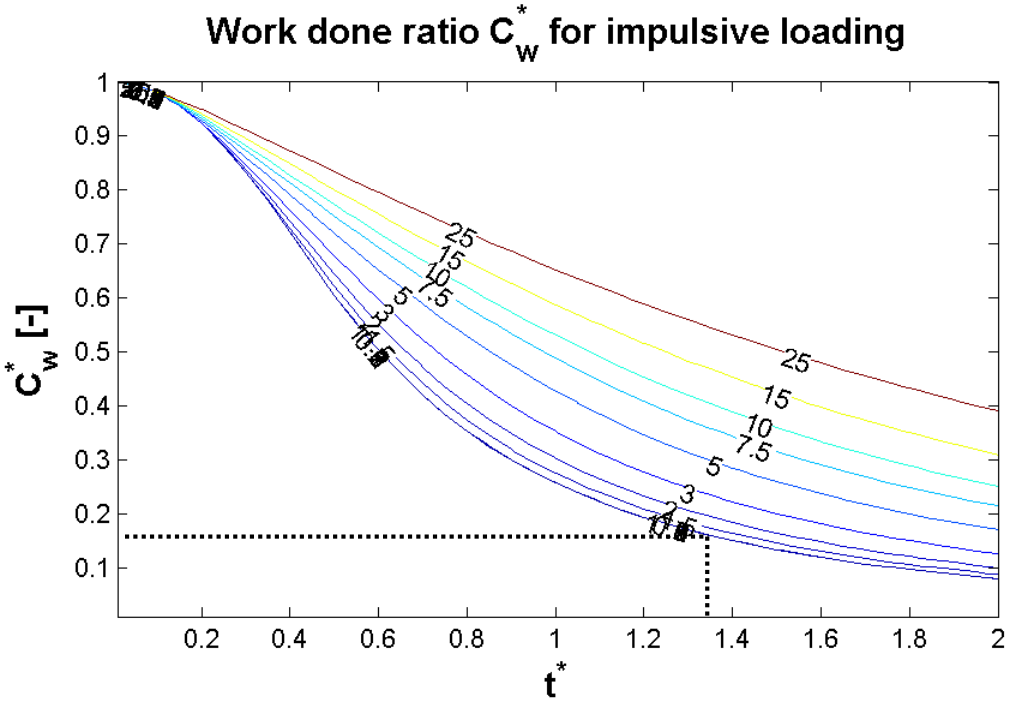

Figure A 29: Normalized Work done ratio, depending on the normalized blast duration and the achieved maximum ductility

$$\Delta E^* = 0.1776 \cdot 5.345 = 0.949$$

In order to solve analytically the maximum achieved ductility, we need to calculate the equivalent bending and membrane stiffness of the system

$$\boldsymbol{k_{Veq}} = k_{eq} = 590300 \; N/m$$

$$\boldsymbol{k_{Heq}} = \frac{k_{H1} \cdot k_{H2}}{2 \cdot (k_{H1} + k_{H2})} \cdot \frac{L^2}{L_1 \cdot L_2} \overset{*}{\rightarrow} \boldsymbol{k_{Heq}} = \frac{2 \cdot k_{H1} \cdot k_{H2}}{(k_{H1} + k_{H2})} = 1.61E7 \; N/m$$

** For symmetrical loading conditions it is valid to assume that $L_1 = L_2 = L/2$*

and the vertical deformation limits for both the yielding of the member and of the lateral connectors:

$$w_{elV} = \frac{R_V}{k_{Veq}} = \frac{2{,}61E4}{590300} = 0.044$$

$$w_{elH} = \sqrt{\frac{\min(R_{H1}, R_{H2}) \cdot L}{k_{Heq}}} = \sqrt{\frac{4 \cdot 7700 \cdot 4.1}{1.61E7}} = 0.089$$

With these values, the non-dimensional stiffness ratio can be calculated to:

$$K_{Stif} = \frac{K_{Heq} \cdot w^2_{elV}}{K_{Veq} \cdot L_1 \cdot L_2} = \frac{1.61E7 \cdot 0.044^2}{590300 \cdot 4.1^2/4} = 0.0126$$

and the adimensional resistance ratio is:

$$K_{Res} = \frac{\min(R_{H1},R_{H2})\cdot L\cdot w_{elV}}{R_V\cdot L_1\cdot L_2} = \frac{4\cdot 7700\cdot 4.1\cdot 0.044}{2.61E4\cdot 4.1^2/4} = 0.051$$

Substituting these values in the analytical solution for the normalized energy:

$$0.949 = \begin{cases} \frac{\mu^2}{2} + 0.0126\cdot\frac{\mu^3}{3} & \text{if} \quad \mu \le 1 \\ \mu - \frac{1}{2} + 0.0126\cdot\left(\frac{1}{12}+\frac{\mu^4}{4}\right) & \text{if} \quad 1 < \mu \le 2.02 \\ \mu - \frac{1}{2} + 0.0126\cdot\left(\frac{1}{12}+\frac{2.02^4}{4}\right) + \frac{0.051}{2}\cdot(\mu^2 - 2.02^2) & \text{if} \quad 2.02 \le \mu \end{cases}$$

Leads to a solution for the maximum achieved ductility of $\mu_{max} = 1.44$

For the longitudinal connectors, the maximum achieved ductility in the connectors can be calculated to:

$$\mu_{Lat,1} = \left(\frac{k_{HLon}}{L} + \frac{1}{2L_1}\right)\cdot\frac{K_{H1}}{R_{H1}}\cdot w_{elV}^2\cdot\mu^2 = \left(0+\frac{1}{4.1}\right)\cdot\frac{1.58E7}{4\cdot 7700}\cdot 0.044^2\cdot 1.44^2 = 0.502$$

$$\mu_{Lat,2} = \left(\frac{k_{HLon}}{L} + \frac{1}{2L_2}\right)\cdot\frac{K_{H2}}{R_{H2}}\cdot w_{elV}^2\cdot\mu^2 = \left(0+\frac{1}{4.1}\right)\cdot\frac{1.58E7}{4\cdot 7700}\cdot 0.044^2\cdot 1.44^2 = 0.502$$

An analytical estimation of the maximum support forces is possible with the expression:

$$F_{support}(\mu) = \left(1 + K_{Stif}\cdot\mu^3\right)\cdot R_V = (1 + 0.0126\cdot 1.44^3)\cdot 2{,}61E4 = \ 27082kN$$

This forces can be distributed between the left (fixed) and right (hinged) support according to the weighting factors 5/8 and 3/8 respectively.

7.2.3.4 Prediction of the response by Design Aids

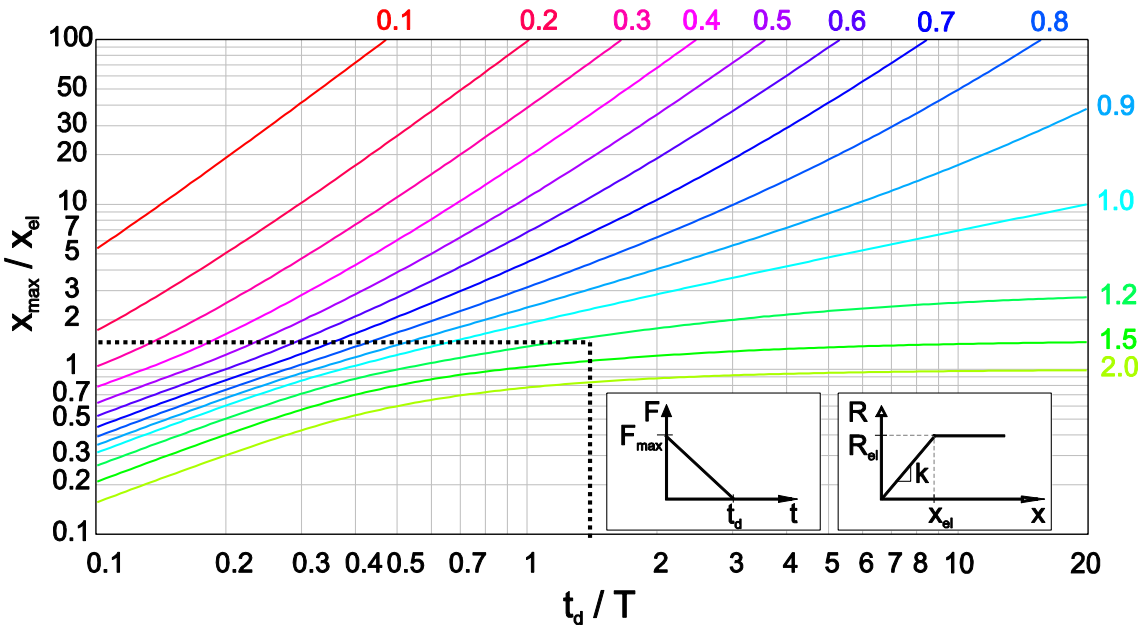

Figure A 30: Normalised response diagram as in [10]

The duration ratio is calculated to: t_d / T = 64 / 48 = 1.33

The force ratio is calculated to: R_V / F_{max} = 2.61E4 / (5000·4.1) = 1.27

From the normalized response diagram, a maximum ductility of ~1.4 can be estimated.

The ADBLAST extension for consideration of membrane effects provides the following diagram for the correction of the estimated ductility:

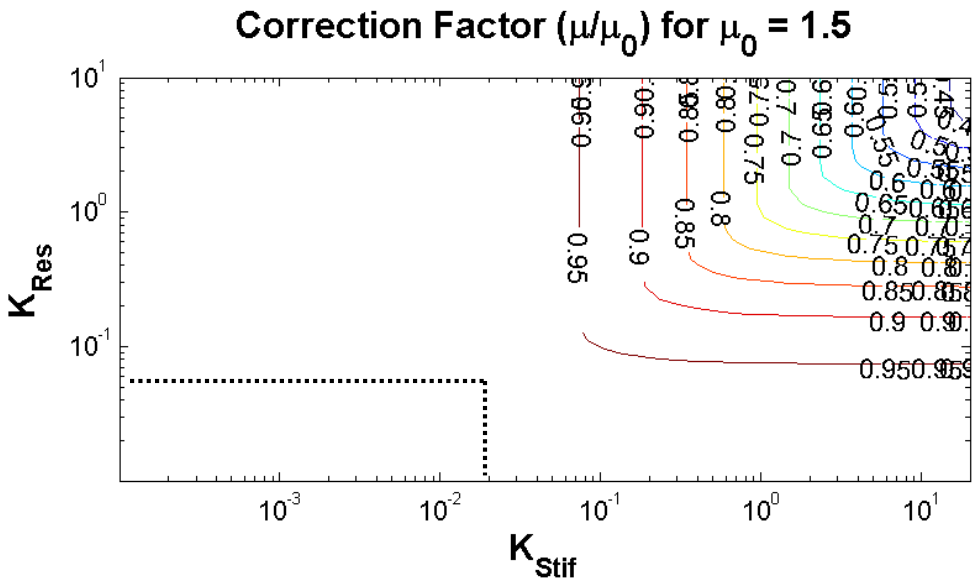

Figure A 31: Correction factor to consider membrane action

In this case, no significant contribution from the membrane action is to be expected.

7.2.3.5 Prediction of the response by Numerical Methods

By means of numerical integration (in case of Norsok and Fabig) and Finite Element Calculations (ADBLAST), the evolution of the response in the time domain can be calculated. For validation purposes, the results of an exact model with beam elements is shown here.

The analytical results are shown here for comparison as well.

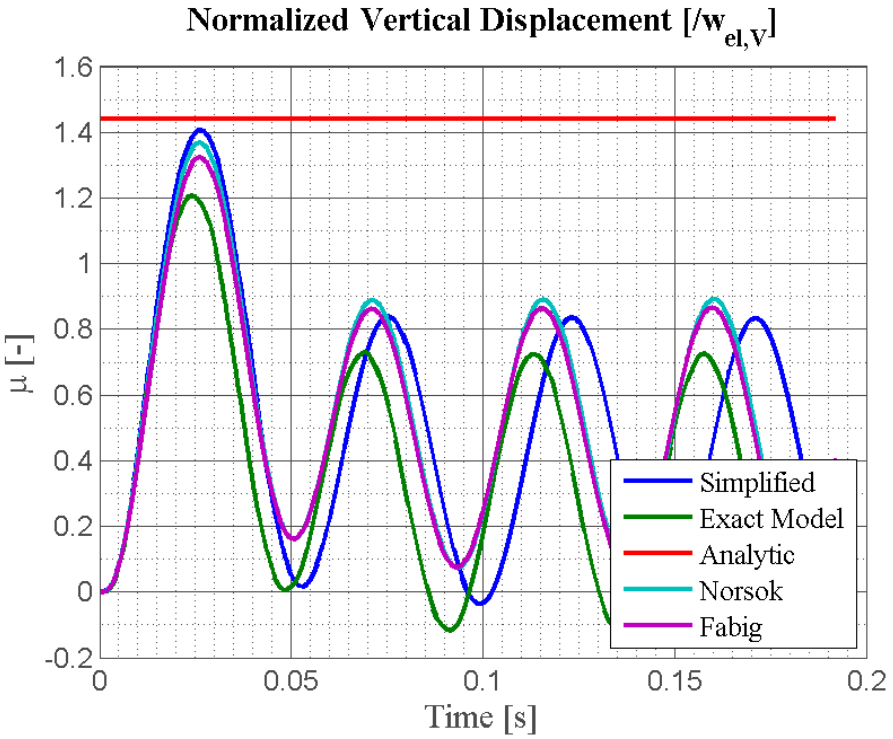

Figure A 32: Normalized Vertical Displacements for the cladding under explosive loading

The longitudinal connector displacements can only be evaluated by means of the new simplified ADBLAST approach as well as be the proposed analytical method:

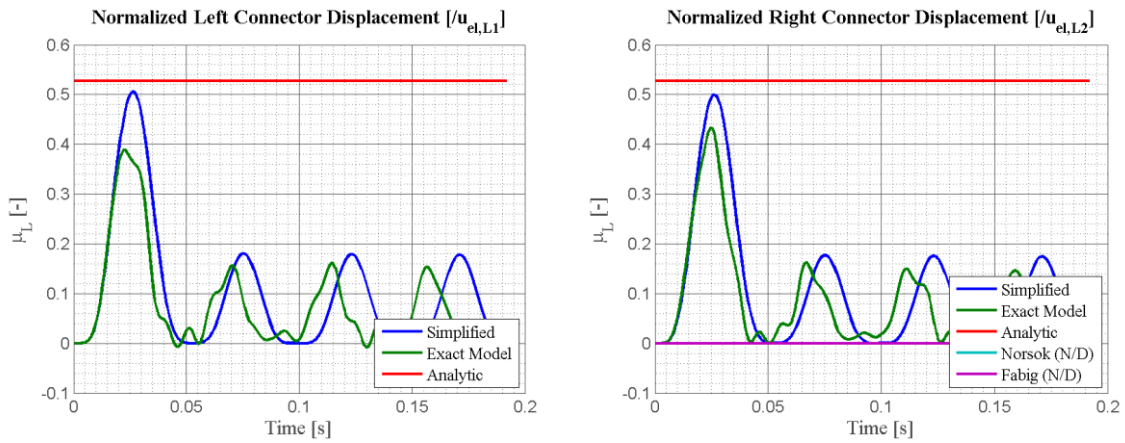

Figure A 33: Normalized Longitudinal Displacement of the left (left) and right (right) connector for the cladding under explosive loading

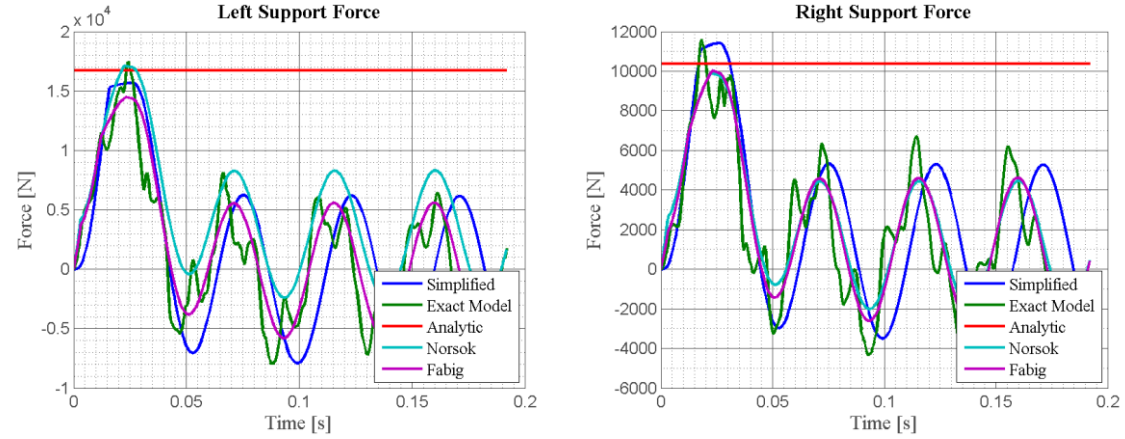

Figure A 34: Transferred Forces on the left (left) and right (right) support (with fixed rotation) for the cladding under explosive loading

7.2.3.6 Design Check

Attending to the presented criteria in Chapter 4, the cladding is required to achieve a maximum ductility of 1.44. This value fulfills all recommendations for blast design according to the different codes.

The maximum support rotation can be estimated by:

$$\varphi_{max} = \mu_{max} \cdot \frac{w_{el,V}}{L/2} = 1.44 \cdot \frac{0.044}{4.1/2} \cdot \frac{180}{\pi} = 1.8°$$

This end rotation is within the acceptable limits for cold form panels.

The detachment of the panels is can happen if the rebound force is enough to cause a pull-through failure of the fasteners. The chosen fasteners have a pull-through resistance of ~9kN each, which compared to the values in Figure A 34, is sufficient.

The maximum shear force that can be absorbed by the trapezoidal cladding is 38.9 kN/m, which is larger than the maximum expected shear force of around ~18 kN.

The cladding will withstand the blast load without any detachment of the panels but with remaining plastic deformations.

7.2.4 Design of the Substructure (Purlins + Cladding)

The purlins consist of U-240 profiles spanning between the frames as a single span beam with total length of 7.0 m. For the design, a single purlin is extracted for consideration. Assuming a

more or less constant distribution of the blast wave over the surface, it is necessary to consider the loaded area both for the total loading as well as for the total mass of the subsystem.

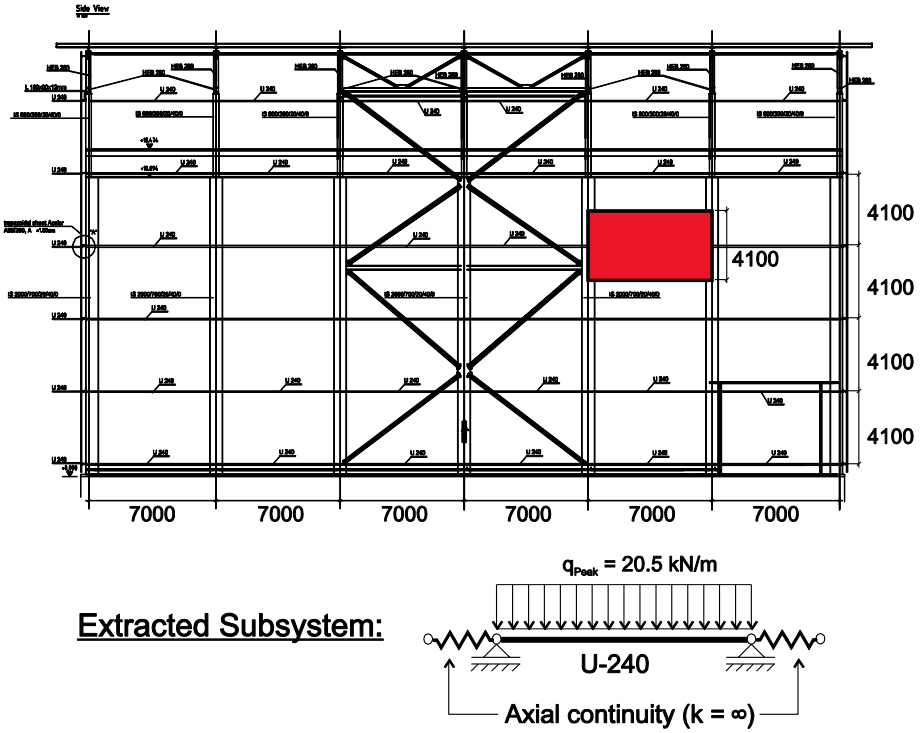

Figure A 35: Overview of the high-rise hall and extracted static subsystem for the analysis of the trapezoidal sheet by simplified methods

7.2.4.1 Subsystem Properties

Purlin (U-240)				
Structure	Length	L =	7.00	m
	Mass	m =	72.571	kg/m²
Material	S235	E =	210000	N/mm²
		f_y =	235	N/mm²
		f_{dy} =	333.5	N/mm²
Section	Type 85/280	A =	35.5	cm²
		I =	2784	cm⁴
		M_{pl} =	108550	Nm
Rottational Connectors				
Left:	Free	k =	0	Nm/m
		M_{pl} =	0	Nm
Right:	Free	k =	0	Nm/m
		M_{pl} =	0	Nm
Longitudinal Connectors				
Left:	Stiff (500 kN limit)	k =	1.00E+09	N/m
		N_{pl} =	500000	N
Right:	Stiff (500 kN limit)	k =	1.00E+09	N/m
		N_{pl} =	500000	N

7.2.4.2 Reduction to a dynamically equivalent system

System reduction Norsok

	K_L	K_{LM}	k_i	R_i	X_i
El (i = 1)	0.64	0.78	1.31E+06	1.24E+05	0.0948
EP (i = 2)	-	-	-	-	-
Pl (i = 3)	0.50	0.66	0	1.24E+05	0.4342
M (i = 4)	0.50	0.66	2.86E+05	-	-

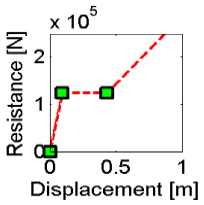

System reduction Fabig

	K_L	K_{LM}	k_i	R_i	X_i
El (i = 1)	0.64	0.79	1.31E+06	1.24E+05	0.095
El-Pl (i = 2)	-	-	-	-	-
El-Pl (i = 3)	-	-	-	-	-
Pl (i = 4)	0.50	0.67	0	1.24E+05	0.186
M (i = 5)	0.50	0.67	1.71E+06	2.05E+05	0.233
M Pl (i = 6)	0.50	0.67	5.71E+05	-	-

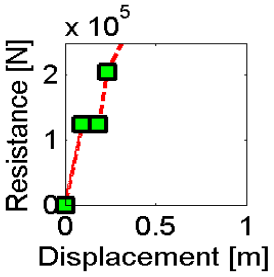

System Reduction ADBLAST

	K_L	K_{LM}	k_i	R_i	X_i	k_{GNR} *2	k_{GNL} *2
El (i = 1)	0.64	0.79	1.31E+06	1.24E+05	0.095	3.97E+08	3.97E+08
EP (i = 2)	-	-	-	-	-	-	-
Pl (i = 3)	0.50	0.67	0	-	-	1.45E+08	1.45E+08
Equivalent *1	0.64	0.79	1.31E+06	1.24E+05	0.095	1.93E+08	1.93E+08

*1: Equivalent system properties are obtained by forcing an elastic-perfectly plastic with equivalent energy dissipation properties.

$$\int_0^{X_2} R(x) \cdot dx = \int_0^{X_2} R_{eq}(x) \cdot dx$$

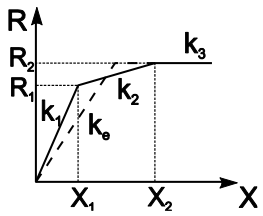

*2: Calculation of k_{H1} and k_{H2}:

Normalized Connector Stiffness: 1.00E9 · *L* / *EA* = 9.4

Looking up in tables for the new ADBLAST Reduction Concept

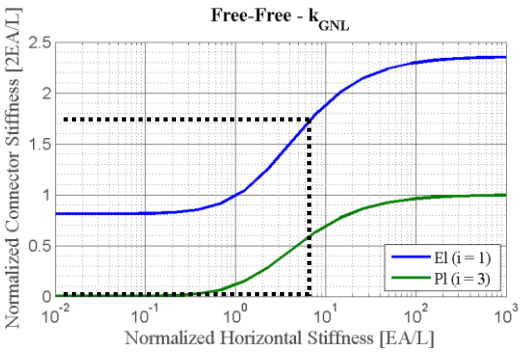

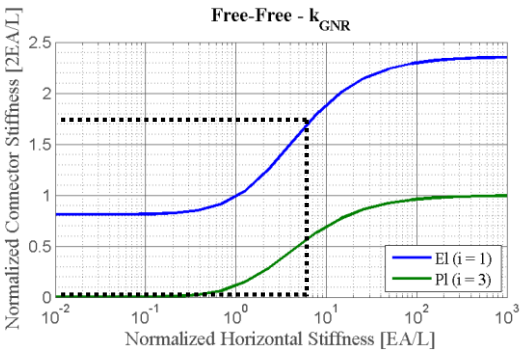

	El (*i*=1)	*EP* (*i* = 2)	*Pl* (*i* = 3)
k_{GNL} [·2*EA*/*L*]	1.86	-	0.68
k_{GNR} [·2*EA*/*L*]	1.86	-	0.68

The values of k_{H1} and k_{H2} for the equivalent model are:

$$k_{H1} = \left(\frac{1}{k_{L1}} + \frac{1}{k_{GNR,eq}}\right)^{-1} \cdot \frac{1}{\mathrm{K_L}} = \left(\frac{1}{1.0E9} + \frac{1}{1.93E8}\right)^{-1} \cdot \frac{1}{0.64} = 2.53E8\ N/m$$

$$k_{H2} = \left(\frac{1}{k_{L2}} + \frac{1}{k_{GNL,eq}}\right)^{-1} \cdot \frac{1}{\mathrm{K_L}} = \left(\frac{1}{1.0E9} + \frac{1}{1.93E8}\right)^{-1} \cdot \frac{1}{0.64} = 2.53E8\ N/m$$

7.2.4.3 Prediction of the response by analytical methods

The eigenperiod of the investigated member can be calculated to:

$$\mathrm{T} = 2\pi \cdot \sqrt{K_{LM} \cdot M/K} = = 2\pi \cdot \sqrt{0{,}79 \cdot 7 \cdot 72.57/1.31E6} = 0.110\ s$$

The duration of the load is 64 ms, therefore an analytical solution is only possible by means of the ADBLAST energetic approach.

The normalized energy input in a purely impulsive case is given by the expression:

$$\Delta E^*_{imp} = 2 \cdot \pi^2 \cdot i^{*^2}$$

In this case:

$$\Delta E^*_{imp} = 2 \cdot \pi^2 \cdot \left(\frac{5000 \cdot 4.1 \cdot 7.0\ x\ 0.064}{2x1.24E5 \cdot 0.110}\right)^2 = 2.237$$

The relation between the actual work done (input) into a structure by a given load and the work done in an impulsive situation ΔE^*_{imp} is characterized by the normalized work done ratio:

$$\Delta E^* = C^*_W \cdot \Delta E^*_{imp}$$

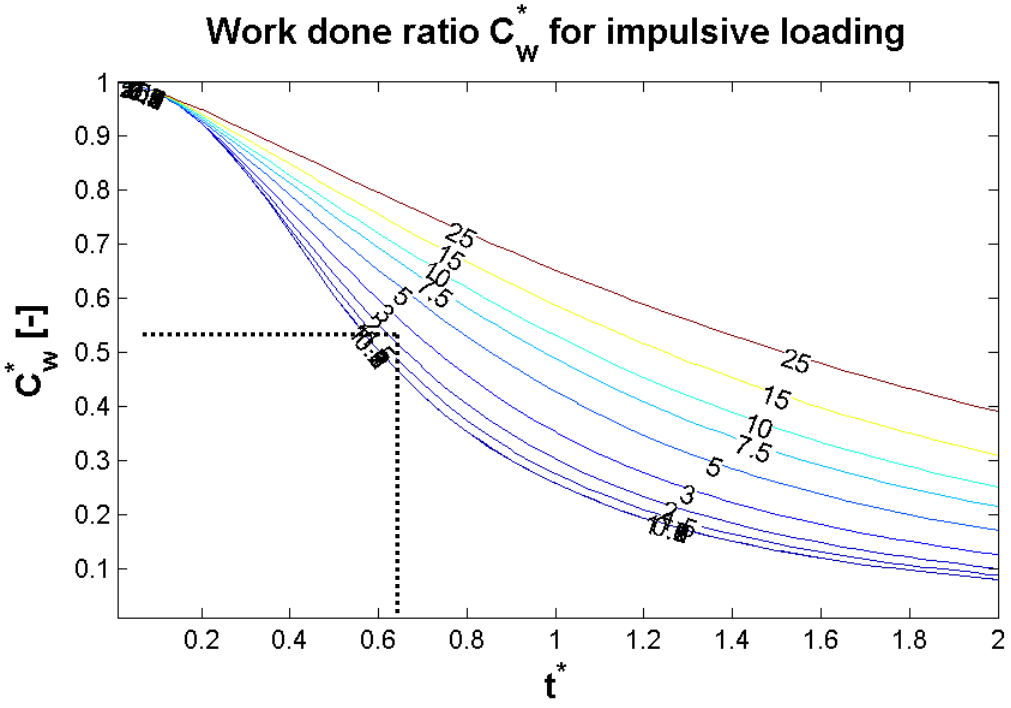

Figure A 36: Normalized Work done ratio, depending on the normalized blast duration and the achieved maximum ductility

$$\Delta E^* = 0.545 \cdot 2.237 = 1.219$$

In order to solve analytically the maximum achieved ductility, we need to calculate the equivalent bending and membrane stiffnesses of the system

$$\boldsymbol{k_{Veq}} = k_{eq} = 1310000\ N/m$$

$$\boldsymbol{k_{Heq}} = \frac{k_{H1} \cdot k_{H2}}{2 \cdot (k_{H1} + k_{H2})} \cdot \frac{L^2}{L_1 \cdot L_2} \overset{*}{\rightarrow} \boldsymbol{k_{Heq}} = \frac{2 \cdot k_{H1} \cdot k_{H2}}{(k_{H1} + k_{H2})} = 2.53E8\ N/m$$

** For symmetrical loading conditions it is valid to assume that $L_1 = L_2 = L/2$*

and the vertical deformation limits for both the yielding of the member and of the lateral connectors:

$$w_{elV} = \frac{R_V}{k_{Veq}} = \frac{1.24E5}{1310000} = 0.095$$

$$w_{elH} = \sqrt{\frac{\min(R_{H1}, R_{H2}) \cdot L}{k_{Heq}}} = \sqrt{\frac{5E5 \cdot 7.0}{2.53E8}} = 0.118$$

With these values, the adimensional stiffness ratio can be calculated to:

$$K_{Stif} = \frac{K_{Heq} \cdot w_{elV}^2}{K_{Veq} \cdot L_1 \cdot L_2} = \frac{2.53E8 \cdot 0.095^2}{1310000 \cdot 7.0^2/4} = 0.142$$

and the adimensional resistance ratio is:

$$K_{Res} = \frac{\min(R_{H1}, R_{H2}) \cdot L \cdot w_{elV}}{R_V \cdot L_1 \cdot L_2} = \frac{5E5 \cdot 7.0 \cdot 0.095}{1.24E5 \cdot 7.0^2/4} = 0.219$$

Substituting these values in the analytical solution for the normalized energy:

$$1.219 = \begin{cases} \frac{\mu^2}{2} + 0.142 \cdot \frac{\mu^3}{3} & \text{if} \quad \mu \leq 1 \\ \mu - \frac{1}{2} + 0.142 \cdot \left(\frac{1}{12} + \frac{\mu^4}{4}\right) & \text{if} \quad 1 < \mu \leq 1.24 \\ \mu - \frac{1}{2} + 0.142 \cdot \left(\frac{1}{12} + \frac{1.24^4}{4}\right) + \frac{0.219}{2} \cdot (\mu^2 - 1.24^2) & \text{if} \quad 1.24 \leq \mu \end{cases}$$

yields a solution for the maximum achieved ductility of $\mu_{max} = 1.544$

For the longitudinal connectors, the maximum achieved ductility in the connectors can be calculated to:

$$\mu_{Lat,1} = \left(\frac{k_{HLon}}{L} + \frac{1}{2L_1}\right) \cdot \frac{K_{H1}}{R_{H1}} \cdot w_{elV}^2 \cdot \mu^2 = \left(0 + \frac{1}{7.0}\right) \cdot \frac{2.53E8}{5E5} \cdot 0.095^2 \cdot 1.544^2 = 1.555$$

$$\mu_{Lat,2} = \left(\frac{k_{HLon}}{L} + \frac{1}{2L_2}\right) \cdot \frac{K_{H2}}{R_{H2}} \cdot w_{elV}^2 \cdot \mu^2 = \left(0 + \frac{1}{7.0}\right) \cdot \frac{2.53E8}{5E5} \cdot 0.095^2 \cdot 1.544^2 = 1.555$$

An analytical estimation of the maximum support forces is possible with the expression:

$$F_{support}(\mu) = (1 + K_{Res} \cdot \mu) \cdot R_V = (1 + 0.219 \cdot 1.544) \cdot 1.24E5 = 165.9kN$$

These forces can be distributed between the left (hinged) and right (hinged) support according to the weighting factors 1/2 and 1/2 respectively.

7.2.4.4 Prediction of the response by Design Aids

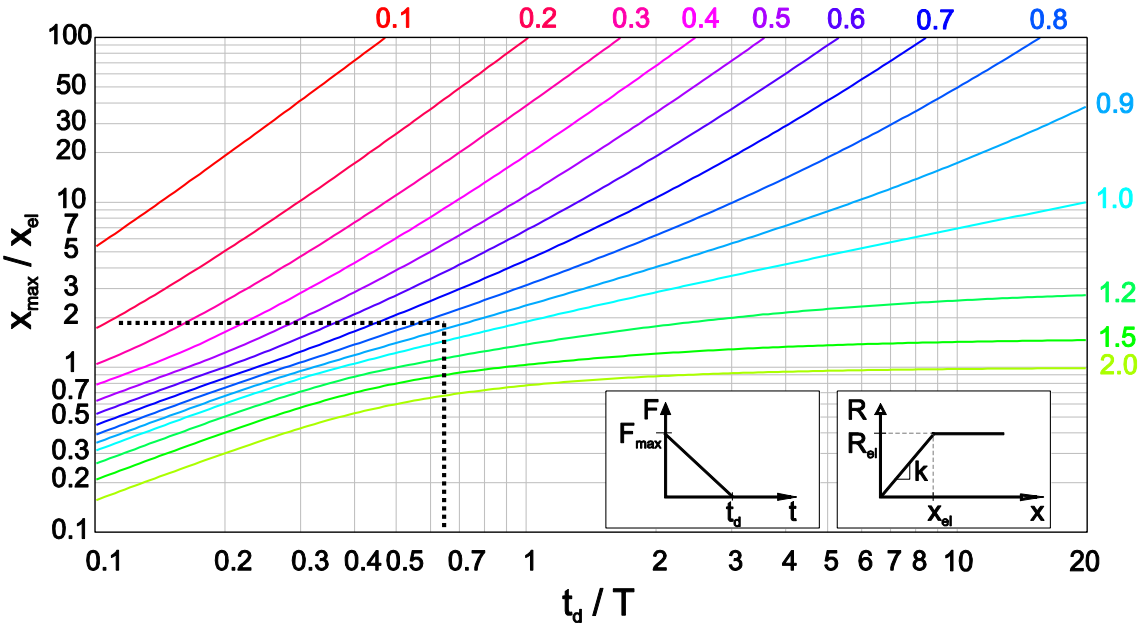

Figure A 37:Normalised response diagram as in [10]

The duration ratio is calculated to: t_d / T = 64 / 110 = 0.58.

The force ratio is calculated to: R_V / F_{max} = 1.24E5 / (5000·7.0·4.1) = 0.864.

From the normalized response diagram, a maximum ductility of ~1.8 can be estimated.

The ADBLAST extension for consideration of membrane effects provides the following diagram for the correction of the estimated ductitlity:

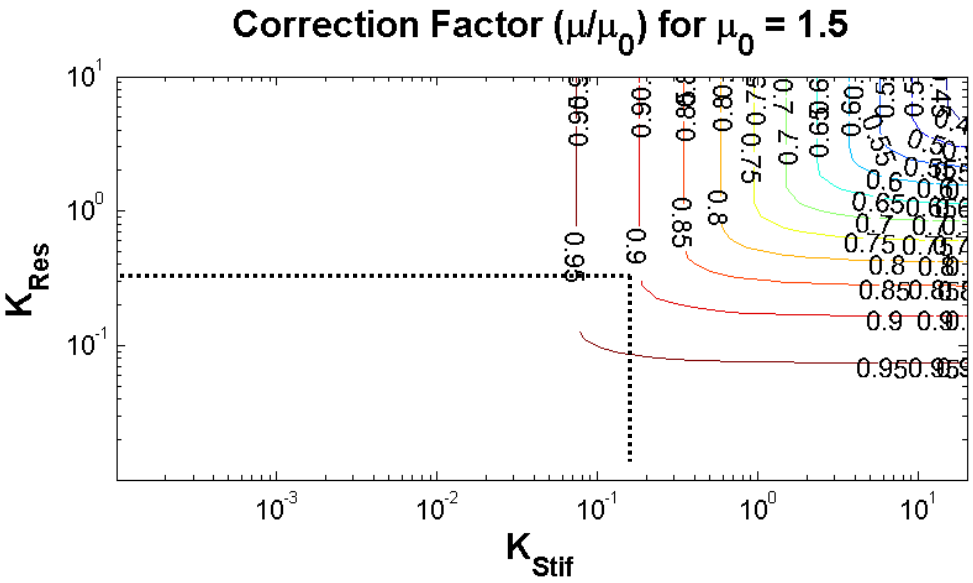

Figure A 38:Correction factor to consider membrane action

In this case, there is a significant contribution from the membrane action. This can be estimated in a reduction of 8% of the expected ductility according to the normalized response diagram. Indeed 0.92·1.8 = 1.656 is closer to the determined solution by means of analytical methods.

7.2.4.5 Prediction of the response by Numerical Methods

By means of numerical integration (in case of Norsok and Fabig) and Finite Element Calculations (ADBLAST), the evolution of the response in the time domain can be calculated. For validation purposes, the results of an exact model with beam elements is shown here.

The analytical results are shown here for comparison as well.

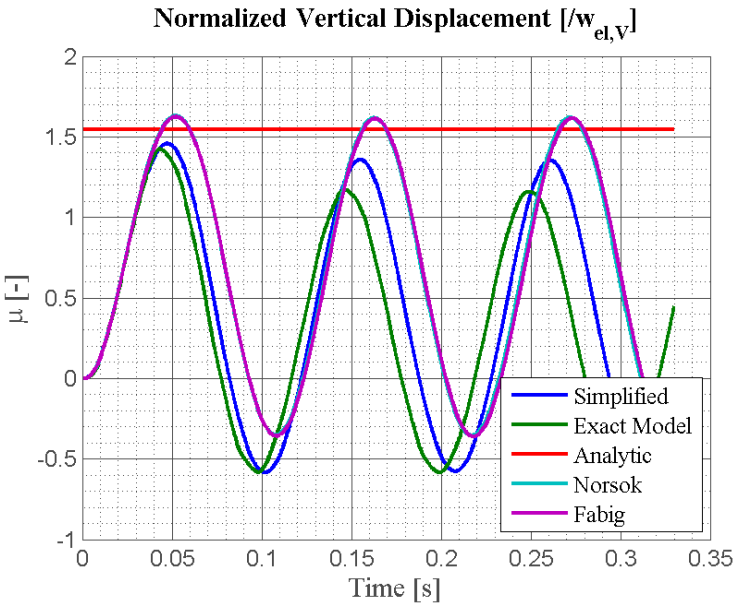

Figure A 39: Normalized Vertical Displacements for the subassembly cladding + purlin under explosive loading

The longitudinal connector displacements can only be evaluated by means of the new simplified ADBLAST approach as well as by the proposed analytical method:

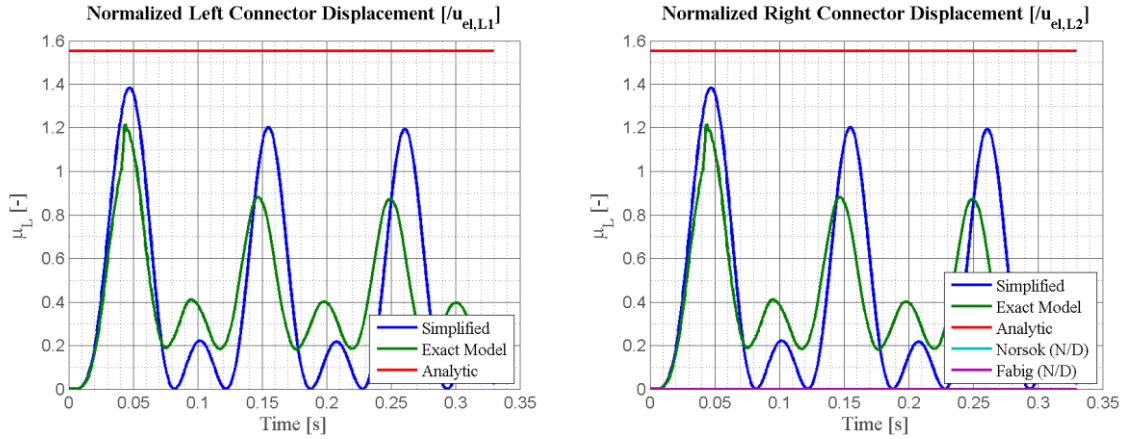

Figure A 40: Normalized Longitudinal Displacement of the left (left) and right (right) connector for the subassembly cladding + purlin under explosive loading

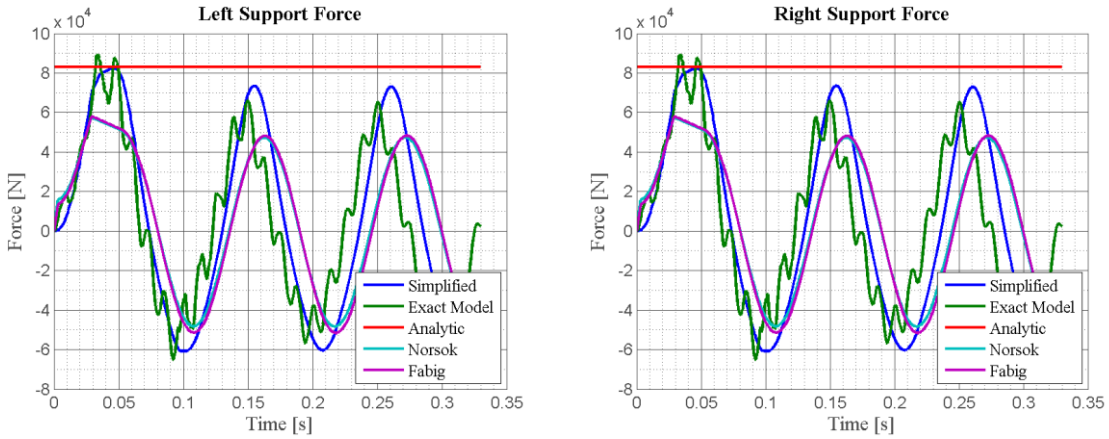

Figure A 41: Transferred Forces on the left (left) and right (right) support (with free rotation) for the subassembly cladding + purlin under explosive loading

7.2.4.6 Design Check

Attending to the presented criteria in Chapter 4, the purlin is required to achieve a maximum ductility of 1.544. This value can be accepted by all recommendations for blast design according to the different codes.

The maximum support rotation can be estimated by:

$$\varphi_{max} = \mu_{max} \cdot \frac{w_{el,V}}{L/2} = 1.544 \cdot \frac{0.095}{7.0/2} \cdot \frac{180}{\pi} = 2.4°$$

This end rotation is not acceptable within level of protection 1 according to UFC (see Table A 5).

The maximum shear force transmitted onto the main structure is of around 82 kN. This force needs to be absorbed by the main structure. Here it is advisable to investigate whether this load can lead to patch loading of the web plate of the main column.

The substructural assembly will resist to the blast load with some damage but without a complete failure.

8 Literature

[1] CEB (1988), Structures under impact and impulsive loading, Bulletin d'Information No 187, Comite Euro-International de Beton, CEB

[2] Soroushian, P. and Choi, K. (1987) Steel mechanical properties at different strain rates. Journal of Structural Engineering, ASCE, 113(4) 663-673.

[3] Bodner, S.R. and Symonds, P.S. (1960) Plastic deformations in impact and impulsive loading of beams. Proceedings of the Second Symposium on Naval Structural Mechanics, Rhode Island, USA, 488-500

[4] United States of America, Corps of Engineers, EM 1110-345-415; Design of structures to resist atomic weapons : Principles of Dynamic Analysis and Design, Washington D.C., 1957.

[5] C. H. Norris, R. J. Hansen, M. J. Holley, J. M. Biggs, S. Namyet und J. K. Minami, Structural Design for Dynamic Loads, New York: McGraw-Hill, 1959.

[6] J. M. Biggs, Introduction to structural dynamics, New York: McGraw-Hill, 1964

[7] Det Norske veritas, DNV-RP-C204: Design against Accidental Loads, 2010

[8] Norsok, N-004: Design of Steel Structures, Oslo, 2013.

[9] Fire and Blast Information Group (FABIG), Simplified methods for analysis of response to dynamic loading, Ascot: Steel Construction Institute, 2002.

[10] United States of America, Department of Defense, UFC 3-340-02: United Facilities Criteria: Structures to Resist the Effects of Accidental Explosions, 2008.

[11] W. Baker, P. Cox, J. Kulesz, R. Strehlow und P. Westine, Explosion Hazards and Evaluation, Oxford: Elsevier Science, 1983.

[12] K. Meskouris, Structural Dynamics, Ernst & Sohn, 2000.

[13] M. Gündel, B. Hoffmeister und B. Hauke, Bemessung von Baustrukturen in Stahl- und Verbundbauweise für Anprall- und Explosionslasten, bauforumstahl e.V., Düsseldorf, 2010

[14] Morison, Colin M. (2006): Dynamic response of walls and slabs by single-degree-of-freedom analysis—a critical review and revision. In: International Journal of Impact Engineering 32 (8), S. 1214–1247. DOI: 10.1016/j.ijimpeng.2004.11.008.

[15] United States of America, Corps of Engineers, PDC TR 06-02, Rev 1: User's Guide for the Single Degree of Freedom Blast Effects design Spreadsheets (SBEDS), 2008

[16] Wriggers, Peter: Nonlinear Finite Element Methods. Berlin, Heidelberg: Springer Berlin Heidelberg, 2008

HOW TO OBTAIN EU PUBLICATIONS

Free publications:

- one copy:
  via EU Bookshop (http://bookshop.europa.eu);
- more than one copy or posters/maps:
  from the European Union's representations (http://ec.europa.eu/represent_en.htm);
  from the delegations in non-EU countries (http://eeas.europa.eu/delegations/index_en.htm);
  by contacting the Europe Direct service (http://europa.eu/europedirect/index_en.htm) or calling 00 800 6 7 8 9 10 11 (freephone number from anywhere in the EU) (*).

  (*) The information given is free, as are most calls (though some operators, phone boxes or hotels may charge you).

Priced publications:

- via EU Bookshop (http://bookshop.europa.eu).

KI-NA-27487-EN-N

Steel structures and components can provide effective systems for blast resistance, yet this potential has not been adequately utilised due to lack of appropriate knowledge and methods.

This project aimed to develop fundamental design guidance for steel structures under external blast loads with emphasis on procedures suitable for typical industrial buildings. The work involved risk assessment and benchmark examples for certain scenarios including safety and performance requirements as well as derivation of pressure impulse loadings for structures.

Analytical methods were used to develop a new simplified model, which allows for a numerical and analytical solution of blast loaded structures. This model allows for an easy design of blast loaded structural elements and full structures including nonlinear effects such as large deformations, membrane (or catenary) action of elements and effects of energy dissipation. This methodology leads to a significantly more efficient and economic design. By including the explicit consideration of fasteners and connectors involved in the membrane effects, the model can even predict connector failure and relate it to the achieved level of transversal deformation.

The method was validated by blast tests, laboratory experiments and by numerical computations. It proved to be applicable for the assessment of steel structures under external blast.

The methodology was comprehensively summarized and made available by preparing a design guide for structural engineers, where several examples are provided.

Studies and reports

Publications Office

ISBN 978-92-79-52096-9
doi:10.2777/141025